EPSC Abstracts
Vol. 10, EPSC2015-15, 2015
European Planetary Science Congress 2015

Non-monotonic potentials near the sunlit side of the Moon

T.M.Burinskaya
Space Research Institute, Moscow, Russia (tburinsk@iki.rssi.ru)

Abstract

The day-side lunar surface is electrically charged due to the joint action of solar ultraviolet radiation and interactions with the plasma environment. Basic equations describing stable non-monotonic altitude profiles of the electric potential arising near the Moon's surface exposed to the solar radiation are obtained for various plasma environments that surround it: the solar wind and the terrestrial plasma sheet. It is found that for both cases the surface potential grows as the photoelectron density increases, but the minimum value of the non-monotonic potential profiles is practically independent of the photoelectron density, and is defined by the parameters of the surrounding plasma. When the lunar surface is irradiated by the solar wind both potentials possess the minimum values in the range of drift velocities typical of the slow solar wind under normal conditions. When the Moon is exposed to both solar radiation and the terrestrial plasma sheet, the surface potential and the minimum value of the non-monotonic profile depend strongly on the temperature of plasma sheet populations, particularly in the range where the ratio of the ion temperature to the electron temperature is less than three.

1. Introduction

On the sunlit side of the Moon the lunar surface is charged due to the joint action of solar ultraviolet radiation, resulting in the photoelectron emission and interactions with the ambient plasma. A number of papers have been done on the formation of electric fields near a surface emitting photoelectrons under the action of solar radiation. It was found that two types of potential distribution can take place: a monotonic distribution that constantly increases or decreases, and a non-monotonic distribution that decreases from the surface to a negative minimum and then tends to zero at infinity; and it was shown that the non-monotonic potential profile is energetically preferred to the monotonic solution, see [1] and references therein. The objective of this paper is to investigate how the key parameter of the non-monotonic potential distribution varies under different plasma conditions in a wide range of the photoelectron densities. Currently we have not the unambiguous data of the parameters and distributions of photoelectrons over the illuminated lunar surface. This problem is discussed in the paper [2], where it is shown that the quantum yield of lunar regolith is the main parameter determining the density, temperature, and distribution function of photoelectrons. At present, this parameter is determined with significant uncertainty analyzed in the above mentioned paper, and the direct measurements on the Moon's surface performed in the framework of future lunar missions are proposed as the best solution of this problem. Taking into account the incompleteness of our knowledge of photoelectron density near the lunar surface, we made calculations in a wide range of densities with a purpose to estimate its influence on the potential profile near the lunar surface. At first, we used the results of [3], examining the lunar regolith samples exposed to sunlight. It was shown that the current density of photoelectrons emitted from the lunar surface could be estimated as 4.5×10^{-6} A/m^2, and the energy distribution could be approximated by a Maxwellian distribution with temperature 1.47 eV. Therefore, the photoelectron density is ~ 1.38×10^{8} m^{-3}. Recently measurements performed on the Lunar Reconnaissance Orbiter have demonstrated the presence of hydrogen-containing regions on the Moon's surface. For these regions the photoemission capability can be higher in comparison with the pure regolith regions. In [2] the photoelectron density was calculated for regions covered with a hydrogen monolayer under assumption that the photoelectric work function is 4 eV. The obtained photoelectron density ~2×10^{14} m^{-3} is much greater than the density for regolith regions. So we have used this value as the highest limit for the photoelectron density. We carried out calculations as well for the photoelectron density ~2×10^{11} m^{-3} found in [2] using the semiempirical dependence of the quantum yield obtained on the experimental database for the work function on the order of 6 eV.

2. Lunar surface in the terrestrial plasma sheet exposed to the solar radiation

We are looking for a steady state non-monotonic distribution of the electric potential along the normal to the lunar surface. The electric potential at the surface is equal to φ_0, an altitude profile of the potential has one minimum $\varphi_1<0$ and tends to zero at infinity. Because the thermal velocity of the solar wind ions is much less than the flow velocity of the solar wind, ions are assumed to be cold and moving with a drift velocity at infinity. The solar wind electrons have a Maxwellian velocity distribution shifted by the drift velocity. Photoelectrons emitted from the lunar surface can be approximated by a Maxwellian distribution. Plasma at infinity is assumed to be neutral with zero net current and zero electric field. We find the set of equations which numerical solutions allow us to construct the altitudes profiles of the electric field above the Moon's surface and the densities of photoelectrons and solar wind electrons as functions of the solar wind velocity and photoelectron density emitting from the surface [4]. Calculations have been performed in a wide range of the ratio of the solar wind velocity to the electron thermal velocity for different values of photoelectron densities. It is shown that, although the thermal velocity of electrons is well above the drift velocity, accounting for the latter in the electron velocity distribution substantially affects the value of the potential, particularly in the lunar regolith regions, where the surface potential halves, while the absolute value of the potential minimum doubles as compared to the calculations made when the electron flow velocity was disregarded. The results of our investigation have shown that the value of the potential minimum φ_1 is practically independent of the photoelectron density, and is defined by the parameters of the solar wind. For a given velocity of the solar wind the surface potential φ_0 grows as the photoelectron density increases. Both potentials possess the minimal values when the ratio of the solar wind velocity to the electron thermal velocity is on the order of 0.23 which corresponds to a slow solar wind for normal solar wind conditions.

3. Lunar surface in the terrestrial plasma sheet exposed to the solar radiation

Large negative potentials detected by the Lunar Prospector Electron Reflectometer (LPER) instrument, when the Moon was in the terrestrial plasma sheet exposed to the solar radiation, were analyzed extensively in [5] by comparison between a sample of measurements obtained onboard the Lunar Prospector and 1-D particle-in-cell simulations. It was found that LPER measurements are best explained by the presence of stable, non-monotonic potential above the lunar surface. However in [5] it was not taken into account that the ratio of ion to electron temperatures in the plasma sheet for distances more than 60 Earth's radius is on the order of 5.5. Taking into account that this parameter is still understood incompletely, we made calculations of key parameters φ_0 and φ_1 controlling the non-monotonic potential profile in a wide range of T_i/T_e ratios for different values of the photoelectron density under assumption that the plasma sheet ions and electrons have Maxwellian velocity distributions, each of them with its temperature. The numerical calculations of obtained equations have shown that a value of the potential minimum φ_1 is defined by the parameters of the terrestrial plasma sheet and does not depend on the photoelectron density [4]. The surface potential grows as the photoelectron density increases but remains negative in a range of parameters under consideration; however the surface charge remains positive and electric field is directed upward from the surface because there is a potential minimum. Both potentials are strongly governed by the temperature of the plasma sheet ions and electrons, and rise sharply in the range $T_i/T_e \leqslant 3$. Then both potentials continue to grow more gradually.

Acknowledgments

This work was partially supported by RFBR grant №15-02-05627.

References

[1] Poppe, A., and M. Horányi: Simulations of the photoelectron sheath and dust levitation on the lunar surface. J. Geophys. Res. 115, A08106, , 2010

[2] Popel, S. I., A. P. Golub, Yu. N. Izvekova, V.: On the distribution of photoelectrons over illuminated part of the Moon. JETP Letters, 99, 115-120, 2014.

[3] Feuerbacher, B., M. Anderegg, B. Fitton, L. D. Laude, R. F. Willis, and R. J. L. Grard: Photoemission from lunar surface fines and the lunar photoelectron sheath. Geochin. Cosmochim. Acta. Suppl. 3, 2655-2663, 1972.

[4] Burinskaya T. M.: Non-monotonic potentials above the day-side lunar surface exposed to the solar radiation, Planet. Space Sci., doi:10.1016/j.pss.2015.03.004, 2015.

[5] Poppe, A., J. S. Halekas, and M. Horányi: Negative potentials above the day-side lunar surface in the terrestrial plasma sheet: Evidence of non-monotonic potentials. Geophys. Res. Lett. 38, L02103, 2011.

EPSC Abstracts
Vol. 10, EPSC2015-29, 2015
European Planetary Science Congress 2015

The researches on selenodesy and lunar dynamics in Kazan

Y. Nefedyev (1), N. Petrova (1), N.Varaksina (1), K. Churkin, R. Zabbarova (1), A. Andreev (1)
(1) Engelhardt Astronomical Observatory Kazan Federal University, Russia (star1955@mail.ru / Fax: +7843-2927797)

Abstract
In this report is presented the brief history of the development of positional observations and rotation of the Moon in Kazan University and Engelhard Astronomical Observatory from the end of the last century until present.

1. Introduction
In Kazan University and Engelhard Astronomical Observatory (EAO) much attention has been given to investigations of the Moon and its rotation. The brief history list of research works on the Moon carried out by workers of EAO are given below.

2. Historical the positional observations of the Moon
The research work on the Moon and its rotation was started more than one hundred years ago in Kazan State University. In 1894 privat-docent A.V. Krasnov returned from Gettingen where he was sent on a mission by professor D. I. Dubjago (the director of the Astronomical Observatory of Kazan University at that time) for acquaintance with a technique of study of lunar physical libration (LPhL) by a heliometr. Krasnov began systematic observations by the Repsold heliometer which was transferred to Kazan by the Peterburg Academy of sciences in 1874. Then assistant A. A. Mihaylovsky carried out 58 measurements of the Mesting A crater from 1900-1905, and they formed the second Kazan series. After A. A. Mihaylovsky changed his place of work, master of astronomy of Warsaw University, T. A. Banahevitch continued the Moon observations by the heliometer. In 1910-1915 he made 130 precision observations of the Mesting A crater. These observations formed the third Kazan heliometric series. Then A.A.Jakovkin continued observations of the Moon. In 1916 he began to form the fourth series of heliometric observations and he has carried out 251 measurements. After A. A. Jakovkin, I. V. Belkovitch carried out heliometric observations of the Moon for more than 17 years (1931-1948). He made 247 measurements of the Mesting A crater. In 1949 the lunar investigations were continued by A. A. Nefedyev. In a period of 38 years he as astronomer-observer formed two series of heliometric observations of the moon including about 400 measurements of the Mesting A crater. Thus, the scholars of Kazan observatory and EAO received by Repsold heliometer seven series of heliometric measurements of the positions of the Mesting A crater relative to the points of the limb of the Moon through1895 – 1958. The reduction of heliometric observations carried out to study the LPhL is the most difficult work in astrometry. It is not surprising that the observers themselves did not reduce the first heliometric observations. Some German astronomers, who had begun to research rotation and figure of the Moon much earlier, were involved in that work. I. V. Belkovitch offered a fundamentally new way for the determination of parameter f revealing the duality of the solution; the parameter f has two significances about 0.62 and 0.71. The first is closer to the significance of f received later on a basis of space observations. Later Y. A. Nefedyev carried out investigations to improve the method of reduction of the heliometric measurements.

2. Theory of rotation of the Moon
The most significant theoretical investigation the Moon's rotation is undoubtedly the work by Sh. T. Habibullin, "The Nonlinear theory of LPhL". The author solved the problem of nonlinear fluctuations of the Moon's rotation with methods of N. M. Krylov, N. N. Bogoljubov and N. G. Malkin. The nonlinear theory in case of a resonance (f=0.622) gives the steadier solution in contrast to the linear theory. In the intervals which are far from the resonance, the nonlinear theory does not reveal essential refinements in comparison with the linear theory, but more authentically describes so called "free libration". The article by Sh. T. Habibullin shows that free libration of the Moon was not more than 0.3". Sh. T. Habibullin and Ju. A. Chikanov [18] considered the problem of lunar free libration and Eilerian movement of its poles that is free libration in great detail.
Currently modern problems in the lunar spin-dynamics are considered in EAO. The accent is done on the fine phenomena of the lunar libration caused by complicated interior structure. Parameters of a free libration are studied as well as the geometrical interpretation of the chandler-like and the free core nutation.

Kazan astronomers led by N.Petrova [1,2] participate in Japanese project ILOM (In situ Lunar Orientation Measurement), which is planned to be realized as one of kinds of observations of lunar rotation. One of the important elements of the project is placing of a small optical telescope on the lunar surface with the purpose to detect the lunar physical libration with high accuracy 0.001 arc sec. Computer simulation of the future observations is being done with the purpose of their optimization: effective placement of measuring system on the lunar surface, testing of sensitivity of new observations to various features of the lunar interior structure. The results of the first stage of the simulation were obtained. At this stage the software for the selection of stars and reduction of their coordinates onto the period of observations is developed, the tracks for the selected stars are constructed and analyzed, their sensitivity to the internal characteristics of the lunar body, in the first place, to the selenopotential coefficients, is tested.

It is shown that selenographic coordinates of polar stars are insensitive to longitudinal librations т (t). Comparing coordinates calculated for two models of a rigid and deformable Moon is carried out and components sensitive to Love number It2 are revealed.

3. Selenodesic system of the coordinates and geometrical figure of the Moon

In EAO carried out the works to study the lunar figure and reference system for its surfaces. Sh. T. Habibullin gave the theoretical substantiation of lunar cartography in the article [3].

A. A. Nefedyev constructed maps of the marginal zone of the Moon [4] on the basis of 5630 altitudes in the marginal zone obtained by heliometric measurements. In this fundamental work the solution of the problem about the zero surface from which the altitudes on the Moon should be measured was found. F. Hayn, T. Weimer and C.B. Watts in solving the similar problem had left this issue opened. Y. A. Nefedyev improved those maps taking into account the "effect of Yakovkin" .

L. I. Rakhimov constructed on the basis of measurements of more than 40000 points of limb on 127 large-scale star-callibrated lunar photographs, the maps of the marginal zone of the Moon for the first time referred to a centre of its mass [5]. These maps should be considered as the most authentic among all other maps of altitudes in the marginal zone of the Moon.

From 1975-1985 Ju. A. Nefedyev made 1500 measurements with the purpose of determining the selenocentric coordinates of 10 craters by referring to stars. Thus for the first time the construction of the completely independent system coordinates of 10 craters was established.

N. G. Rizvanov investigated a geometrical figure of the near side of the Moon on large-scale star-callibrated lunar photographs [6]. The average values of the heights of these areas determine the absolute heights of appropriate areas. It turned that the relief of the Moon surface, according to the catalogue [6], to the north from parallel +10 degrees was up to 2 km below the standard level determined with other ground-based observation of the Moon. This effect was confirmed by the analysis of photographs of the Moon from spacecraft "Zond-6,-8" and other space experiments.

Relief of the lunar near side with data of six selenodesic catalogues constructed on ground-based observations was investigated. The analysis of the physical surface was made by means of the expansion of the absolute heights of craters in terms of spherical functions.

M. I. Shpekin on the basis of the analysis of photographs of the Moon from spacecraft "Zond-6,-8" gave a quantitative description of the region of the sea East.

At the present time Y.Nefedyev and N.Varaksina [8] have made the selenocentric dynamical reference net which covers the visible and far sides of the Moon and contains 248200 objects.

4. Summary and Conclusions

Thus, Kazan is one of the developed centers to explore the Moon and the results obtained by Kazan astronomers are an important contribution to the lunar planetology.

Work was supported by grants RFBR 15-02-01638-a, 15-02-01638-a and 14-02-31296-mol-a.

References

[1] Petrova N., Hanada H. (2012) Planetary and Space Science, V. 68, 86-93.
[2] Petrova N., Abdulmyanov T., Hanada H. (2012) J. Adv. Space Res, V. 50, 1702-1711.
[3] Habibullin Sh.T. (1968) Astr. Journ, 45, 3, 663-674.
[4] Nefed'ev A.A. (1955) Trans. EAO, 29, 21-110
[5] Rakhimov L.I. (1993) Trans. EAO, 57, 69-113.
[6] Habibullin Sh. T., Rizvanov N.G. (1984) Earth, Moon and Planets, 30, 1, 1-19.
[7] Nefedyev, Y., Valeev, S., Mikeev, R., et al. (2012) , Advanced in Space Research, №50, 1564 – 1569.

EPSC Abstracts
Vol. 10, EPSC2015-31, 2015
European Planetary Science Congress 2015

Using Huber's robust method in astronomy for reduction of the selenodesic observations

Y. Nefedyev (1), V.Bezmenov (2), S. Demin (1), K,Churkin, A. Andreev (1)
(1) Engelhardt Astronomical Observatory, Kazan Federal University, Russia (star1955@mail.ru / Fax: +7843-2927797)
(2) Kazan Federal University, Russia

Abstract

Modern robust methods reduction of the observations permit to exclude faulty measurements, which by use of a classical method of the least squares (MLS) can deform of estimates. We used Huber's method of M estimated. It is shown on example reduction item geliometrical observations of the lunar craters relative to stars.

1. Introduction

In astronomy the observations of many phenomena (factors) in difference from experiments in physics, chemistry cannot be repeated. Therefore each such measurement presents large value. On the other hand some part astronomical observations, as experiments in other natural sciences, can be faulty. We will not analyze the reasons of occurrence of errors. We will note only, that they can be stipulated by many factors: conditions of astroclimate, the moments of observation, malfunction of an equipment, human factor and etc.
Therefore the large influence to final results accuracy can render choice of an effective reductions method of observations which would allow excluding "abnormal" observation. At present known many mathematical methods of statistics, in particular, robust methods [1]. The testing such methods in astronomy on example reduction of lunar craters with stars heliometrical observation is below resulted. In parallel these observations were reduced by classical method MLS. The results received by this two methods reduction were caparisoned. The final purpose of this work is to show efficiency of use of Huber's robust method in astronomy.

2. Method

The main purpose of robust method is to eliminate interference of gross measuring errors. Today various robust methods of estimators are known, and the method based on maximum likelihood is respected as the best one. For the first time the present method was offered by Huber [2]. He called one by M - estimators method since there are the proximity to estimators of the maximum likelihood. The method was described in works [1, 3 ,4]. M-estimators method is widely applied while analyzing various kinds of measurements containing gross errors. The reason is that method is relatively simple in comparison with other robust methods and it allows to use standard calculation procedure of MLS.
Under certain conditions (no irregular measurements; measurements are independent; etc.) the results obtained by robust method must concur with results obtained by MLS method.
From the general point of view the models of investigated phenomenon can be presented in the following way:

$$S = G(p; q) + \varepsilon, \qquad (1)$$

were $S = [S_1, S_2, \ldots, Sn]$ is vector of measured distances and $P = [p_1, p_2, \ldots, p_n]$ is vector of position angles of the craters – stars vectors, $\varepsilon = [\varepsilon_1, \varepsilon_2, \ldots, \varepsilon_n]$ - is vector accumulated errors, q - is vector of parameters to be determined m values.
It's necessary to note that vector q concrete form will be determined by equation

$$q = [\xi, \eta, \zeta]; \qquad (2)$$

were ξ, η, ζ is selenocentric rectangular coordinates. Vector of accumulated errors ε will consist of errors in observations of distances vector ε_s, and vector of ε_0 - response to measurement errors of position angles ε_p

$$\text{epsilon} = \varepsilon_s + \varepsilon_0 \qquad (3)$$

In formula (3)

$$\varepsilon_0 = G(\varepsilon_p; q_u), \qquad (4)$$

were q_u is vector q true value.
In general case q' solution consists the calculation of vector $\triangle q$ of amendments to q_0 initial values. For this purpose we have to solve the system equations.

$$A \triangle q + \varepsilon = Z, \quad (5)$$

were A - is equations factors matrix and Z is vector of free members

$$Z = S - S0, \quad (6)$$

were S_0 is vector of dimensions calculated values.

If we apply method of least squares we'll get the following solution of the system (5):

$$\triangle q' = (A^T PA)^{-1} A^T PZ, \quad (7)$$

were P is weight (diagonal) matrix.

Well known MLS formulae $Q = (A^T PA)^{-1}$ for covariational matrix are applied to estimate the accuracy of the solution obtained for vector $\triangle q'$ components which are situated obliquely in the matrix Q.

Some the heliometric observations are erroneous. Their part in heliometric series can exceed 20%. It is known that MLS estimators are very sensitive to gross errors in observations. In practice various methods are applied to filter measurement information for irregular observations/ The heliometric observations are not an exception. Usual irregular observations are detected:

1. By analysis of notes in observational journals;
2. By examination of condition $|Zi| < \delta\Lambda^{add}$.

The apprehension that not all irregular observations can be detected and eliminated is enough valid. Reliability of the lunar rectangular dynamic coordinates determination can be increased by applying robust method together with MLS.

It is shown that Huber's function ψ must be limited and continued. Several ψ functions can be listed, as examples, possessing above mentioned properties. For instance, Huber determined function shape for normal cluttered distribution.

3. Heliometric observations analysis results

Dynamic coordinates of the lunar craters have been obtained from absolute heliometric observations (positioning relatively the stars). It is possible to note considerable difference between estimations for coordinates of the craters Kepler A, Egede A and Sinas while comparing results obtained by MLS - method and the robust method. Repeated analysis of the vector of the free members of equations (5) (for each of the mentioned craters) allowed regarding at least two measurements as erroneous. In case these measurements the M – estimators method (a = 1:500) must be taken for estimators of the craters Kepler A, Egede A, Sinas coordinates. Concerning other craters the difference between MLS - estimators and M - estimators is not considerable. Data for the mentioned craters has been examined repeatedly and erroneous measurements have been not detected. t is possible that M - estimators of dynamic coordinates of the craters Messier A, Pons P, Hesiodus B, Flamsteed A, Archimedes A, Luther and Mesting A it would be preferable

4. Summary and Conclusions

In general, results of analysis of the lunar heliometric observations obtained by means of two alternative kinds of statistical procedure (MLS - method and robust method) allow to conclude the following: 1. after measurement information has been filtered some measurements remain which may be regarded as doubtful if not erroneous. 2. We consider that if those measurements not eliminate, then it is possible to take M - estimators for estimations of the lunar craters dynamical coordinates as well.

Work was supported by grants RFBR 15-02-01638-a, 15-02-01638-a and 14-02-31296-mol-a.

References

[1] Huber, P.J., (1981), Robust Statistics (Wiley, New York).

[2] Huber, P.J., (1964), Ann. Math. Statist, 1, 35.

[3] Gardiner, B.G., A.R. Webb, A.F. , et al, (1993), Env. Tech., bf series, 14(1), 25-43.

[4] Huber, P.J., (1977), Robust Statistical Procedures,CBMS-NSF Regional Conference Series in Appl. Math.. SIAM, Philadelphia.

EPSC Abstracts
Vol. 10, EPSC2015-32, 2015
European Planetary Science Congress 2015

The analysis of the lunar centre masses position

A. Andreev (1), Y. Nefedyev (1), N. Petrova (1), N.Varaksina (1), K. Churkin, R. Zabbarova (1), (1)
Engelhardt Astronomical Observatory Kazan Federal University, Russia (star1955@mail.ru / Fax: +7843-2927797)

Abstract

The relative position of lunar center masses relative to center of the figure in Kazan was customized. The expansions by spherical harmonics N=5 degree and order of the lunar function h(λ, β) with using the package ASNI USTU were executed. Module of the expansion of the local area to surfaces to full sphere was used. The parameters of cosmic missions are given for comparison (SAI; Bills, Ferrari).

The normalized coefficients from expansions for eight sources hypsometric information are obtained: Clementine (N=40), Kazan (N=5), Kiev (N=5), SAI (N=10; Chuikova (1975)), Bills, Ferrari, - Kaguya (Selena, Japan mission), ULCN (The Uuified Lunaz Control Network 2005).

The displacements of the lunar centre figure relative to lunar centre of the masses were defined from equations [1]. The results of the obtaining relative position of the lunar centre masses and centre of the figure in Kazan selenocentric catalogue give good agreement with modern cosmic mission data..

1. Introduction

The knowledge of the center of mass position of the Moon relative to its center of the figure is important for researches the lunar origin, structure and evolution and in terms of precision solutions circumlunar navigation tasks. To date this task is the most relevant and demanded for cosmic lunar missions.

2. Models, methods and software for the expansion of the lunar topography into spherical harmonics

The research work on the Moon and its rotation was Just as in [1] offsets Δ center of the figure (CF) were obtained relative to the center of the coordinate system any catalogue. The formulas used in [1] are as follows:

$$\Delta\xi = \sqrt{3}\overline{C}_{11}, \Delta\eta = \sqrt{3}\overline{S}_{11}, \Delta\zeta = \sqrt{3}\overline{C}_{10},$$

where ξ is the axis directed toward the Earth, η is equatorial axis directed perpendicular to ξ , ζ is rotation axis of the Moon, are the normalized amplitudes of the harmonics of the first order expansion of the relief. Next, we consider below:

- mathematical models in the form of expansions in spherical functions - methods for estimating the model parameters
- information technology data processing.

As a model describing the behavior of the relief on the lunar sphere is used the expansion of the height in a series of spherical harmonics [2] in the form of a regression model GA [3]:

$$h(\varphi,\lambda) = \sum_{n=0}^{N}\sum_{m=0}^{n}\left(\overline{C_{nm}}\cos m\lambda + \overline{S_{nm}}\sin m\lambda\right)\cdot\overline{P_{nm}}(\cos\varphi) + \varepsilon$$

where φ,λ are (latitude, longitude) coordinates of well-known lunar objects; C_{nm}, S_{nm} are normalized harmonic amplitudes ; $\overline{P_{nm}}$ is normalized associated Legendre functions; ε random error of regression.

3. Theory of rotation of the Moon

The solution of an overdetermined system GA for different sources of hypsometric information conducted within the framework of regression modeling approach [3]. It is providing for addition to the usual steps (the postulation of the model GA and the estimation of amplitudes C_{nm} , S_{nm}) using a number of statistics quality including external measures:

- diagnosis of the basic conditions of the method of least squares;
-the adaptation when they are violated. As the computational schemes of the method of least squares are used Gauss-Jordan and Householder schemes.

Main violations of conditions when used the method of least squares for workup GA are the availability of [3]:

-the redundant (noise) of harmonics resulting in decreased accuracy of prediction both individual heights and isohypses;
- correlated with each other amplitudes of the harmonics in the application of GA to describe the relief on the segment of a sphere or in a strong inhomogeneous distribution of objects. In this case the digital model (the method of least squares

estimates of amplitudes) must be considered incorrect.

Using stepwise regression it is possible to adapt to two specified violations using the known procedure of regression analysis [3]. It will be very effective for estimating the parameters of the model GA if the following conditions are carried out:

a) the objects are non-uniformly distributed throughout the sphere;
b) the expansion's order defined as the number of points should be relatively small (n less than 15). Otherwise the calculation time will increase sharply.

For a uniform distribution of objects across the sphere is enough to eliminate statistically insignificant harmonics and execute the calculations again.

The direct use of the model **GA** for the individual sections of the sphere (hemisphere, etc.) is difficult because there are interdependencies (multicollinearity) between the coefficients of the expansion. In earlier works to describe the topography on the near side of the Moon was used "mirror" display of objects in the opposite direction which of course is unacceptable to describe the relief of individual segments which are smaller area of the hemisphere. In [4] was proposed a method of estimating the amplitudes of the model **GA** by first expanding the segment to a complete sphere which allows to eliminate the effect of multicollinearity. Then the noise harmonics are removed by stepwise regression.

To obtain the expansions **GA** in spherical harmonics in order to create a digital model and determine estimations of the center of mass position of the Moon relative to its center of the figure required in the future was used ASSR "Sphere" (an automated system of scientific research [3], [4].

ASSR "Sphere" is intended to describe the distribution of various values of the parameters (topography, gravity, magnetic, and other types of potential fields) on the sphere and its parts which were measured in points with known coordinates. With using this bundled software can generate models of the form **GA**, carry out forecasting in the form of cross-sections, contour, tone and three-dimensional representation of the distribution of values of characteristics. The formation of models **GA** is accompanied by an estimation of their quality and diagnostic of adherence of method of least squares conditions. When they are violated the relevant methods of adaptation are used.

ASSR "Sphere" in the "splitting" mode can be applied to models of large orders for parallel processing.

For describing the potential field areas on sphere (gravity anomalies, magnetic field, the soil characteristics, etc.) can be used known software package SURFER which is similar to the ASSR "Sphere". Through the use of expansions in spherical harmonics with the expansion to the full scope in ASSR "Sphere" and other properties as described above the using this complex for analyze the earth's surface allows for increased accuracy of description and prediction of 40% or more beside with SURFER.

- The main results
- Digital models of the relief for the full sphere and the visible side of the Moon

4. Summary and Conclusions

It should be noted that that the "KSC-1162" catalogue, which was made in the center of mass and principal axes of inertia of the Moon, has the closest agreement with the results of recent space missions if using the objects outside its coverage area on sphere of the Moon.

It should be noted that the correction of the first measurements of the "Clementine" mission data which were made by the authors of the "ULCN 2005" catalogue It was apparently related to the data on the visible side of the Moon because the amplitudes and offsets for the ("KSC-1162" + "Clementine") variant close to the results of the "ULCN 2005" but not "Clementine".

Work was supported by grants RFBR 15-02-01638-a, 15-02-01638-a and 14-02-31296-mol-a.

References

[1] Chuikova N. , (1975), Astronomical Journal, V.52, N.6, 1279-1292.
[2] Sagitov, M., (1979), Moskow, Science, 1-432.
[3] Valeev, S., (2001), Kazan, FEN, 1-296.
[4] Valeev, S., Samohvalov, K., (2006), Kazan, Reports International conference "Near-earth astronomy – 2005", 373-375.

EPSC Abstracts
Vol. 10, EPSC2015-34, 2015
European Planetary Science Congress 2015

The making of selenocentric dynamical catalogue in lunar libration zone

Y. Nefedyev (1), N. Petrova (1), N.Varaksina (1), K. Churkin (1), R. Zabbarova (1), A. Andreev (1)
Engelhardt Astronomical Observatory, Kazan Federal University, Russia (star1955@mail.ru / Fax: +7843-2927797)

Abstract

1. Introduction

Currently the Moon is a subject of research in many space experiments in astronomy and planetary science. Modern space missions "Clementine" and "Lunar Prospector" swiftly and radically changed the situation in the study of the Moon. Today there are the prospects in industrial and robotic exploration of the Moon and creating long-term manned lunar bases. Development of these space technologies imposes special requirements on the results of coordinate - time support. It is including the development of reference systems, establishing mutual orientation of dynamic and inertial coordinate systems and investigation of the dynamics and geometry of the celestial bodies. This fully applies to the dynamic and geometric parameters of the Moon referred to its center of mass. However despite the outstanding results in this direction, derived from observations of space missions "Apollo" and "Zond", the task of creating a global selenocentric network still not completely solved.

The libration zone of the Moon represents rather unknown region. Nowadays there is a large heliometric and photometric observational series and occultations for measuring of a profiles lunar marginal zone. "But they couldn't be used in selenodesic researches, because data were obtained for the different zero surfaces" [1].

2. The method of making catalogue in lunar libration zone

It is known Watts's maps are more correctly [2] However, the coordination system of this map is not coincide with fundamental star's system, therefore the maps of lunar marginal zone "Kazan" has been create in Engelhardt Astronomical Observatory (EAO). In contrast to other previous maps, which were created in a practice, the physical surface within maps "Kazan" [3] is treated to the fundamental sky's coordination system, to ephemeris center of the moon masses and main axis of inertia. So, the method of creating of the selenodesic catalogue for the objects in libration zone consists of the main steps: reduction of the Watts's maps with Morrison's correction [4] to the map's system "Kazan"; authentication of craters on a marginal zone's map with the Total moon map [5], created by SAI MSU and Survey service of USSR under the guidance of Lipsky, and their reduction to the coordination system of Watts's maps accordance with the maps "Kazan". The selenocentric net of the libration moon's zone was obtained by EAO. This catalogue will be used to attach the selenocentric dates of the lunar far side to the selenodesic catalogue system KSK -1162.

The comparison of the maps lunar marginal zone in the range of Gain longitudes from P = 120° to P = 130° is shown in Fig. 1. It is presented for the corresponding libration zone of the Total maps of the Moon, which is obtained within SAI. As can be seen from Fig. 1 there is a good agreement for reliefs for both cases. This confirms the possibility of definition of coordinates for control points in libration zone with the using the maps lunar marginal zone.

3. The comparison of maps for the lunar marginal zone

The inverse problem was solved for identification of the objects of the lunar libration zone.

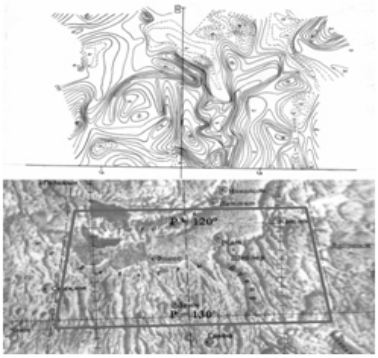

Figure 1: Comparison of the maps "Kazan" in the range on the Gain longitudes from P = 120° to P = 130° with the corresponding libration zone for the Total lunar maps obtained due to SAI

The inverse problem was solved for identification of the objects of the lunar libration zone [6].
The reference selenocentric network contains the coordinates of 1 300 objects of the lunar libration zone. This networks is widely - spread relative the Moon limb, and it is built in the center of mass system of the Moon. It is necessary to note the investigations in this direction are continued now.

4. Summary and Conclusions

On the basis of positional observations in lunar marginal zone was obtained catalog containing 1 300 positions of reference objects selenocentric coordinates in the dynamic coordinate system.

Table 1: The tenderloin from the libration reference catalogue

N п/п	ξ_K	η_K	ζ_K	λ_K	φ_K	H_K
1	0.56791	0.78234	0.25213	66.06	51.54	1736.5
2	0.62688	0.72582	0.27826	66.06	46.62	1735.7
3	0.62250	0.73011	0.27644	66.05	46.98	1735.5
4	0.63555	0.73262	0.23999	69.31	47.16	1736.6
5	0.68287	0.72879	-0.03232	92.71	46.83	1736.8
6	0.68495	0.72272	-0.07804	96.50	46.35	1736.0
7	0.76860	0.62317	-0.13514	99.97	38.60	1735.8

Catalog of selenocentric reference objects (Table 1) contains the following data: the first column indicates the number of the order, the second, third and fourth columns contain selenocentric rectangular coordinates of lunar objects ξ, η, ζ (in fractions of the lunar radius 1738,1 km), the fifth column contain radius vectors R of the craters measured from the center of lunar mass. Further along the selenographic longitude and latitude (λ and φ). Selenographic dynamic rectangular coordinate system ξ, η, ζ tied to the center of mass of the Moon and its axes of inertia. The axis ζ is directed towards the Earth, the axis ξ is directed to the north pole of the Moon and the axis η completes the system of coordinates to the right. All of these axes lie in the principal axes of inertia of the ellipsoid of inertia of the Moon.
Work was supported by grants RFBR 15-02-01638-a, 15-02-01638-a and 14-02-31296-mol-a.

References

[1] Gavrilov I.V., Duma A.S. (1971) Astrometry and astrophysics N 1354-61.
[2] Watts C.B. (1963) Astron. Pap. Americ. Ephem. V 1 1-951.
[3] Rakhimov L.I. (1992) Izvestia EAO N 5789-113.
[4] Morrison L.V. (1979) Monthly Notices N 187 41 -82.
[5] Science leader Yu.N. Lipsky (1979) "Nauka", Moscow
[6] Nefedyev, Y, Varaksina N., et al (2012) Georesurses, № 1 (43), 62 – 64.

EPSC Abstracts
Vol. 10, EPSC2015-47, 2015
European Planetary Science Congress 2015

Petrological Mapping of the Crater Boguslawsky

C. Wöhler (1), N. A. Evdokimova (2), E. A. Feoktistova (3), A. Grumpe (1), K. Kapoor (1), A. A. Berezhnoy (3), V. V. Shevchenko (3)
(1) Image Analysis Group, TU Dortmund University, Dortmund, Germany, (2) Space Research Institute, Moscow, Russia, (3) Sternberg Astronomical Institute, Moscow State University, Moscow, Russia.

Abstract

An analysis of orbital spectral data of the crater Boguslawsky, the intended target region of the Russian Luna-Glob mission, is performed. We have constructed a high-resolution DEM of the crater Boguslawsky, based on which the temperature regime on the surface is investigated. The depth of the OH absorption feature is analysed. The content of the main elements is estimated, and a petrologic map is constructed accordingly.

1. Crater Boguslawsky as a Proposed Landing Site for Russian Luna-Glob mission

The crater Boguslawsky with a diameter of about 95 km [1] is located in the southern lunar highlands. This crater has been chosen as a landing site of the Russian Luna-Glob mission [1]. According to the geologic study in [2], the crater is of Nectarian age, and its floor corresponds to a single geologic unit except a part of the eastern wall which is covered by ejecta material of the smaller crater Boguslawsky D. In [1], the Boguslawsky region is assigned to six different geological units based on a variety of orbital image, laser altimetry and radar data sets as well as counts of small craters and boulders.

2. DEM and Temperature Regime

A digital elevation model (DEM) of the Bogulawsky region has been constructed based on a combination of GLD100 stereo data [3] and Moon Mineralogy Mapper (M^3) radiance data [4] using the method described in [5] (Fig. 1a). The obtained DEM and spectral reflectance data were used for the raytracing-based approach in [6] to model the surface temperature in the vicinity of the crater Cabeus. An alternative, simpler temperature estimation approach is described in [7], where the surface radiance is modelled as the weighted sum of a standard laboratory radiance spectrum and a black body emission spectrum. This method, however, does not yield accurate results for surface temperatures below 250–300 K. Hence, we implemented a further method which extends the thermal equilibrium based approach in [8] by an iterative mutually consistent estimation of spectral reflectance and surface temperature. The result obtained for morning illumination (about 81 hours after local sunrise) is shown in Fig. 1b. For comparison, a map of the DIVINER-based surface temperature [9] at the same illumination is shown in Fig. 1c.

3. Possible OH Presence

The three described methods were used to investigate the influence of the method used for thermal emission removal on the depth of the hydroxyl (OH) absorption near 3 µm wavelength. A M^3-based map of the R_{2657} / R_{2817} reflectance ratio, which can be used as a proxy for the OH absorption depth, is shown in Fig. 1d. The general behaviour is such that the warmer southwestern crater wall displays a weaker OH absorption than the cooler crater floor.

4. Elemental Composition and Petrological Mapping

Global maps of M^3-derived spectral parameters describing the two primary absorption features near 1 µm and 2 µm were used in combination with Lunar Prospector Gamma Ray Spectrometer (LP GRS) [10] data to infer a regression model of the wt% values of Ca, Al, Fe and Mg [7] (cf. also [11]) (Fig. 1e). Using spectral parameter maps of the Boguslawsky region of full M^3 resolution, we then constructed elemental abundance maps and a petrological map of the relative abundances of three endmember rocks (basalt, Mg-rich rock, anorthosite) (Fig. 1f). The floor and walls of Bogulawsky are mainly of typical highland character, only a few small regions on the crater floor (e.g. in the southern part of the western landing ellipse; red, orange and green in Fig. 1f) have a high basalt and/or Mg-rich rock content.

5. Conclusions

We constructed maps of the surface temperature, the OH absorption depth, the main elemental abundances and a petrologic map. The obtained results can be used for preparation of the scientific program of the Russian Luna-Glob mission.

References

[1] Hiesinger, H. et al. (2014) *Geology of the Lunar Glob Landing Sites in Boguslawsky Crater*. LPSC XXXXV, abstract #2370.

[2] Ivanov, M. A. et al. (2014) *Geological context of potential landing site of the Luna-Glob mission.* Solar Syst. Res. 48(6), 391-402.

[3] Scholten, F. et al. (2012) *GLD100: The near-global lunar 100 m raster DTM from LROC WAC stereo image data.* JGR 117, E00H17, DOI: 10.1029/2011JE003926.

[4] Pieters, C. M. et al. (2009) *The Moon Mineralogy Mapper (M³) on Chandrayaan-1*. Current Science 96(4), 500-505. Data download from http://pds-imaging.jpl.nasa.gov/volumes/m3.html

[5] Grumpe, A. et al. (2014) *Construction of lunar DEMs based on reflectance modelling.* ASR 53(12), 1735-1767.

[6] Berezhnoy, A. A. et al. (2012) *Origin and stability of lunar polar volatiles.* ASR 50(12), 1638–1646.

[7] Wöhler, C. et al. (2014) *Integrated topographic, photometric and spectral analysis of the lunar surface: Application to impact melt flows and ponds.* Icarus 235, 86-122.

[8] Shkuratov, Y. et al. (2011) *Optical measurements of the Moon as a tool to study its surface.* PSS 59(13), 1326-1371.

[9] Paige, D. A. et al. (2010) *The Lunar Reconnaissance Orbiter Diviner Lunar Radiometer Experiment.* SSR 150(1-4), 125-160. Data download from http://pds-geosciences.wustl.edu/missions/lro/diviner.htm

[10] Lawrence, D. J. et al. (1998) *Global elemental maps of the Moon: The lunar prospector gamma-ray spectrometer*. Science 281 (5382), 1484-1489.

[11] Shkuratov, Y. et al. (2005) *Derivation of elemental abundance maps at intermediate resolution from optical interpolation of lunar prospector gamma-ray spectrometer data*. PSS 53(12), 1287-1301.

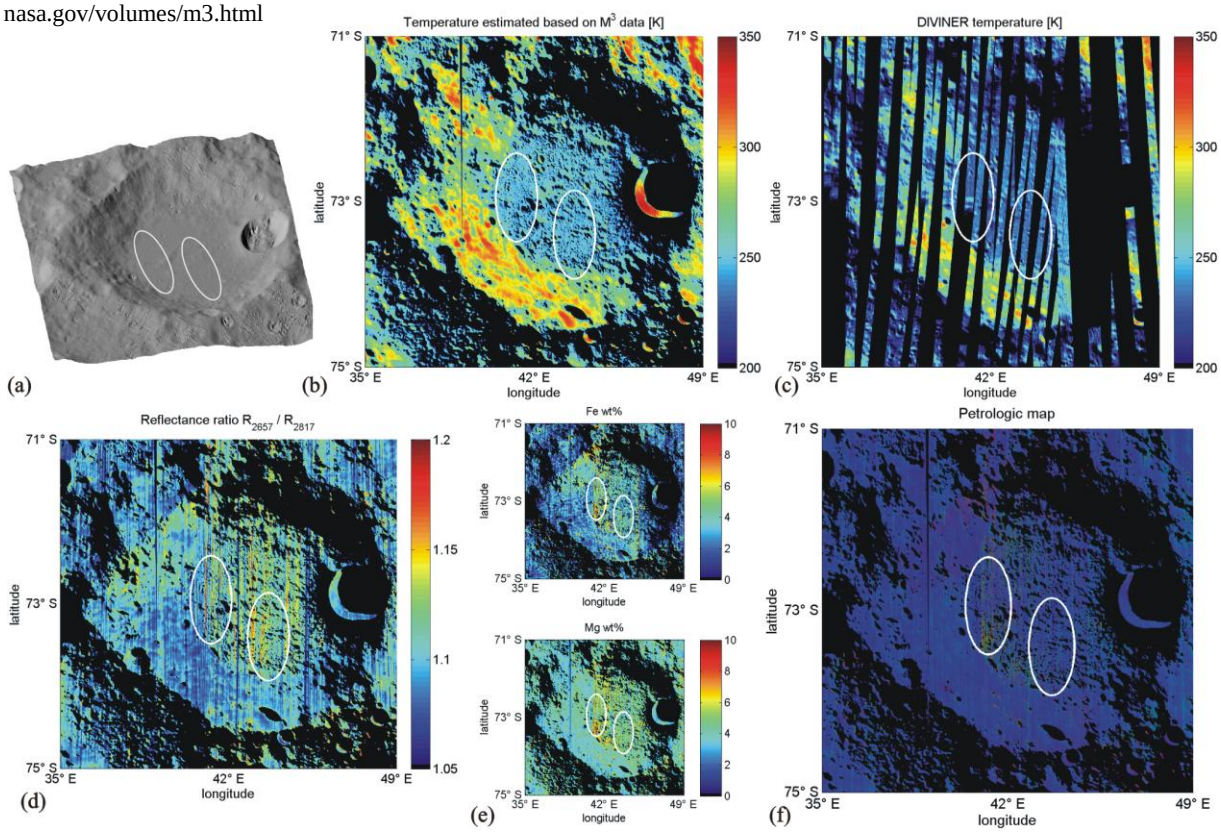

Figure 1: (a) DEM. (b) Map of DIVINER-based surface temperature map under morning illumination (about 81 hours after local sunrise). (c) Map of M³-based surface temperature under morning illumination (extension of method in [8]). (d) OH absorption depth as indicated by the R_{2657} / R_{2817} spectral ratio. (e) Estimated Fe (top) and Mg (bottom) abundances in wt%. (f) Petrological map. In all maps, black denotes missing data. Landing ellipses according to [1].

EPSC Abstracts
Vol. 10, EPSC2015-64, 2015
European Planetary Science Congress 2015

Lunar investigations at the Kazan University: the physical libration – analytical and numerical approach, the lunar coordinate systems

Petrova N. (1,2), Nefediev Yu. (1), Zagidullin A. (1), Kosoulin V. (2)

(1) Kazan Federal University, Kazan, Kremlevskya str., 18, Russia (nk_petrova@mail.ru)

(2) Kazan Power Engineering University, Kazan, Krasnoselskaya str., 51, Russia

Abstract

The theory of physical librations is one of traditional field of investigation at the Kazan University. At the present time it is necessary to develop the model of lunar rotation in order to achieve in the theory the accuracy of 0.1 milliseconds of arc, which is the requirement of modern laser ranging observations and other experiments to determine the parameters of the physical libration.

Both numerical and analytical approaches are very important, since the first provides greater accuracy, and the second - allows a qualitative analysis of the observed data, revealing features that are sensitive to the different physical phenomena that affect the rotation of the Moon.

In particular, the analytical theory has found effective application in computer simulating a new type of observation, such as the ILOM [1], with the purpose to estimate possibilities of the experiment.

One of the important application of the libration theory is the developing the selenocentric coordinate system useful for navigation tasks in the near-moon space. Such kind of the system the Union Selenocentric Reference System was constructed at the university on the basis of absolute coordinates of lunar craters, obtained with simultaneous photographing craters and stars.

1. Computer simulating the planned observation from the lunar surface

Over the past 10 years a creative cooperation has been formed between scientists of the Kazan University and the National Astronomical Observatory of Japan (Mizusawa). The project ILOM (In situ Lunar Orientation Measurement), planned in the frame of SELENE-2 or -3 missions, is aimed at obsevating the physical libration of the Moon. The Russian side has taken over some of the theoretical tasks to ensure the planned observations. One of the important elements of the project is placing of a small optical telescope on the lunar surface with the purpose to detect the lunar physical libration with millisecond accuracy [1].

Computer simulation of the future observations is being done with the purpose of their optimization: effective placement of measuring system on the lunar surface, testing of sensitivity of new observations to various features of the lunar interior structure. The results of the first stage of the simulation are presented. At this stage the software for the selection of stars and reduction of their coordinates onto the period of observations is developed, the tracks for the selected stars are constructed and analyzed, their sensitivity to the internal characteristics of the lunar body, in the first place, to the selenopotential coefficients, is tested [2-3].

Inverse problem of lunar physical libration is formulated and solved. It is shown that selenographic coordinates of polar stars are insensitive to longitudinal librations $\tau(t)$. Comparing coordinates calculated for two models of a rigid and deformable Moon is carried out and components of lunar libration sensitive to Love number k_2 are revealed [4].

Currently, the inverse problem is used by us to test the effect on the libration parameters of error in the coordinates of the observed stars. Preliminary calculations of the effect of errors in stellar coordinates show (see Fig. 1) that the error in 10 milliseconds in the ecliptical coordinates leads to a short-period variations of residual differences with a period of 1 month (27.23 days - the argument F) in 0.05ms $\Delta\rho$ and 0.3 ms in $I\Delta\sigma$.

Analytical theory of physical libration was very convenient tool for modeling the upcoming observations. The main outcome of this collaboration was the understanding of the strategy and tactics of building an improved analytical theory of physical libration.

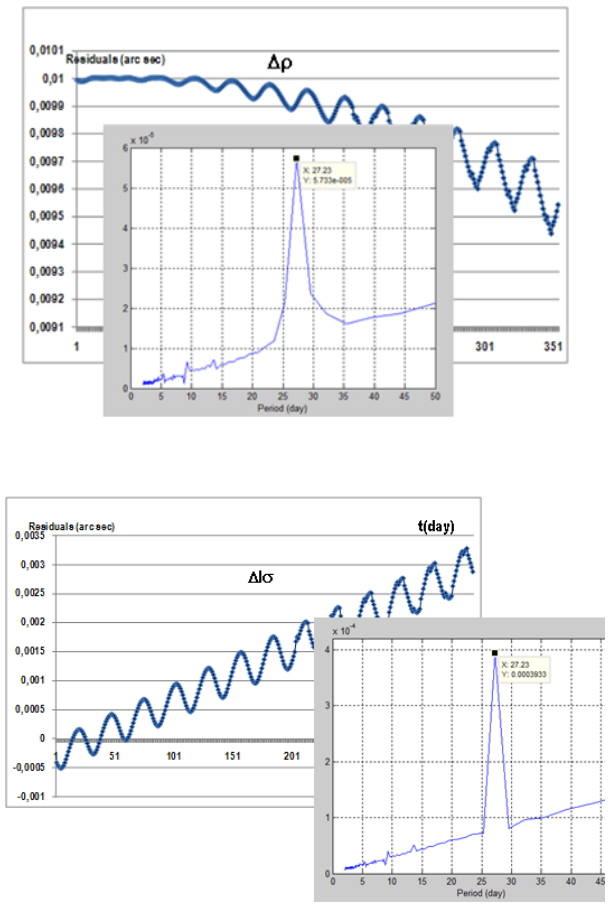

Fig. 1 Residuals arising due to inaccuracy of stellar coordinates

2. The first stage of numerical approach to construction of the libration theory

The urgency to develop numerical theory is also obvious. Ever-increasing accuracy of observations requires improving the theory describing the spin-orbit dynamics of the Moon. Analytical theory, for all its virtues, has inaccuracies inherent in the method itself for obtaining solutions. Moreover, the inclusion in the model of the lunar rotation dissipation effects of different origins, the presence of a two-layer core effects significantly complicates obtaining analytical solutions.

Numerical approach can give solution in such situations relatively fast, and sometimes it is the only way, to get information about the internal structure of the Moon and external factors affecting its dynamics. Dynamic ephemeris (DE) developed to the present time in the JPL NASA, are the standard that specifies the direction vector for developing the numerical theory.

To date, we have developed an integrator based on Runge-Kutta method of order 10, which in the solution of the linear problem of physical libration provides accuracy of 10^{-9} seconds in the interval of 10 years when compared with the exact analytical solution.

3. The Union Selenocentric Reference System

Three tasks were addressed in this research [5]:

a) the analysis of the mathematical model of the orthogonal coordinate transformation accuracy;

b) the identification of the basic dynamic reference system objects with ones that are contained in reducing catalogues;

c) the extension of the base points net of the basic dynamic reference system.

The construction of the system were performed using the developed software package "Transformation selenodesic coordinates" (TSC). During the processing, the following steps were carried out:

a) the analysis and investigation of the accuracy of the basic net contained in DSC;

b) the decryption of common objects for the coordinate systems that are being explored;

c) the extension of the mathematical content package TSC.

Acknowledgements

The work is performed according to the Russian Government Program of Competitive Growth of Kazan Federal University, and was supported by grant RFBR 13-02-00792-a.

References

[1] Hanada et al. Intern. Ass. Geodesy Symp. Vol.28, (2005), pp 163-168

[2] Petrova, N., Hanada, H. Planetary and Space Science (2012), Vol. 68. p. 86 – 93.

[3] Petrova N., Hanada H., Solar System Research, (2013), Vol. 47, No. 6, pp. 463–476.

[4] Petrova, N., Abdulmyanov T., Hanada H. J. Adv. Space Res. (2012), v50, 12, p. 1702-1711

[5] Nefedyev Y.A. S.G.Valeev, N.Y.Varaksina, R.R.Zabbarova, V.S.Borovskih. Georesources.- (2012)- 1(12).- P. 40 - 42.

EPSC Abstracts
Vol. 10, EPSC2015-67, 2015
European Planetary Science Congress 2015

Numerical approach to constructing the lunar physical libration: results of the initial stage

Zagidullin A. (1), Petrova N. (1,2), Usanin V. (1), Nefedief Yu. (1), Glushkov.M (1)

(1) Kazan Federal University, Kazan, Kremlevskya str., 18, Russia (arhtur.zagidullin@ya.ru)
(2) Kazan Power Engineering University, Kazan, Russia

Abstract

So called "main problem" it is taken as a model to develop the numerical approach in the theory of lunar physical libration. For the chosen model, there are both a good methodological basis and results obtained at the Kazan University as an outcome of the analytic theory construction. Results of the first stage in numerical approach are presented in this report.
Three main limitation are taken to describe the main problem:
- independent consideration of orbital and rotational motion of the Moon;
- a rigid body model for the lunar body is taken and its dynamical figure is described by inertia ellipsoid, which gives us the mass distribution inside the Moon.
- only gravitational interaction with the Earth and the Sun is considered. Development of selenopotential is limited on this stage by the second harmonic only. Inclusion of the 3-rd and 4-th order harmonics is the nearest task for the next stage.
The full solution of libration problem consists of removing the below specified limitations: consideration of the fine effects, caused by planet perturbations, by visco-elastic properties of the lunar body, by the presence of a two-layer lunar core, by the Earth obliquity, by ecliptic rotation, if it is taken as a reference plane.

1. Mathematical Formulation of the problem

The technique of mathematical description of the lunar rotation and solution obtaining was developed by Khabibullin [1] and later by Petrova [2]. The rotation of the Moon as a rigid body is described by a trihedron of its principle inertia axes, which are rigidly bounded with the lunar body. This trihedron, whose origin from the lunar center of mass, is called Dynamical Coordinate System (DCS). The motion of the lunar body is described by the angles μ, ν, π (Fig. 1).

The kinematical equations

$$\Omega_x = -\dot{\mu}\times\sin\nu - \dot{\pi}$$
$$\Omega_y = -\dot{\mu}\times\cos\nu\times\sin\pi + \dot{\pi}\times\cos\pi$$
$$\Omega_z = \dot{\mu}\times\cos\nu\times\cos\pi + \dot{\pi}\times\sin\pi$$

give us projections of the rotation angular velocity Ω on the reference axes, which are taken from ecliptical coordinate system.

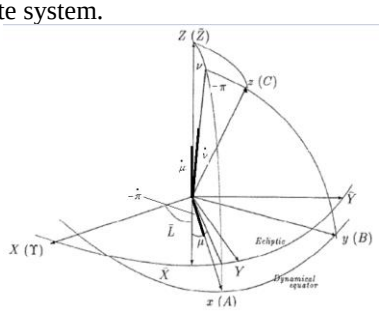

Fig 1: To the conclusion of the kinematic equations

The equations of the lunar rotation are being built in Hamilton formalism, where the canonical variables are $q_1 = \mu, q_2 = \nu, q_3 = \pi$ and the conjugate canonical momenta are p_1, p_2, p_3. Initial values for the numerical integration are calculated according to the analytical theory [2]. The same theory has been used as a reference to verify the accuracy of the numerical integrator.

The equations obtained were greatly simplified to accelerate the debugging programs for the numerical integration: trigonometric functions were expanded into series on small variables (q_1, q_2, q_3) till the terms of the first order of smallness $O(q_1^2, q_2^2, q_3^2)$. In fact, the resulting system of equations

$$\dot{q}_1 = p$$
$$\dot{q}_2 = (1+\kappa_1)p_2 - \kappa_1 n q_3$$
$$\dot{q}_3 = (1+\kappa_2)p_3 - n q_2$$
$$\dot{p}_1 = Q_{100}(t)$$
$$\dot{p}_2 = -n^2 q_2 + n p_3 + Q_{010}(t)$$
$$\dot{p}_3 = -\kappa_1 n^2 q_3 + \kappa_1 n p_2 + Q_{001}(t)$$

corresponds to a linear problem of physical libration. Here the function Qijk (t) are the trigonometric series coming from expansion of selenopotential till the 2nd

order. The advantage of the system (2) is that it allows obtaining exact analytical solutions. This system was solved numerically.

2. Numerical Integration of Lunar libration equation

The one-step Runge Kutta (RK) method of 4^{th} (RK-4) and 10^{th} (RK-10) orders of accuracy [3] was used to numerical integration.

On the Fig. 2a, 2b we can see the behavior of error in dependence on a step in the interval of 1020 days. The optimal step for RK-10 is ½ day. Fig. 3a, 3b demonstrate results of calculation in the 10 years interval: that is difference between numerical and exact solutions.

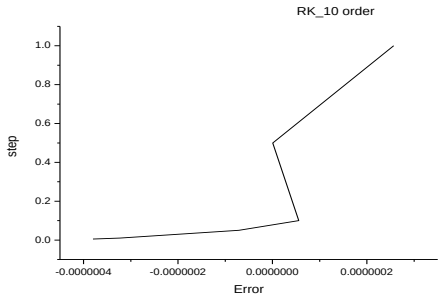

Fig 2a: Error for RK 10 order

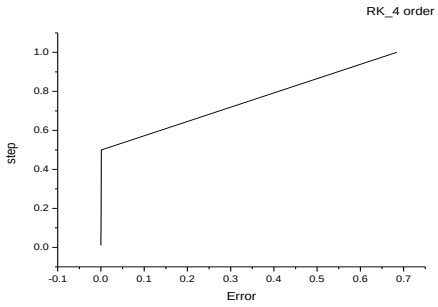

Fig 2b: Error for RK 4 order

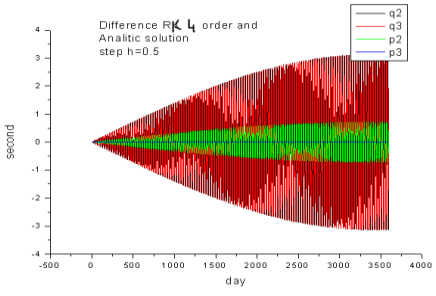

Fig 3a: Error in the interval of 10 years for RK-40.

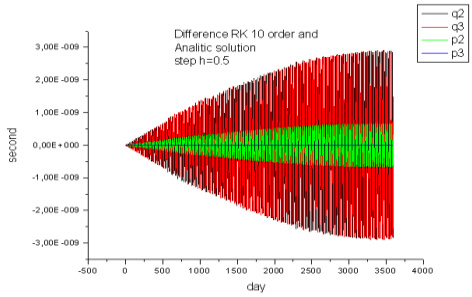

Fig 3b: Error in the interval of 10 years for RK-10.

Analyzing of the curves leads to the conclusion, that the RK-10 is on 4 order better than RK-4. Decreasing of a step in the method of RK-4 leads to the accuracy of the method of RK-10, but the calculation time increases in several times. Because of this we choose the RK-10 as main integrator. The 1/2 day is a good step for the physical libration, because there are no so short harmonics in lunar libration.

3. Summary and Conclusions

The modern accuracy of the lunar laser ranging has an accuracy of 0.0001 arc seconds for lunar physical libration parameters [4]. The high accuracy is necessary and for other space experiments, such as the planned Japanese project ILOM (In situ Lunar Orientation Measurement), which is directed to obtain millisecond accuracy in determination of the lunar libration [5].

Integrator RK-4 shows a stable error ±5 seconds at the 10-years interval, while the RK-10 has accuracy 10^{-9} second and an acceptable calculation time at the same time interval. We believe this method will justify itself in solving more complex, actual, equations of libration.

The work is performed according to the Russian Government Program of Competitive Growth of Kazan Federal University, and was supported by grant RFBR 13-02-00792-a.

References

[1] Kabibullin Sh. (1966) Trudy Kazan GorAO (in Russian)
[2] Petrova N. Earth, Moon and Planets, Vol. 73, 1996. No 1, p. 71-99.
[3] E. Haire: A Runge-Kutta Method of Order 10. J. Inst. Maths Applics (1978) 21, 47-59
[4] Williams J.G., Boggs D., Yoder Ch., Ratcliff J., Dickey J., J. Geoph.Res., 2001. V.106, No E11, pp. 27, 933-27, 968.
[5] Hanadaet al. Application of a PZT telescope to In situ Lunar Orientation Measurement (ILOM). Intern. Ass. Geodesy Symp. Vol.28, (2005), pp 163-168

EPSC Abstracts
Vol. 10, EPSC2015-94, 2015
European Planetary Science Congress 2015

Virtual Moon atlas Pro 6.0 freeware

Christian Legrand[1] and Patrick Chevalley[2], [1]Software designer / Ch. Legrand 668 Rue du Tour de Préaux 76160 PREAUX (France) / chlegrand76@hotmail.fr , [2] Software programer / P. Chevalley 160 Route d'Aire CH-1219 AIRE (Switzerland) / pch@ap-i.net.

Abstract

Since 2002, we develop "Virtual Moon Atlas" a freeware to help Moon observing and to improve interest for Moon in general public.

1. Introduction

VMA Pro" version uses datas coming from NASA, USGS, JPL, from Dr Robinson, Binder, Gaddis, Zuber and Salamuniccar teams, and from Kaguya, and Chang'é missions

The software includes management of a complete database (Near 60 000 entries) of named or satellite or anonymous features of Moon two sides.

Pictures libraries presenting each formations and coming from LPI resources and amateurs shootings are associated and contain more than 8 000 pictures. PHOTLUN © is a specific included pictures manager. VMA Pro 6.0 is presently available for Windows, Linux and Mac 0S.

VMA software has been reviewed in main amateur astronomy magazines [1],[2],[3],[4]…,

Translations are available (FR/EN/GE/SP/IT/CN…) .

VMA software has been downloaded near 900 000 times. It is or has been used by several professional organizations such as Kitt Peak, National Japan Observatory, University College London (K. Joy), , several French astronomy magazines and astronomy writers (P. Harrington, T. Plotner …) . Recommended by ESA, registered as educational software by French ministry for education.

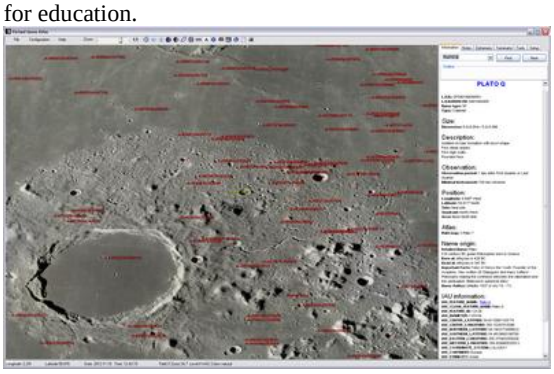

Picture 1 : Plato area with LRO texturel

2. Detailed description

2.1 Freeware features :

- « Map » window with various functions thumbnails « Information », « Ephemeresis », « Notes», Tools »
- Full rotating Moon globe with coordinates grid
- Double window ability permitting comparisons between different textures and overlays combinations
- Real time or choosen phase and librations display
- Orientation of the lunar disk with powerful zoom
- Formations search function starting from name
- Formations names display according to zoom power
- Orbital viewing simulation
- Integrated notepad for your own notes
- Size and distance measurement tool on maps
- Context menu on right mouse click
- Maps and databases printing with captions setup
- Eyepieces and CCD cameras field simulation
- Full screen display for public videoprojections

2.2 Databases : Included databases contains more than 60 000 formations:

- Nearside & Farside named and satellite formations
- First anonymous craters database
- Human exploration sites (Historical)
- Lisa Gaddis pyroclastic deposits
- ALPO domes databases

For each formation, included informations about : Formation geology, localization on lunar disk, detailed description, detailed name origin, official IAU 2012 datas

All these databases include the "LUN / Lunar Universal Number" conceived by ourselves and permitting "naming" and localization of any lunar formation more than 0.1 arc minute wide.

DATLUN © is a specific database manager using

menus or SQL requests on every data.

Picture 2 : DATLUN main screen

2.3 Mapping textures: JPL shaded relief with albedo (1500 m/pix) and without albedo (1000 m / pix), Dr Robinson teams Clementine (200 m / pix) and LRO (120 m/pix), USGS Lunar Orbiter and CNSA Chang'é 2 (60 m per pixel) HR textures**.**

2.4 Historical textures: Permitting easy comparisons of these pioneers works with present datas: (Langrenus 1645 / Hevelius 1647 / Cassini 1679 / Tobias Mayer 1791)

2.5 Scientific overlays: 44 different ones : Gravity, temperature, altimetric, geologic, various elements as thorium, iron, several neutrons varieties… overlays can be applied on each texture.

2.6 Pictures libraries: VMA includes lunar pictures libraries (More than 9 000 pictures) from :
- Lunar Orbiter Photographic Atlas of Moon
- Lunar probes
- Apollo missions mapping and 70 mm
- Consolidated Lunar Atlas
- Lunar Astronautical Charts and Lunar Maps
- Best amateur lunar imagers pictures

PHOTLUN © specific pictures manager with editing possibilities permitting basic processing included.

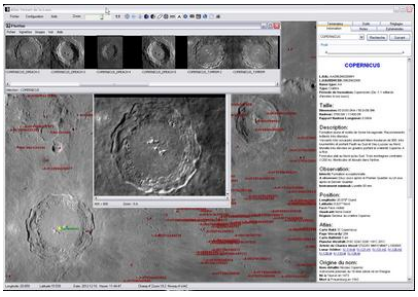

Picture 3 : PHOTLUN main screen

2.7 Internet connection : The WEBLUN © module using a special lunar Internet sites database permits connection and interactivity while using VMA.

2.8 Delivery: VMA Pro 6 version and all add-ons collection are freeware and downloadable free from our Web site http://www.ap-i.net/avl/en/start
We maintain a discussion forum and we encourage other languages translations. We also listen continuously to our users requests, (including professionals), trying to update the software with new useful functionalities.

OTHERS SCREEN CAPTURES :

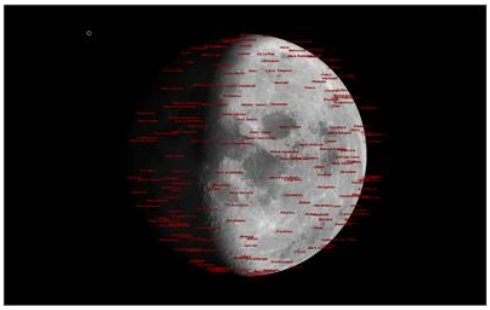

Picture 4 : Full screen for public education events

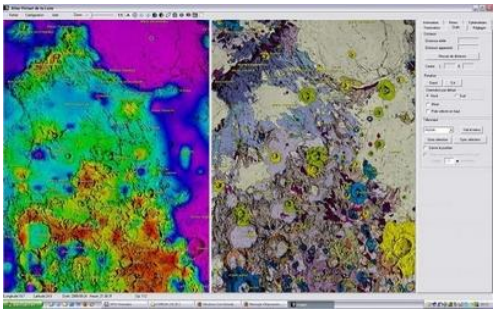

Picture 5 : Double window with altitude & geology overlay for correlation search

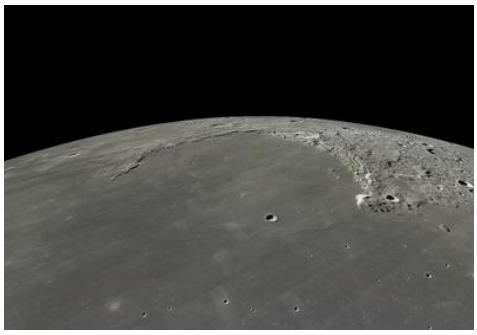

Picture 6 : Sinus Iridum fly over with LRO texture

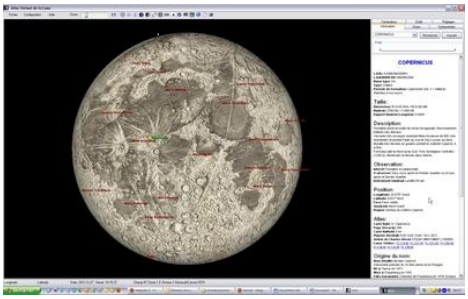

Picture 7 : Cassini 1679 historical texture

References

[1] G. Seronik. (2003) Sky & Telescope.
[2] R. Bartlett (2003) Astronomy Magazine.
[3] J.L. Dauvergne (2012) Ciel & Espace

EPSC Abstracts
Vol. 10, EPSC2015-165, 2015
European Planetary Science Congress 2015

The Application of Chang'e-3 Moon-based Extreme Ultraviolet Camera Geometric Positioning

W. Yan, J.J. Liu, W.R. Wang, F.F. Wang, X.G. Zeng, X.Y. Gao
Key Laboratory of Lunar and Deep Space Exploration, National Astronomical Observatories, Chinese Academy of Sciences, Beijing, China. (yanw@nao.cas.cn/ Tel: +86 01064880607-8012)

Abstract

The moon-based extreme ultraviolet camera (EUVC) mounted on the Chang'e-3 (CE-3) lander is used to observe Earth's plasmasphere. Geometric positioning is critical for the EUVC observations to determine Earth center in each image. In this paper, calculation accuracy of Earth center's Solar Magnetic System (SM) coordinates is analyzed by comparing the results obtained by geometric positioning and image recognition respectively. The conclusion is geometric positioning results are more accurate so that the original images should be modified to ensure its accuracy for further scientific researches.

1. Introduction

The CE-3 lunar probe successfully landed in the northwestern part of Mare Imbrium at 13:11 on 2013 December 14 (UTC), making China the third country to achieve a soft landing on the Moon. The EUVC is one of four payloads on the CE-3 lander. It has taken photos of Earth's plasmasphere from a perspective on the side during about one year (Ip et al. 2014).

1.1 Scientific Goals

The scientific goals of the EUVC are as follows. (1) Image Earth's plasmasphere at 30.4 nm from the perspective of the side at different positions along the orbit of the Moon to investigate three-dimensional structures in the plasmasphere. (2) Continuously image the plasmasphere over a relatively long duration to monitor evolution of the plasmaspheric density and structure with geomagnetic activity.

1.2 Technical Requirements

The specifications for the EUVC are listed in Table 1 (Chen et al. 2014).

Table 1: Specifications for the EUVC

Parameter	Value
Central wavelength (nm)	30.4 ± 0.5
Spectral bandwidth (nm)	⩽5.0
Field of view (◦)	15.00 ± 0.75
Angular resolution (◦)	⩽0.10
Exposure time (min)	2, 10 or 20
Dynamic range (Rayleigh)	0.1_10.0
Sensitivity (count s^{-1} $Rayleigh^{-1}$)	⩾0.10
Sensitivity ratio at 30.4 nm and 58.4 nm	⩾70.0

1.3 Geometric Positioning

The EUVC images (Figure 1) can be obtained after image processing such as geometric calibration, photometric calibration, and so on. The plasmasphere, plasmapause, airglow and the Earth's shadow can be seen clearly in the image. In Figure 1, the red cross is the center of the image, which is corresponding to the optical axis pointing of the EUVC, and the black cross indicates Earth's center, which is corresponding to the geocentric pointing of the image and can be calculated by image recognition as mentioned in (He et al. 2011).

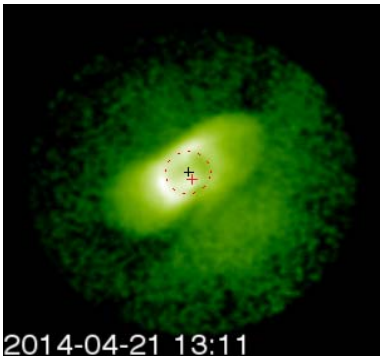

Figure 1: The EUVC image

The purpose of geometric positioning is determining the optical axis pointing, the geocentric pointing and any other pointing of the EUVC images at SM system. Its process is transforming the initial pointing vector which obtained by image coordinates to SM system through a series of coordinate conversion. The coordinate systems involved in this process are instrument coordinate system, the CE-3 lander body coordinate system, moon-fixed coordinate system, geocentric mean equator coordinate system for epoch J2000.0, SM system, and so on. Conversion equation is as follows in which $\vec{V}_{SM}$,$\vec{V}_O$ and $T_{SM\leftarrow O}$ denotes pointing vector in SM system, in the initial system, and the conversion matrix respectively.

$$\vec{V}_{SM} = T_{SM\leftarrow O}\vec{V}_O \quad (1)$$

2. Experiment and Results

The angle formed by the optical axis pointing and the geocentric pointing (noted as AOG) can be obtained by geometric positioning and image recognition respectively. In theory, the two results should be equal to each other. However, we found there are differences between them, which are even larger than 1° sometimes. To analyze the reason of this phenomenon, the change trend of AOG with time by the two methods is calculated as Figure 2.

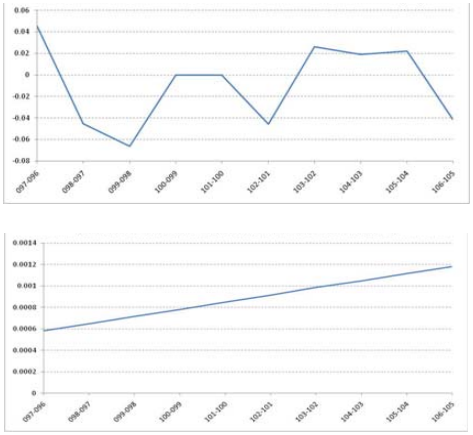

Figure 2: The change trend of AOG with time(°)

Because the optical axis pointing of the EUVC is fixed during the experimental period while the geocentric pointing is changed regularly according to the rotation of Earth and Moon, it can be seen from Figure 2 that the change trend of AOG obtained by geometric positioning is more reasonable. Geometric positioning results can be used to modify the original EUVC images.

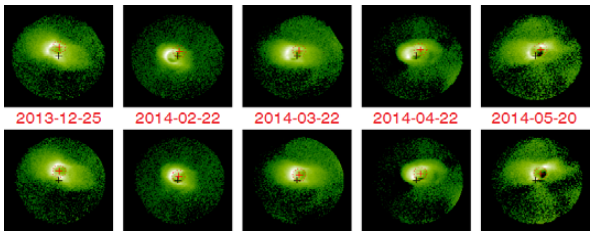

Figure 3: The original EUVC image modification

Figure 3 illustrated the effect of the original EUVC image modification using geometric positioning results. The top and bottom parts show images before and after modification respectively. The red cross denotes Earth center determined by geometric positioning. It can be seen that bright spot center which is the principle of Earth center chosen by image recognition is overlapped with red cross after image modification.

3. Summary and Conclusions

Geometric positioning is one of key technical steps for the EUVC images processing. It can provide accurate geocentric pointing to determine Earth center and to achieve scientific goals of the EUVC. Calculation of measured data shows that geometric positioning results can also be used to modify the original EUVC images. So geometric positioning can ensure the reliability of the EUVC observation data.

References

[1] Ip,W.-H., Yan, J., Li, C.-L.,& Ouyang, Z.-Y.: Preface: The Chang'e-3 lander and rover mission to the Moon, RAA(Research in Astronomy and Astrophysics), Vol. 14, No. 12, 1511-1514, 2014.

[2] Chen B., Song K.-F., Li Z.-H., et al.: Development and calibration of the Moon-based EUV camera for Chang'e-3, RAA, Vol. 14, No. 12, 1654–1663, 2014.

[3] He F., Zhang X.-X.,2 Chen B., et al.: Reconstruction of the plasmasphere from Moon-based EUV images, JOURNAL OF GEOPHYSICAL RESEARCH, VOL. 116, A11203, 2011

EPSC Abstracts
Vol. 10, EPSC2015-168, 2015
European Planetary Science Congress 2015

A miniature laser ablation mass spectrometer for in situ chemical composition investigation of lunar surface

M.B. Neuland (1), K. Mezger (2), A. Riedo (1), M. Tulej (1) and P. Wurz (1)
(1)Physics Institute, Space Research and Planetary Sciences, University of Bern, Sidlerstrasse 5, CH - 3012 Bern, Switzerland,
(2) Institute of Geological Sciences, University of Bern, Baltzerstrasse 1+3, CH - 3012 Bern, Switzerland,
Contact: neuland@space.unibe.ch , Tel.: +41 (0)31 631 44 24, Fax: +41 (0)31 631 44 05

Abstract

A miniature laser ablation mass spectrometer (LMS) is presented. The LMS is designed as a flight instrument for planetary and space research and optimised for in situ measurements of the chemical composition of rocks and soils on a planetary surface. By means of measurements standard reference materials of soil and a sample of the Allende meteorite we demonstrate that LMS is a suitable instrument for in situ measurements of elemental and isotopic composition with high precision and accuracy. Furthermore, it is shown that LMS data allows deriving of the material mineralogy and petrology with high spatial resolution, lateral and vertical, and the application of in situ age dating methods.

1. Introduction

The chemical composition of planetary bodies, moons, comets and asteroids is a key to understand their origin and evolution [1]. Measurements of the elemental and isotopic composition of a rock yield information about the formation of the planetary body, its evolution and following processes shaping the planetary surface [2]. From the elemental composition, conclusions about modal mineralogy and petrology can be drawn. Isotope ratios are a sensitive indicator for past events on the planetary body and yield information about origin and transformation of the matter, back to events that occurred in the early solar system. Finally, measurements of radiogenic isotopes make it possible to carry out analyses of the age of rocks. All these topics, particularly in situ dating analyses, quantitative elemental and highly accurate isotopic composition measurements, are top priority scientific questions for future lunar missions. An instrument for precise measurements of chemical composition will be a key element in scientific payloads of future landers or rovers on lunar surface.

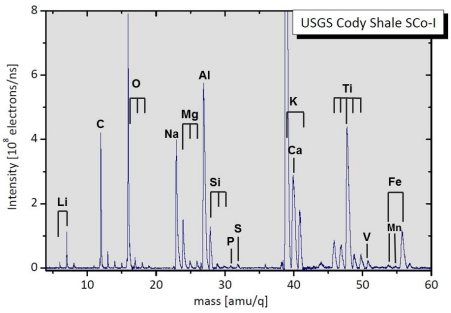

(a) USGS Cody Shale SCo-I

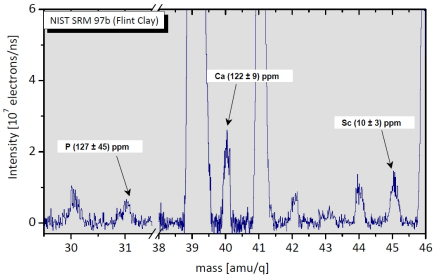

(b) NIST 97b Flint Clay

Figure 1: Typical spectra on standard soil samples.

2. Instrument

The LMS instrument combines a laser ablation/ionisation ion source with a time-of-flight mass analyser. A focused laser beam is pointed on the sample of interest, surface atoms are ablated and ionised. Electric fields guide the produced ions through the ion–optical system on the micro channel plate detector [3]. Measurements in multiple channels with different gain levels assure a high dynamic range allowing the detection of all elements even down to tens of ppb level [5]. Each laser shot results in a full mass spectrum from 0 to 250 amu/q. The laser that is used is a fs–laser in the near infrared with a repetition rate of 1 kHz. Together with the custom-made data recording and processing

chain, this allows for very fast measurements on spots of less than 10 µm in diameter [6].

3. Lab Measurements, Preparatory Work

We carried out measurements on a series of soil standards. Measurements of these samples are used to confirm known sensitivity coefficients of the instrument and to prove the power of LMS for quantitative elemental analyses. Fig. 1a) shows the lower end mass scale of a typical spectrum on one of the standard soils (USGS Cody Shale). A few major and minor elements are assigned. Fig. 1b) shows a zoom into a spectrum of the NIST97b (Flint Clay) sample, which demonstrates detection of elements in the low ppm range with high SNR. For demonstration of the capability of LMS to measure the chemical composition of extraterrestrial material we use a sample of Allende meteorite. 4'000 measurements were carried out on the CV3 meteorite, where the measuring plan focused on high spatial resolution with regard to mineralogical analysis of small inclusions and resolution of different regions inside chondrules. Fig. 2 displays the preliminary analysis of one measurement area, where the chemical composition of 680 locations with 50 µm spacing was measured on Allende. Fig. 2a) and b) show the measured relative abundance of Fe and Mg for each single locations. It is noticeable that a certain geometrical feature occurs in both of the maps. Comparing to the optical image of the same region (Fig. 2c), the LMS measurements correctly identifies two different mineral entities separated by the shown contours. Further analysis of such measurements yield detailed information about mineralogy [9]. Investigation of layered samples confirm the high spatial resolution in vertical direction of LMS. It was found that the depth resolution on solid samples is in nm range [8], which allows in situ studying of past surface processes on a planetary surface. Measurements on solid NIST samples focused on the analysis of Pb and application of the ^{207}Pb/^{206}Pb system for age determination. With the measured correlation between isotope abundance and relative accuracy, an estimate was derived for the uncertainty of the radio-isotope chronology. It results that the statistical uncertainty for the age determination by LMS is about $\pm$ 100 Myrs, if abundance of ^{206}Pb and ^{207}Pb is 20ppm and 2ppm respectively. For comparison: in lunar KREEP these Pb isotopes have abundances of tens to hundreds of ppm [7].

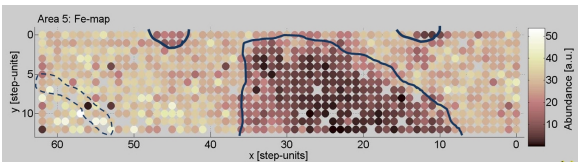

(a) Fe

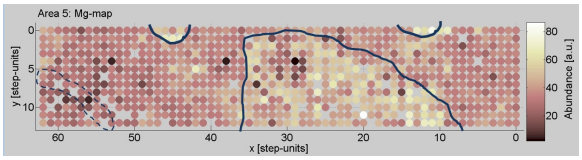

(b) Mg

(c) Optical image

Figure 2: LMS measurements of Fe (a) and Mg (b) on a sample of Allende meteorite. The contours found in the element maps agree with a feature also found in the optical image (c) of the same region.

4. Towards Lunar Measurements

We present a miniature laser ablation mass spectrometer for planetary and space research. We established the measurement capabilities of LMS for petrographic and mineralogical analyses, for isotopic studies and dating analyses, which are key topics for future missions to the Moon. Having the LMS instrument installed on a lunar rover would allow to measure the chemical composition of many rock and soil samples, distributed over a certain area, inside the South Pole Aitken Basin for example. LMS measurements would yield valuable conclusions about age and mineralogy.

Acknowledgments

This work is supported by the Swiss National Science Foundation (SNF).

References

[1] Wurz, P. et al., 2009, *AIP Conf.Proc.*, CP1144:70-75.

[2] McSween, H., Huss, G., 2010, Cosmochemistry, *Cambridge University Press*.

[3] Tulej, M. et al.,2012, *Int.J.Spec.*, Article ID 234949.

[4] Tulej, M. et al., 2014, *GGR* 38(4):441-466.

[5] Riedo, A. et al., 2013, *J.Mass Spectrom.*48:1-15.

[6] Riedo, A. et al., 2013, *J.Anal.Atom.Spectrom.* 28(8):1133-1356.

[7] Riedo A. et al., 2013, *Planet. Space Sci.* 87: 1-13.

[8] Grimaudo V. et al., 2015, *Anal.Chem.* 87: 2037-2041.

[9] Neuland, M.B. et al., 2014, *Planet.Space Sci.* 101:196-209.

EPSC Abstracts
Vol. 10, EPSC2015-170, 2015
European Planetary Science Congress 2015

The Impact of Craters on Neutron Fluxes and Lunar Polar Hydrogen Abundances

V.R. Eke (1), K.E. Bower (1), S. Diserens (1), M. Ryder (1), P.E.L. Yeomans (1), L.F.A. Teodoro (2), R.C. Elphic (3), W.C. Feldman (4), B. Hermalyn (5), C.M. Lavelle (6), D.J. Lawrence (6), S. Maurice (7)
(1) Institute for Computational Cosmology, Department of Physics, Durham University, South Road, Durham. DH1 3LE, UK, (2) BAER, Planetary Systems Branch, Space Science and Astrobiology Division, MS 245-3, NASA Ames Research Center, Moffett Field, CA 94035, USA, (3) Planetary Systems Branch, Space Science and Astrobiology Division, MS 245-3, NASA Ames Research Center, Moffett Field, CA 94035, USA, (4), Planetary Science Institute, 1700 East Fort Lowell, Suite 106, Tucson, AZ 85719, USA, (5) University of Hawaii, Honolulu, HI, USA, (6) The Johns Hopkins University Applied Physics Laboratory, Laurel, MD 20723, USA, (7) IRAP, Toulouse, France. (v.r.eke@durham.ac.uk)

Abstract

Hydrogen abundances in lunar polar cold traps are investigated using remotely-sensed neutron count rates. The effect of neutron beaming from craters is measured using data from the Lunar Prospector Neutron Spectrometer (LPNS) and understood in the context of a simple model. This enables a reanalysis of data near the lunar poles, accounting for the topographical impact on the neutron count rates, leading to improved estimates of the hydrogen abundance in the various cold traps. For the case of Cabeus, taking into account the topographical effect increases the inferred water-equivalent hydrogen weight percentage from $\sim 1\%$ to $\sim 4\%$, consistent with that measured using the LCROSS impactor.

1. Introduction

The composition of the near-surface lunar regolith can be inferred using the spectrum of neutrons leaking from the Moon following cosmic ray spallation events [3, 2]. Neutron spectroscopy has been used to create maps of the hydrogen abundance within 70 cm of the surface, allowing conclusions to be drawn about the spatial distribution of volumetrically significant water ice deposits [3, 8]. This search has focused on polar cold traps where water ice is stable against sublimation. However, these efforts have yet to account for the geometrical impact of craters on the detected neutron fluxes. The weak beaming of neutrons normal to the emitting surface might combine with a concave crater surface to focus neutrons over the crater. This would increase the remotely-sensed neutron count rate, opposing the decrease in epithermal neutron count rate produced by a hydrogen-rich regolith. In order to make an unbiased estimate of the hydrogen content in polar cold traps, this factor should be understood and accounted for. We will: 1) quantify how neutron count rates change as the detector moves relative to craters, 2) describe a model that can account for these observations and 3) discuss the consequences of our findings for estimates of hydrogen concentrations in polar cold traps, with reference to previous results such as that from the LCROSS impactor [1].

2. Data and model

The LPNS epithermal neutron data are used [6] in order to quantify the variation in neutron count rate with cratercentric distance, because this dataset has the best spatial resolution of the available lunar neutron datasets [9]. In order to model the effect of topography, the Lunar Orbiter Laser Altimeter (LOLA) global $1^\circ/64$ digital elevation model is used [7]. The set of craters being considered is chosen to be a "highland" subset of those found by [4], where this is defined as craters with centres having latitude$> -30^\circ$, |longitude|$> 90^\circ$ and radii, $r_c > 10$km.

The model is essentially the result of a numerical integration over the entire surface visible from the detector. It takes into account the varying cosmic ray flux impacting into the azimuthally-symmetric crater embedded into an otherwise spherical surface. The crater topography includes a central flat infill region, a constant radius of curvature wall leading up to the uplifted rim, with a constant gradient outer uplifted slope back to the unperturbed lunar surface. The neutron flux from the surface is beamed like $\sqrt{\cos\theta}$, where θ is the angle to the surface normal, as advocated by Monte Carlo neutron transport simulations [5]. In addition, 75% of neutrons aimed at the lunar surface are

allowed to be reemitted, rather than being absorbed into the regolith.

3. Results

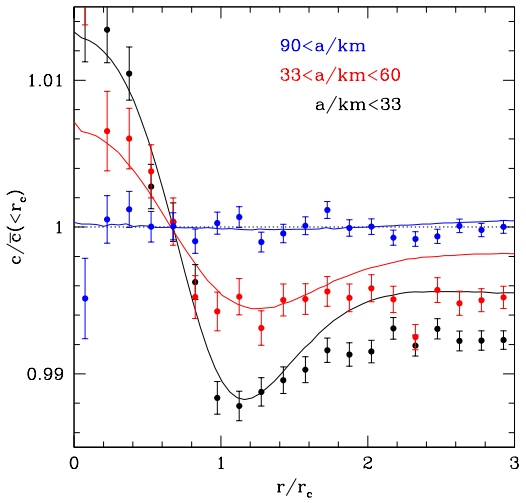

Figure 1: The stacked, normalised epithermal neutron count rate profile for the LPNS (points) and model (lines), for craters with radii in the range $40 - 50$ km. The results have been split by detector altitude, a.

The comparison of LPNS and model epithermal neutron count rate profiles around craters with $r_c = 40 - 50$ km is shown in Fig. 1 with the observations split by detector altitude. In order to decrease the size of the uncertainties in the LPNS profiles, all 115 craters within this radius range have been stacked together. The count rates, c, have been normalised by the average count rate within the crater before stacking together craters. A central bump is seen in the count rate, when the detector is sufficiently low for its footprint to be small enough to resolve this feature. From low altitude, the mean count rate over the crater is $\sim 0.8\%$ greater than that measured outside the crater. The model, as described in the previous section, shows very similar features, but overpredicts the normalised count rate at $r/r_c > 2$ by $\sim 0.25\%$. To make the model fit the LPNS profiles as well as is shown in Fig. 1, the flux emitted from within $2r_c$ has been increased by 0.35%. While the underlying physical justification for this is unclear, it may be the result of localised surface, or near-surface, roughness that might enhance the emitted neutron flux.

For some of the larger polar craters containing permanently shaded regions, there are sufficient observations that useful individual profiles can be constructed. Of particular interest is Cabeus crater. In order to fit the epithermal neutron count rate profile around Cabeus, the model needs the equivalent of ~ 4.5 wt% WEH placed into a circular disc covering the central 275 km^2 in a $r_c = 42$ km crater with the best-fitting topographical model parameters for Cabeus. This is over 4 times as large as the value inferred by [8], who did not account for the effect of topography.

4. Summary and Conclusions

The impact of topography on the remotely sensed neutron count rate has been quantified and largely understood using LPNS data and a simple geometrical model. Focussing of neutrons over craters increases the count rate, which looks like a reduction in hydrogen concentration. Taking into account this topographical effect can significantly change the inferred volatile content in polar cold traps.

References

[1] Colaprete, A., et al.: Detection of Water in the LCROSS Ejecta Plume, Science, Vol. 330, pp. 463-468, 2010.

[2] Elphic, R., et al.: Lunar Fe and Ti Abundances: Comparison of Lunar Prospector and Clementine Data, Science, Vol. 281, pp. 1493-1496, 1998.

[3] Feldman, W., et al.: Fluxes of Fast and Epithermal Neutrons from Lunar Prospector: Evidence for Water Ice at the Lunar Poles, Science, Vol. 281, pp. 1496-1500, 1998.

[4] Head, J., et al.: Global Distribution of Large Lunar Craters: Implications for Resurfacing and Impactor Populations, Science, Vol. 329, pp. 1504-1507, 2010.

[5] Lawrence, D., et al.: Improved modeling of Lunar Prospector neutron spectrometer data: Implications for hydrogen deposits at the lunar poles, JGR, Vol. 111, E08001, 2006.

[6] Maurice, S., et al.: Reduction of neutron data from Lunar Prospector, JGR, Vol. 109, E07S04, 2004.

[7] Smith, D., et al.: Initial observations from the Lunar Orbiter Laser Altimeter (LOLA), GRL, Vol., 37, L18204,2010.

[8] Teodoro, L., Eke, V., Elphic, R.: Spatial distribution of lunar polar hydrogen deposits after KAGUYA (SELENE), GRL, Vol. 37, L12201, 2010.

[9] Teodoro, L., et al.: How well do we know the polar hydrogen distribution on the Moon? JGR, Vol. 119, pp. 574-593, 2014.

EPSC Abstracts
Vol. 10, EPSC2015-190, 2015
European Planetary Science Congress 2015

Regolith thickness at the Chang'E-3 landing site from the Lunar Penetrating Radar and impact craters

Wenzhe Fa (1), Meng-Hua Zhu (2) and Tiantian Liu (1)
(1) Institute of Remote Sensing and Geographical Information System, Peking University, Beijing 100871, China (wzfa@pku.edu.cn) (2) Space Science Institute, Macau University of Science and Technology, Macau, China.

Abstract

The Chang'E-3 lunar penetrating radar (LPR) observations reveal a newly formed regolith layer (<1 m), an ejecta layer (~2-6 m), and a palaeoregolith layer (~4-9 m) from the surface to a depth of ~20 m. The thicknesses of the newly formed regolith layer and the palaeoregolith layer are consistent with the estimations based on the excavation depth and morphology of small fresh craters.

1. Introduction

Lunar regolith structure is critical to studying the geology and impact history of the Moon [1]. To date, direct study of the regolith structure was only available at a few landing sites through core tube experiments, where regolith was sampled to a maximum depth of 3 m [1]. On December 14, 2013, China's Chang'E-3 (CE-3) spacecraft successfully landed in the northern Mare Imbrium [2]. The CE-3 landing site is within a geologic unit (I22) consisting of high-titanium basalt, with a model-surface age of 2.96 Gyr [3]. The landing site is ~50 m away from the east rim of a 500 m diameter crater (unofficially named as CE-3 crater) [4]. The age of the CE-3 crater is estimated to be ~100 Myr according to its morphology prominence [5]. For the first time, a rover-deployed ground penetrating radar is used to characterize the structure and dielectric property of the regolith over the landing site. Here we report the LPR observations at the high-frequency channel (500 MHz).

2. Regolith stratigraphy from the LPR observations

The LPR started working on December 15, 2013, and its surface traverse is ~110 m during its effective observation time of ~8.3 hours (Fig. 1a). The collected raw data were processed through horizontal band removal, band-pass filtering, compensation of geometrical spreading and dielectric attenuation, and range migration. The processed LPR data are displayed in B-scan format as a function of horizontal distance and apparent depth (Fig. 1b) [4]. The real depth is the apparent depth divided by the square root of the dielectric permittivity (3 as in [4]).

The most prominent features within the first meter are the three to five bright irregular layers with typical thickness of 0.3-0.5 m. These layers are probably ejecta from small local craters that were later modified by micrometeorite bombardment and solar wind. This region is interpreted as the newly formed surface regolith.

At an apparent depth from ~1 to 10 m, is a region with bright radar echo. This region contains numerous, chaotic, irregular layers, and hyperbolic curves. These layers might result from irregular interface geometry, or densely distributed rocks smaller than the LPR wavelength [4]. We interpreted this region as the continuous ejecta from the CE-3 crater.

Below the ejecta layer is a region with weak radar echoes. The thickness of this layer decreases from ~9 m to 4 m with increasing distance from the CE-3 crater. This region is relatively homogeneous, and only few hyperbolic curves are visible. This region is probably the regolith layer produced on top of the mare basalt during 2.96 Gyr and was later buried by the ejecta of the CE-3 crater. Thus, this region can be regarded as a paleoregolith.

Beneath the palaeoregolith layer, at an apparent depth of ~20 m, the strength of the radar echoes increases and numerous irregular layers appear again. This should be the transition zone between the palaeoregolith layer and the underlying mare basalt.

3. Regolith thickness from impact craters

Images from the CE-3 landing camera show 9 craters with diameters ranging from 2 to 16 m (Fig.

1a). The excavation depths of these small fresh craters are <2 m, which are consistent with the LPR observed thickness of the newly formed regolith.

Crater counting results from high-resolution LROC image show that, within an area of 8.1 km × 12.2 km surrounding the landing site, there are 1688, 237, and 54 normal, flat-bottomed, and concentric craters, respectively. Using the relation between regolith thickness and crater morphology [6], cumulative distribution of regolith thickness is obtained (Fig. 1c). The median regolith thickness is estimated to be 6.5 m. Meanwhile, 867 small craters of distinctly blocky (type A), a few blocks (type B), and no blocks (type C) [7] were also counted, of which 7 are type A, 55 are type B, and 805 are type C. Fig. 1d shows the relative distribution of the counted A, B, and C type craters, and the threshold diameter between types A, B and type C is ~55 m. Therefore, the regolith thickness is ~5.5 m using a simple crater depth/diameter ratio of 1/10 [7]. These two estimations are consistent with the thickness of the palaeoregolith layer as observed by the CE-3 LPR.

4. Conclusions

The CE-3 LPR observations at 500 MHz show a surface regolith layer less than 1 m, an ejecta layer of ~2-6 m, and a palaeoregolith layer of ~4-9 m from the surface to a depth of ~20 m. The observed thicknesses of the surface regolith layer and the palaeoregolith layer are consistent with the estimations based on the morphology and excavation depth of small fresh craters. The revealed regolith stratigraphy, in combination with surface age from crater counting, indicates a complex regolith evolution at the CE-3 landing site.

References

[1] Heiken, G. H., Vaniman, D. T., and French, B. M.: Lunar Source-Book: A User's Guide to the Moon, Cambridge Univ. Press, 1991.

[2] Fang, G. Y. et al.: The Lunar Penetrating Radar (LPR) onboard Chang'E-3 mission, Research in Astron. Astrophys., 14, 1607–1622, 2014.

[3] Hiesinger, H., Jaumann, R., Neukum, G. and Head, J. W.: Ages of mare basalts on the lunar nearside, J. Geophys. Res., 105, 29239–29275, 2000.

[4] Fa, W., Zhu, M.-H., Liu, T., and Plescia, J. B.: Shallow subsurface structure of the Moon at the Chang'E-3 landing site as revealed by the lunar penetrating radar, Proc. Lunar Sci. Conf., 46, Abstract 1136, 2015.

[5] Basilevsky, A. T.: On the evolution rate of small craters, Proc. Lunar Sci. Conf., 7, 1005–1020, 1976.

[6] Fa, W., Liu, T., Zhu, M.-H., and Haruyama, J.: Regolith thickness over Sinus Iridum: Results from morphology and size-frequency distribution of small impact craters, J. Geophys. Res., 119, 1914–1935, 2014.

[7] Wilcox, B. B., Robinson, M. S., Thomas, P. C., and Hawke B. R.: Constraints on the depth and variability of the lunar regolith, Meteorit. Planet. Sci., 40, 695–710, 2005.

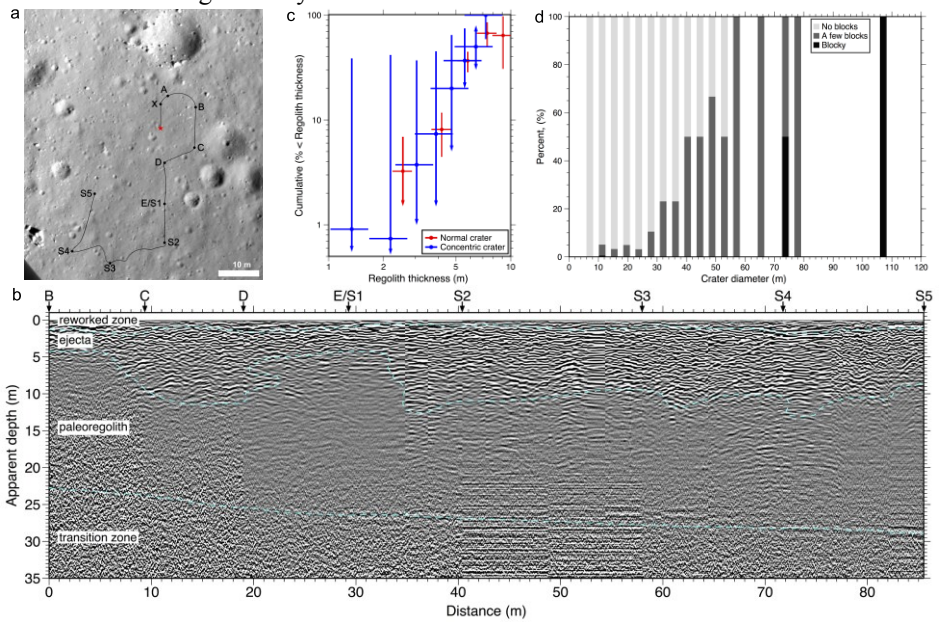

Figure 1. (a) An optical image from CE-3 landing camera showing the LPR survey line. (b) LPR image at 500 MHz from Point B to S5 along the survey line. (c) Cumulative distribution of regolith thickness estimated from normal (red) and concentric (blue) craters. (d) The distribution of blocky craters types A, B, and C as a function of diameter for the region surrounding the CE-3 crater.

EPSC Abstracts
Vol. 10, EPSC2015-191, 2015
European Planetary Science Congress 2015

Dust particle release from the lunar surface: role of adhesion and meteoroid impacts

S.I. Popel (1,2), A.P. Golub' (1), **Yu.N. Izvekova** (1,2), G.G. Dol'nikov (1), A.V. Zakharov (1) and L.M. Zelenyi (1,2)
(1) Space Research Institute, Russian Academy of Sciences, Moscow, Russia, (2) Moscow Institute of Physics and Technology (State University), Dolgoprudnyi, Moscow region, Russia (besedina_yn@mail.ru / Fax: +7-495-3331248)

Abstract

Effects important for dust particle release from the lunar surface are discussed. The emphasis is given to adhesion and effects of meteoroid impacts.

1. Introduction

It is now almost universally accepted that the dust over the lunar surface is a component of a plasma-dust system (see, e.g., [1-3]). The first lunar dust observations were made during the Surveyor and Apollo missions. The Surveyor lunar missions revealed that sunlight was scattered in the terminator region, and this led to the generation of the lunar horizon glow and streamers above the lunar surface [4]. Subsequent observations showed that the sunlight was scattered most probably by the charged dust particles originating from the lunar surface [5]. The analysis of the data obtained by the Surveyor landers led to a conclusion that the dust particles with a diameter of about 5 μm might levitate at a height of about 10 cm above the lunar surface.

The description [1-3] makes clear some features of dusty plasma system over the Moon. However, there are unsolved problems concerning its parameters and manifestations [6]. In particular, significant uncertainty exists as to the physical mechanism through which dust particles are released from the surface of the Moon. Adhesion has been identified as a significant force in the dust particle launching process which should be considered to understand particle launching methods [7].

The problem of the dust particle release from the lunar surface can be solved, for example, by considering meteoroid impacts onto the surface of the Moon. Here, we consider lunar dust particle launching process due to meteoroid impacts. A significant attention is paid to the importance of the adhesive force.

2. The force of adhesion

In [7] dust particles with smooth surfaces have been considered. The effect of surface roughness results in significant attenuation of the effect of adhesion in comparison with the results [7]. Indeed, the calculation of the force of adhesion between a plane with an asperity of the radius r and a spherical particle of radius a gives

$$F = \frac{AS^2}{24\Omega^2}\left(\frac{ra}{r+a} + \frac{a}{\left(1+rS/(2\Omega)\right)^2}\right), \quad (1)$$

where A is Hamaker's constant, S is the surface cleanliness, and $\Omega = 0.132$ nm characterizes the diameter of oxygen ion. For lunar regolith Hamaker's constant is $4.3\cdot10^{-20}$ J; surface cleanliness varies in the range of 1 to 0 and for lunar dayside is calculated as $S = 0.88$ [8]. Calculations based on Eq. (1) show that the effect of roughness results in two-three orders of magnitude attenuation of the effect of adhesion in comparison with the case of a smooth particle. Nevertheless, even considering the roughness of lunar regolith particles, the electrostatic forces required to launch dust particles from the lunar surface, as a rule, do not exceed the adhesive forces. Dust particle launching can be explained if the dust particles rise at a height of about dozens of nanometers owing to some processes (e.g. meteoroid impacts, etc.). This is enough for the dust particles to acquire charges sufficient for the dominance of the electrostatic force over the gravitational and adhesive forces, and finally to rise above the lunar surface.

3. Meteoroid impacts and dust particle release

When high-speed meteoroid impacts the lunar surface the substances of the impactor and the target are strongly compressed and heated. Under the action of high pressure strong shock wave is formed. The shock propagates and weakens moving away from the impact epicenter. Finally the weakening shock transforms into linear acoustic wave. The zones (around the impact epicenter) of evaporation of the substance, its melting, destruction of particles constituting lunar regolith, their irreversible deformations are formed due to the propagation of the weakening wave. Beyond the zone of irreversible deformations the zone of elastic deformation is created which is characterized by the magnitudes of the pressure in acoustic wave less than dynamic limit of elasticity.

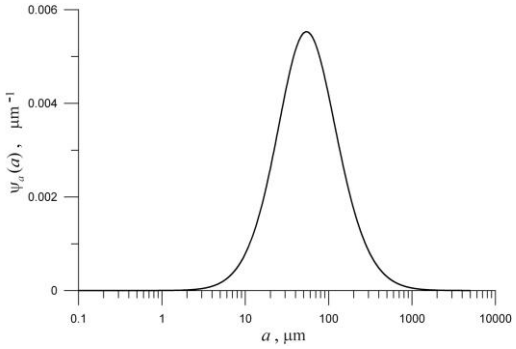

Figure 1: The size-distribution function of particles released from the lunar surface due to meteoroid impacts.

Considering the balance between the maximum force of pressure in the blast wave and the sum of the adhesive, electrostatic, and gravitational forces we determine the radius of the zone around the impact epicenter which restricts the region where dust particles are released from the surface of the Moon due to meteoroid impacts. Furthermore, we estimate the speeds of the released particles, find their size-distribution (Fig. 1), and evaluate maximum heights of dust particle rise.

4. Conclusions

Thus to consider dust particle release from the lunar surface one has to take into account (among other effects) both the adhesion and meteoroid impacts. A possibility of the rise of micrometer-sized dust particles above the lunar surface is shown. In particular, dust particles with a diameter of about 5 μm can be present at a height of about 10 cm above the lunar surface that explains the data obtained by the Surveyor landers.

Acknowledgements

This work was carried out as part of the Russian Academy of Sciences Presidium program no. 9 “Experimental and Theoretical Research of Objects of the Solar System and Planetary Systems of Stars” and was supported by the Russian Foundation for Basic Research (project no. 15-02-05627-a) and the Russian Federation Presidential Program for State Support of Young Scientists (project no. MK-6935.2015.2).

References

[1] Popel, S.I., Kopnin, S.I., Golub', A.P., Dol'nikov, G.G., Zakharov, A.V., Zelenyi, L.M., and Izvekova, Yu.N.: Dusty plasma at the surface of the Moon, Solar System Research, Vol. 47, pp. 419-429, 2013.

[2] Popel, S.I., Morfill, G.E., Shukla, P.K., and Thomas, H.: Waves in a dusty plasma over the illuminated part of the Moon, J. Plasma Phys., Vol. 79, pp. 1071-1074, 2013.

[3] Popel, S.I., Golub', A.P., Izvekova, Yu.N., Afonin, V.V., Dol'nikov, G.G., Zakharov, A.V., Zelenyi, L.M., Lisin, E.A., and Petrov, O.F.: On the distributions of photoelectrons over the illuminated part of the Moon, JETP Lett., Vol. 99, pp. 115-120, 2014.

[4] Rennilson, J.J. and Criswell, D.R.: Surveyor observations of lunar horizon-glow, Moon, Vol. 10, pp. 121-142, 1974.

[5] Zook, H. and McCoy, J.: Large scale lunar horizon glow and a high altitude lunar dust exosphere, Geophys. Rev. Lett., Vol. 18, pp. 2117-2120, 1991.

[6] Popel, S.I. and Zelenyi, L.M.: Dusty plasmas over the Moon, J. Plasma Phys., Vol. 80, pp. 885-893, 2014.

[7] Hartzell, C.M. and Scheeres, D.J.: The role of cohesive forces in particle launching on the Moon and asteroids, Planet. Space Sci., Vol. 59, pp. 1758-1768, 2011.

[8] Perko, H.A., Nelson, J.D., and Sadeh, W.Z.: Surface cleanliness effect on lunar soil shear strength, Journal of Geotechnical and Geoenvironmental Engineering, vol. 127, pp. 371–383, 2001.

EPSC Abstracts
Vol. 10, EPSC2015-208, 2015
European Planetary Science Congress 2015

On the Chemical Evolution of the Impact-Generated Protolunar Disk

B. Brugger (1), O. Mousis (1), S. Charnoz (2), P. Vernazza (1), and M. Ali-Dib (3)
(1) Aix Marseille Université, CNRS, LAM (Laboratoire d'Astrophysique de Marseille) UMR 7326, 13388, Marseille, France (bastien.brugger@lam.fr)
(2) Laboratoire AIM-LADP, Université Paris Diderot/CEA/CNRS, F-91191 Gif sur Yvette, France
(3) Université de Franche-Comté, Institut UTINAM, CNRS/INSU, UMR 6213, Observatoire des Sciences de l'Univers de Besançon, France

Abstract

We investigate the evolution of the protolunar disk's chemical composition, which is assumed to have formed from a collision between the early Earth and a Mars-sized object. We use a two-phase model (solid and gas) for the silicate-dominated composition of the disk, based on the minimization of the Gibbs free energy, and that includes a chemical network with hundreds of chemical reactions. A thorough study of the parameters space of our model allows us to propose several observational tests that may trace back the thermodynamic evolution of the impact-generated disk.

1. Introduction

The giant impact theory suggests that the Moon was formed as a result of the collision between the planet Earth and a Mars-sized object, named Theia, about 30-50 million years after condensation of the first solids in the solar system. This collision is supposed to have formed a silicate-rich disk with both materials from the impactor and Earth's mantle, which led to the formation of the Moon after thermodynamic and chemical evolution.

2. Model and Methods

In this work, we used a two-phase model for the silicate disk, consisting of a melt layer surrounded by a vapor atmosphere, in order to investigate the evolution of the disk's chemical composition in previously set thermodynamic conditions. This model allows phase changes of the species as well as the formation and dissociation of new chemical species, and does not take into account the disk's dynamic evolution since the time needed to reach chemical equilibrium is negligible in comparison to the dynamic time of the system. Our initial conditions are those proposed by [1]: for a temperature range between 1800 K and 4200 K, the saturation vapor pressure values derive from [2], and the chemical elements used in the model are O, Na, Mg, Al, Si, K, Ca, Ti, Fe and Zn. Formed with these ten elements, 83 chemical species are selected to appear in the disk, whose initial composition is taken close to the Earth's mantle composition because of the collision.

In order to compute the disk's equilibrium composition, we utilized the commercial software *HSC Chemistry*, which is widely used in the fields of geophysics and planetary science. When comparing our equilibrium calculations against those made by [1], we found that both set of results are very close in the temperature range explored by these authors (i.e. 1800-4200 K) : the gas phase of the disk is dominated by Na, SiO, Fe, O_2 and O in this temperature range. One of their conclusions was that the high abundances of O and O_2 could be the direct signature of impact-generated disks.

3. Results and Conclusions

After validating our model against the results of [1], we decided to go further in our study of the protolunar disk. Because recent models suggest that the silicate disk's temperature range could be more extended, we investigated the disk's chemical composition in the 1000 K to 4500 K range. The first observation we make with these new temperature ranges is the strong decrease of O and O_2 abundances at T < 1500 K, which immediately shows that the conclusions made by [1] cannot be extrapolated outside the temperature range they chose. In contrast to this previous study, we find that species like Zn and K, whose abundances were magnitude orders

below those of O and O_2 at T > 1800 K, become predominant at lower temperatures. We have thus obtained more accurate conclusions on the characteristics of the chemical composition at equilibrium of an impact-generated disk.

Figure 1 shows the partition of all elements found both in vapor and melt phases as a function of temperature in the 1000-4500 K range. This simulation shows that volatile elements in the disk essentially remain in solid phase, except in the 2000-4500 K range where their abundances increase in the gaseous phase. The trend is particularly true for species constituted from Na and K, the only ones for which the gas phase abundances exceed the solid abundances in the 2000-4500 K range. Our calculations show that the investigation of the gaseous abondances of Na and K should also be useful to trace back the thermodynamic evolution of an impact-generated disk.

4. Figures

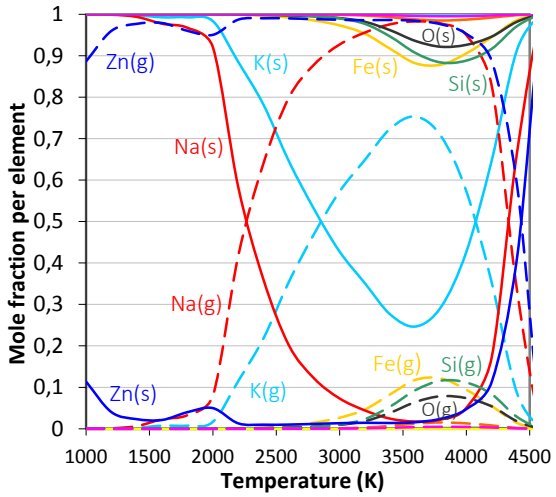

Figure 1: Distribution of elements in the two phases - solid (s) and gas (g) - of the protolunar disk as a function of temperature. For each element, the sum of mole fractions in solid and gaseous phases is normalized to the unity. In the temperature range 1000-2000 K, the abundances of all elements (except Zn) in the solid phase converge towards 1 (i.e. gaseous phase is negligible). In the 2000-4500 K range, the abundances of solids decrease in favor of those of gases.

References

[1] Visscher, C. & Fegley, B. Jr. 2013. *Chemistry of Impact-generated Silicate Melt-vapor Debris Disks*. The Astrophysical Journal 767, L12.

[2] O'Neill, H. St. C. 1991. *The Origin of the Moon and the early History of the Earth – A chemical Model*. Geochimica et Cosmochimica Acta 55, 1135.

EPSC Abstracts
Vol. 10, EPSC2015-241, 2015
European Planetary Science Congress 2015

Bidirectional Reflectance of icy Samples: Application to water ice detection on the Moon and Mercury.

Z. Yoldi Martínez de Mandojana (1), A. Pommerol (1), B. Jost (1), O. Poch (2), J. Gouman (1) and N. Thomas (1).
(1) Physikalisches Institut, University of Bern, Switzerland, (2) Center for Space and Habitability, University of Bern, Switzerland

Abstract

The reflectance of water ice and lunar regolith simulant (JSC-1AF) mixtures has been measured under different geometries. We have found that considerable amounts of water ice can be mixed within the soil without producing any noticeable photometric signature, as the relation between the reflectance and the amount of ice in the sample is strongly non-linear. Some reflectance models have been tested to try to reproduce this non-linearity.

1. Introduction

Some permanently shadowed craters at the poles of the Moon and Mercury are thought to host ice in their walls [1, 2, and references therein]. Laser altimeters and cameras can be used to search for potential changes of the surface reflectivity caused by the presence of ice. Laser altimeters currently in orbit around the Moon and Mercury have provided data showing some spatial variability in the reflectance of the polar areas of both bodies. In both cases, the possibility of finding the ice mixed within the regolith as in an intimate mixture is explored [3, 4]. To estimate the quantity of ice present in the craters, reflectance models are applied to the reflectivity measured by the laser altimeters [3]. Several authors have studied the reflectance of ice-free binary mixtures, showing that the models work well for predicting the mixture components abundancies [5]. Experimental studies involving water ice appear much more seldom in the literature, because the measurement of icy samples requires special equipment and procedures. We have produced intimate binary mixtures of water ice and JSC-1AF and measured their Bidirectional Reflectance Distribution Function (BRDF) with the PHIRE-2 instrument; a gonio-radiometer that allows characterizing the BRDF of ice-bearing samples in the VIS-NIR (400-1100 nm) spectral range [6]. Small (20°) and large (70°) incidence angles have been used. Null phase angle measurements are relevant for applications to laser altimetry, whereas higher phase angle measurements are relevant for the case of indirect illumination of the surface by light scattered from nearby topography. Then, we have tested the Hapke model [7] of reflectance and the "isograin" model [8] to achieve a better understanding on how these models deal with the reflectance of icy regolith analogues.

2. Methods

The particulate water ice has been created in our laboratory. Two sizes of ice particles (diameters of 5 and 70 microns) and several percentages of ice within the sample have been tested. The procedure for sample preparation was accurately defined and followed for all samples in order to guarantee a good reproducibility and mitigate the influence of the sample preparation on the reflectance of the sample. The samples show the same BDRF at 750 nm than at the laser altimeter's wavelength (1064 nm). The measurements have been made at 750 nm in order to reduce the duration of the measurements and avoid the metamorphism of the ice.

3. Results

Phase curves presenting the reflectance as a function of the emission angle are shown in Fig. 1 for fine-grained ice (Fig. 1a) and coarse-grained ice (Fig. 1b). The phase curves measured at low incidence angle are dominated by the opposition effect, which produces a relatively strong increase of reflectance (25%) as the phase angle decreases below 10°. At high incidence angle, the reflectance increases as well at high phase angle and reaches a maximum in the forward scattering direction, for ice-rich samples. In both cases we observe that, when mixed intimately, relatively high amounts of ice within the sample do not significantly affect its reflectance. In the case of the coarse-grained ice (Fig. 1b), very high amounts of ice are required to produce a photometric signature. The reflectance measured at high phase angle

however, shows a much stronger dependence on the amount of ice in the sample.

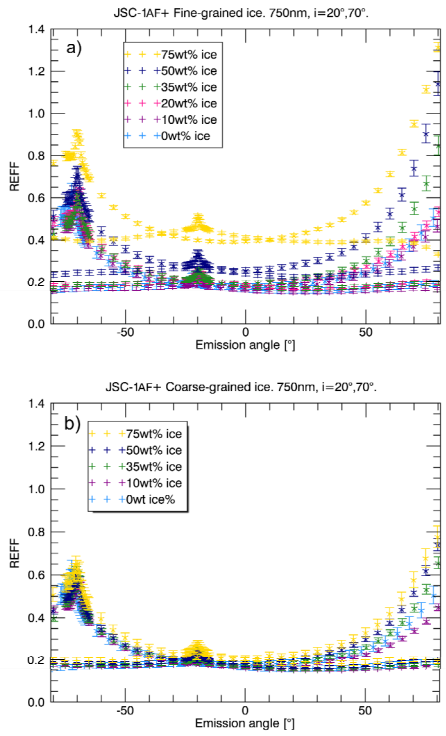

Figure 1: Reflectance phase curves for binary mixtures of JSC-1AF and water ice. a) ice diameter: 5 microns b) ice diameter: 70 microns

4. Discussion

Our results demonstrate in a few particular cases how difficult it is to detect water ice intimately mixed within a lunar-type regolith from its VIS-NIR photometric signature. For example, looking at a surface at 0°-phase and low incidence angle, one would not be able to distinguish between a dry soil and a soil containing up to 75wt% of 70 micrometer-sized water ice particles. The results for high incidence: i=70° show that high phase angles may be the best opportunities to detect water ice, due to the strong forward scattering peak in ice-rich samples. In order to expand our experimental findings from a few particular cases to more general trends, we use our data to test existing reflectance models. In particular, we have tested the Hapke and the "isograin" models, to compare their different approaches to compute the reflectance of binary mixtures from the properties of the end members.

5. Conclusions

Experimental results show that ice is more difficult to detect when it is present as bigger particles and when it is observed at low incidence and phase angles. Looking for ice at high phase angles results in better chances of detection. With regard to the reflectance models, they work well in a relative way; they are able to reproduce the shape of the phase curves described by the reflectance, as long as the mixing coefficients are correctly estimated. Calculating ice concentrations from reflectance data without any knowledge of the mixing coefficients, which strongly depend on the size/shape of the grain, results in very large errors.

References

[1] Feldman et al. Evidence for water ice near the lunar poles. Journal of Geophysical Research, Vol. 106, No E10, Pages 23,231-23,251, October 25, 2001

[2] Lawrence et al. Evidence for Water Ice Near Mercury's North Pole from MESSENGER Neutron Spectrometer Measurements. Science 339, 292 (2013)

[3] Lucey et al. (2014) The global albedo of the Moon at 1064nm from LOLA, J. Geophys. Res. Planets, 119, 1665-1679, doi: 10.1002/2013JE004592

[4] Neumann et al. Bright and Dark Polar Deposits on Mercury: Evidence for Surface Volatiles. Science 339, 296 (2013)

[5] Mustard and Pieters, 1987. Quantitative abundance estimates from bidirectional reflectance measurements. J. Geophys. Res., Vol 92, No B4, E617-E626.

[6] Pommerol et al., 2011. Photometry and bulk physical properties of Solar System surfaces icy analogs: The Planetary Ice Laboratory at University of Bern. Planetary and Space Science 59, 1601-1612.

[7] Hapke. Bidirectional reflectance spectroscopy: 1. Theory (1981). J. Geophys. Res, Vol 86, Issue B4 10 April 1981 Pages 3039–3054

[8] Hiroi and Pieters, 1992. Effects of Grain Size and Shape in Modeling Reflectance Spectra of Mineral Mixtures. Proc. Of Lunar and Planet. Science, Vol 22, 313-325

EPSC Abstracts
Vol. 10, EPSC2015-277, 2015
European Planetary Science Congress 2015

Dust accelerator tests of the LDEX laboratory model

Y.W. Li(1), S. Bugiel(1), B. Hofmann(1), M. Horanyi(2) Z. Sternovsky(2) and R. Srama(1,3) (1) IRS, University of Stuttgart, Germany, (2) LASP, University of Colorado, Boulder, Colorado 80309, USA, (3) Baylor University, Waco, TX 76706, USA (li@irs.uni-stuttgart.de / Tel.:+49-621-516557)

Abstract

The LDEX (Lunar Dust EXperiment) sensor onboard lunar orbiter LADEE (Lunar Atmosphere and Dust Environment Explorer) was designed to characterize the size and spatial distributions of micron and sub-micron sized dust grains. Recent results of the data analysis showed strong evidence for the existence of a dust cloud around the moon. LDEX performs in situ measurements of dust impacts along the LADEE orbit. The impact speed of the observed dust grains is close to 1.7 km/s (the speed of the spacecraft), since the dust grains are considered on bound orbits close to the maximum height of their ballistic motion.

LDEX is an impact ionization dust detector for in situ measurements. The detection of a dust grains is based on measuring the charge generated by high speed impacts ($>$ 1km/s) on a rhodium coated target. The impact charge Q is a function of both the speed v and the mass m of the impacting dust particle. The characteristic values are dependent on the instrument geometry, the impact surface properties (material), the impact geometry (impact angle) and the particle properties (material, density, speed, mass, shape). In our tests we used PPy-coated olivine and PPy-coated ortho-pyroxene with impact speeds around 1.7 km/s.

A LDEX laboratory model was designed and manufactured by the University of Stuttgart. The model is used to support calibration activities of the Univ. of Colorado and to perform special tests (impact angle and impact location variations) at the dust accelerator facility at MPI-K (Heidelberg) which is operated by the IRS of the University of Stuttgart.

1 Instrument Description

The laboratory model of LDEX is a to-scale model of the LDEX flight model. It uses the same target material and dimensions. The instrument consists of a hemispherical rhodium target with a size of approx. 10 cm in diameter, an ion grid and a MCP detector in the center. A dust grain impacts at the hemispherical target and generates an impact plasma. An electric field between the ion focusing grid with negative bias potential and the grounded target separates the electrons and negative ions from positive ions. The electrons and negative ions are collected at the target and they are measured by a charge sensitive amplifier (CSA). The positive ions in the center create an induced charge on the ion focusing grid and are measured by a second CSA. Depending on the grid transmission, an ion current is measured as well. After flying through the ion focusing grid, the positive ions are detected by a microchannel plate (MCP) behind the focusing grid. The MCP output is directly connected to a transient recorder to measure the ion signal of individual impacts.

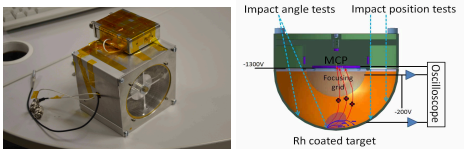

Figure 1: The LDEX laboratory model in the laboratory(left) and the cross section of LDEX with experimental parameters (right). The electrodes are shielded by an aluminum housing and entrance grids. An electronics box is seen at the top.

2 Experiment set up

The LDEX laboratory model was tested and calibrated at the Dust Accelerator Facility at Max Plank Institute for Nuclear Physics, which is operated by Institute of Space Systems at University of Stuttgart, Germany. We used polypyrrole (PPy) costed olivine (ρ = 3.32 g/cm^3) and ortho-pyroxene to (ρ = 3.4 g/cm^3) simulate the mineral dust grains in the lunar environment.

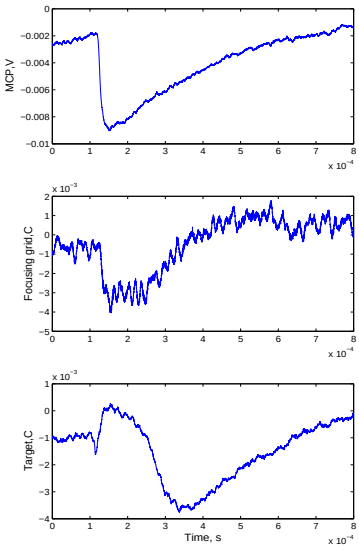

Figure 2: Typical LDEX signals created by a PPy-coated latex dust grain with a mass of 1.5 $\times 10^{-12}$ g, a projectile speed of 1.72 km/s and a primary charge of 1.44 fC. The signals are from the MCP (top), the grid (middle) and the target (bottom)

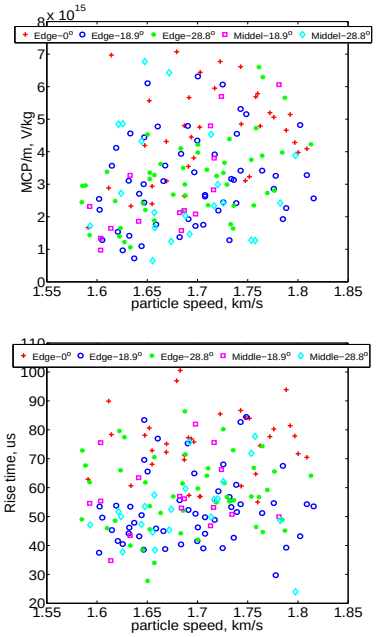

Figure 3: The impact calibration data using PPy-coated Olivine dust grains with different distances from the axis of the symmetry of LDEX. The speeds of impactor are in the range of 1.55 -1.85 km/s.

As comparisons, iron and PPy-coated Latex particle were also used for the calibration. The instrument was bombarded by micron and submicron sized dust grains with the speeds of between 0.5 km/s and 60 km/s. Figure 2 shows an example of typical MCP, focusing grid and target waveforms recorded at the dust accelerator facility.

3 Initial Calibration

We do analyse the impact signals with respect to their amplitde in order to determine the exponents of the relation between particle speed v, particle mass m and impact charge Q of $Q = \alpha m v^{\beta}$. We analysed both, the negative target signal Q_{target} and the positive ion yield Q_{MCP}. We found the following equations

$$m \approx (7.56 \cdot 10^{-5}) \cdot Q_{MCP}^{1.0542 \pm 0.029} \cdot v^{-3.544 \pm 0.11} \quad (1)$$

$$m \approx 0.046 \cdot Q_{target}^{1.115 \pm 0.047} \cdot v^{-2.903 \pm 0.13} \quad (2)$$

where m is the mass of the impactor with a unit of kg; and Q_{MCP} and Q_{target} are the detected charges by the MCP and the target with a unit of C, respecitvely; v is the speed of the impactor with a unit of km/s.
Figure 3 indicates that the charge amplitude and the rise time are independent on the location and on the impact angle.

References

[1] M. Horanyi, Z. Sternovsky, M. Lankton et al.: The Lunar Dust Experiment (LDEX) onboard the Lunar Atmosphere and Dust Environment Explorer, Space. Sci. Rev., 2014, 185:93-113.

[2] Sternovsky, Z., Horanyi, M., Gruen, E., et al.: The calibration of the Lunar Dust Experiment (LDEX) instrument, AGU, Fall Meeting 2011, abstract P43A-1666

EPSC Abstracts
Vol. 10, EPSC2015-282, 2015
European Planetary Science Congress 2015

Designed and Implementation of Lunar Immersive Visualization System Based on Chang'E-3 Data of Panoramic Camera

Gao Xingye, Liu Jianjun, Ren Xin , Mu Lingli, Li Chunlai,Yan Wei,Wang Fenfei,Wang Wenrui,Zeng Xingguo
National Astronomical Observatories, Chinese Academy of Sciences, Beijing 100012, China(gaoxy@nao.cas.cn/ Fax:+86-10-64888703)

Abstract

In this paper, we present a lunar immersive visualization system that was developed for assisting lunar scientist to establish science mission goals in Chang'E-3 mission. Based on data of panoramic camera and star catalogue, the system enables the operator to visualize the terrain and the celestial background from the rover's point of view in 3D in combination with 4-pipe-projection system.

1. Introduction

China's Chang'E-3 lunar probe that consisted of the Chang'E-3 lander and the 'Jade Rabbit' rover successfully landed on the Moon on December 14, 2013[1]. The 'Jade Rabbit' rover contain stereo panorama camera which take images to assist lunar scientists learn Chang'E-3 rover's surroundings [2, 3]. Utilizing stereo 360-degree imagery from panorama camera of Yutu rover, we designed and implemented a lunar immersive visualization system. The system enables the operator to visualize the terrain and the celestial background from the rover's point of view in 3D. To avoid image distortion, stereo 360-degree panorama stitched by 112 images is projected onto inside surface of sphere according to panorama orientation coordinates and camera parameters to build the virtual scene. Stars can be seen from the Moon at any time. So we render the sun, planets and stars according to time and rover's location based on Hipparcos catalogue as the background on the sphere. Immersing in the stereo virtual environment, the operator can zoom, pan to interact with the virtual lunar scene and mark interesting objects. Hardware of the lunar immersive visualization system is made up of four high lumen projectors and a huge curve screen which is 31 meters long and 5.5 meters high. This system contributed heavily to establishment of science mission goals in Chang'E-3 mission.

2. System Design

Data manager module, simulate module, render module and four-chanel projectors system make up the lunar immersive virtualization system(Fig 1). Data manager module manage the Hipparcos database and panoramic images of Chang'E-3. Simulate module is key module of the system which takes the charge of time and space coordinates transformation, projection transformation and user interaction. Render module render the virtual scene. Four-chanel projector system show the virtual scene of the Moon on the huge curve screen which is 31 meters long and 5.5 meters high.

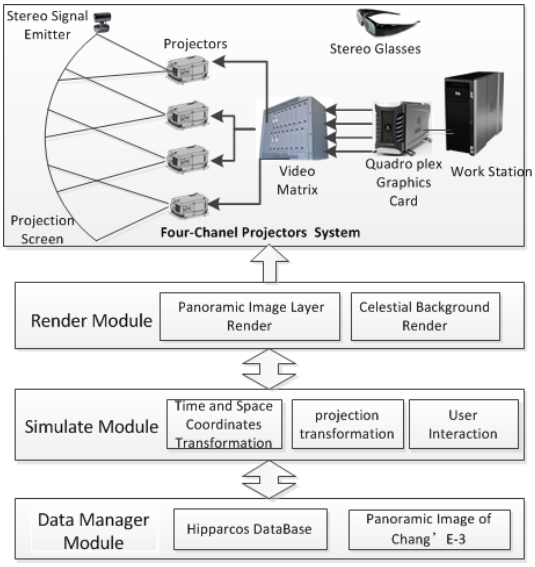

Figure 1: System structure diagram

3 Implementation

3.1 Modelling the scene

Stars and panoramic images are textured on celestial sphere based on horizontal coordinate for modelling the virtual scene of the Moon in real time. Firstly, based on Hipparcos catalogue and vsop87 program,

planets and stars are transform form Earth-centered Earth Mean Equator and Equinox of Epoch J2000 coordinate to Horizontal coordinate system according to Chenag'E-3's location(Figure 2). And then, panoramic images and celesta background are projected onto the spherical surface according to orientation and time. Celesta background layer is on the bottom layer and panoramic layer is on the top(Figure 3).

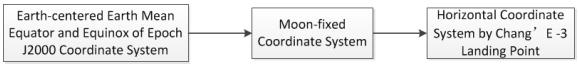

Figure 2: Space and time coordinate transform

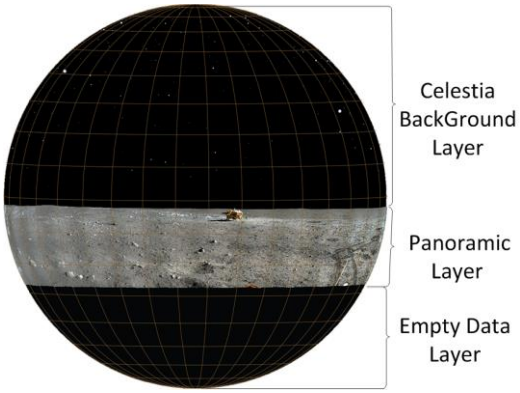

Figure 3 : Projected on celestial sphere

3.2 Reprojection to view plane

Utilizing Gnomonic projection, cylindrical and stereographic projection , the virtual scene of the Moon is reprojeected from spherical surface to view plane for the operator to see on the screen(Figure 4).

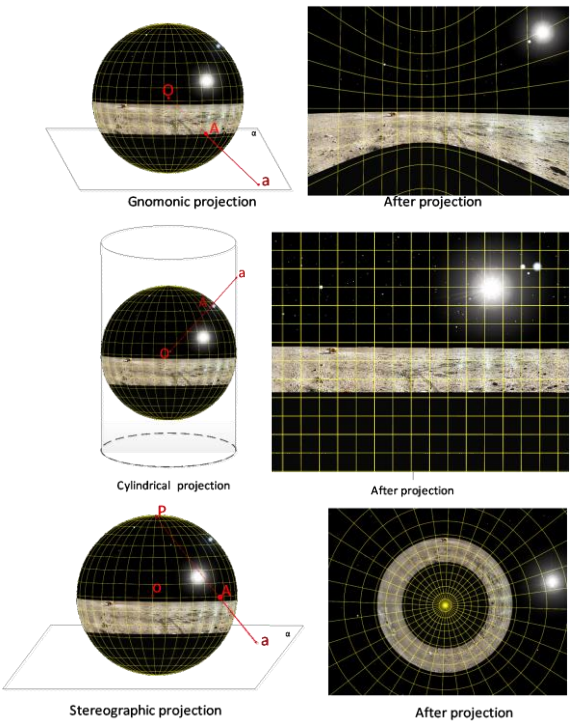

Figure 4: Gnomonic projection , cylindrical and stereographic projection methods

4. Result

We create a virtual scene of the Moon surface by this system(Figure 5). The system not only contributed heavily to Chang'E-3 mission, but also plays an import role in science popularization about the Moon after Chang'E-3 mission.

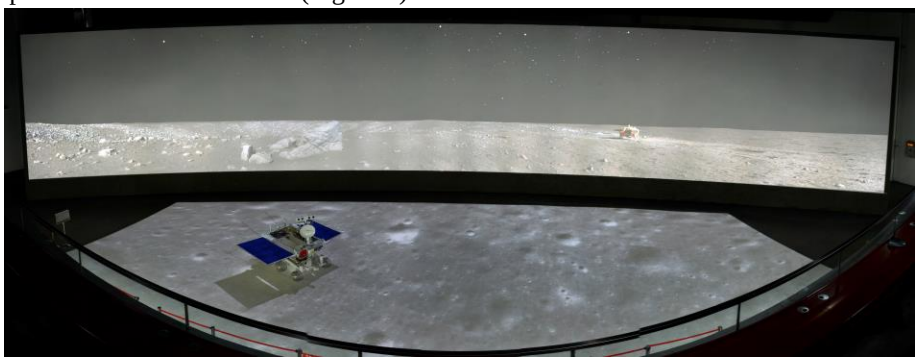

Figure 5: Scene created by lunar immersive visualization system with model of Yutu and ground screen

Acknowledgements

We are grateful for support from the five systems in the Chinese Lunar Exploration Project. We are thankful to the Ground Research and Application System.

References

[1] Wu Weiren, Zhou Jianliang, Wang Baofeng, Liu ChuanKai.: Key technologies in the teleoperation of Chang'E-3 "Jade Rabbit" rover, Science China, Vol. 44(4), pp. 425-440, 2014

[2] Ye Peijian, Rao Wei.: Application of photoelectricity technology for deep space exploration in China, Spacecraft Recovery & Remote Sensing, Vol. 32(2), pp.1-11, 2011

[3]Wu Fanlu, Liu Jianjun, Ren Xin, LiChunlai.: Research on panoramic mosaics method of Chang'E-3 Pancam Images, Acta Optica Sinica, Vol. 34(9), pp. 1-8,2014

EPSC Abstracts
Vol. 10, EPSC2015-299, 2015
European Planetary Science Congress 2015

Wave phenomena at Moon: the solar wind–magnetic anomalies interaction

A. Skalsky and **A. Sadovski**
Space Research Institute of Russian Academy of Sciences (IKI RAS) (asadovsk@iki.rssi.ru / Fax: +7-495-3331248)

Abstract

One of the most interesting effect of solar wind interaction with Lunar surface is the formation of such called mini-magnetosphere above the anomalous magnetic regions. The anomalies magnetic field and forming magnetic field discontinuity (shock structure) may reflect solar ind ions and electrons. We perform the review of different mechanisms for the wave generation in plasma environment near such mini-magnetosphere regions.

1. Introduction

The lunar plasma environment seems to be very simple matter but the observations of the interaction in Moon-plasma system has proven that the physical processes are complex and varied. Especially it should be noted that the interaction have a kinetic nature and must be studied using kinetic theory.

One of important processes is the solar wind interaction with Moon surface. There are regions of enhanced crustal magnetic field so called magnetic anomalies, where a magnetic field may reach till several hundred nT [1, 2, 3]. The observations of Kaguya and Chandrayaan revealed that significant deflected proton fluxes exist over magnetic anomalies at the lunar surface [4, 5, 6, 7]. Such deflection may imply that the magnetic anomalies may act as magnetosphere-like obstacles (mini-magnetospheres), modifying the upstream plasma. Moreover the observations of energetic neutral atoms showed that the enhanced fluxes of deflected particles may exist [9, 8].

We perform the review of different mechanisms for the wave generation in plasma environment near such mini-magnetosphere regions.

2. Solar wind interaction with magnetic field anomalies

The interaction of the solar wind with magnetic anomalies may result in formation of miniature magnetosphere. The main observational features revealing such concept are the existence of the MHD waves with 40–80 km/s speed in the solar wind reference frame, the growth of the plasma density.

The possibility of the minimagnetosphere formation depends upon two conditions:

- the magnetic field pressure should be big enough to balance the solar wind dynamic pressure;
- the characteristic minimagnetosphere size should be bigger than the proton gyroradius.

For typical solar wind conditions magnetic field necessary for the mini-magnetosphere formation should be 7–230 nT. The magnetic field in magnetic anomalies may be more than 20–27 nT. In papers [10, 11] authors presented the simple model for the ion reflection from anomaly. The main conclusion was that the some shock structure may forms and great deflection of electrons is possible. However, presented model of reflection may be appropriate only for strong magnetic anomalies and the amount of deflected ions should be very sensitive to the solar wind conditions.

However if we estimate the solar wind electron energy after shock it appears to be equal $E_e \sim 3 \times 10^{-12}$ erg/nuc. Maximum energy, that may be gained to proton deceleration is $E_i \leq 10E_e$, but the energy of proton solar wind component is $E_{SW} \sim 9 \times 10^{-10}$ erg/nuc. So the energy gain is too low to stop the protons and they fill the magnetic cavity.

3. Wave activity near the Moon

Variety of electric fluctuations was observed during the passage of Wind spacecraft across the lunar wake: langmuir waves, electrostatic modes above electron

cyclotron frequency, whistlers [12]. The investigations by Kuncic and Cairns [13] revealed emissions on plasma frequency and its first harmonic. Electron reflection at quasi-shock at leading edge of magnetic anomaly could drive the electric field oscillations. The generation mechanism is similar to that known for foreshock of planetary bow shock.

In KAGUYA [14] and Lunar Prospector [15] missions the monochromatic whistlers near the Moon were observed as narrow band magnetic fluctuations with frequencies close to 1 Hz, and are mostly left-hand polarized in the spacecraft frame. The waves are generated by the solar wind interaction with lunar crustal magnetic anomalies. The conditions for observation of the waves strongly depend on the solar zenith angle (SZA), and a high occurrence rate is recognized in the region of SZA between 40 to 90° with remarkable north-south and dawn-dusk asymmetries. It is suggested that ion beams reflected by the lunar magnetic anomalies are a possible source of the waves.

Also large-amplitude monochromatic ULF waves were observed on Kaguya spacecraft [16]. The dominant periods of waves are of 120–100 s. The amplitude was as large as 3 nT. The occurrence rate is high above the terminator and on the dayside surface. The direction of the propagation is not exactly parallel to the interplanetary magnetic field, but shows a preference to the direction of the magnetic field and the direction perpendicular to the surface of the moon below the spacecraft. The sense of rotation of the magnetic field was left-handed with respect to the magnetic field in 53% of the events, while 47% showed right-handed polarization. The possible generation mechanism is the cyclotron resonance of the magnetohydrodynamic waves with the solar wind protons reflected by the moon. Most of events occur in the southern hemisphere of the Moon over region of lunar magnetic anomalies.

Non-monochromatic fluctuations of the magnetic field over the frequency range of 0.03-–10 Hz were detected by Kaguya [17] at an altitude of 100 km above the lunar surface. The fluctuations were almost always observed on the solar side of the moon, irrespective of the local lunar crustal field. They were also detected just nightside of the terminator (SZA $< 123°$), but were absent around the center of wake. The level of the fluctuation enhanced over the wide range from 0.03 to 10 Hz, with no clear peak frequency. The fluctuations had the compressional component, and the polarization was not clear. The fluctuations were supposed to be whistler waves generated by the protons reflected by the lunar surface.

4. Summary and Conclusions

Waves occur in wide frequency range from f_{ci} to f_{pe}. Observations of wide band electric noise (above f_{ce}) seem to be related to short electric spikes. Wave phenomena observed at Moon are mostly associated with the wake boundary and lunar crust magnetic anomalies. Most of emissions are detected simultaneously with enhanced fluxes of reflected from the Moon surface (crust anomaly) ions and electrons.

Acknowledgements

This work was supported by Presidium of RAS programm P-9, Science scientific school NSh-248.2014.2.

References

[1] Coleman, P.J., Lichtenstein, B.R., Russell, C.T. et al.: Magnetic fields near the moon, Proc. Lunar Planet. Sci. Conf. Vol. 3, pp. 2271, 1972.

[2] Lin, R.P.: Constraints on the origins of lunar magnetism from electron reflection measurements of surface magnetic fields, Phys. Earth Planet. Int. Vol. 20, pp. 271, 1979.

[3] Lin, R.P., Mitchell, D.L., Curtis, D.W., et al.: Lunar surface magnetic fields and their interaction with the solar wind: Results from Lunar Prospector, Science, Vol. 281, pp. 1480–1484, 1998.

[4] Holmström, M., Wieser, M., Barabash, S., Futaana, Y., Bhardwaj, A.: Dynamics of solar wind protons reflected by the Moon, J. Geophys. Res., Vol. 115, pp. A06206, 2010.

[5] Saito, Y., Yokota, S., Tanaka, T. et al.: Solar wind proton reflection at the lunar surface: Low energy ion measurement by MAP-PACE onboard SELENE (KAGUYA), Geophys. Res. Lett., Vol. 35, pp. L24205, 2008.

[6] Saito, Y., Yokota, S., Asamura, K. et al.: In-flight Performance and Initial Results of Plasma Energy Angle and Composition Experiment (PACE) on SELENE (Kaguya), Space Sci. Rev., Vol. 154, pp. 265–303, 2010.

[7] Wieser, M., Barabash, S., Futaana, Y. et al.: Extremely high reflection of solar wind protons as neutral hydrogen atoms from regolith in space, Planet. Space Sci., Vol. 57, pp. 2132–2134, 2009.

[8] Wieser, M., Barabash, S., Futaana, Y. et al.: First observation of a mini-magnetosphere above a lunar magnetic anomaly using energetic neutral atoms, Geophys. Res. Lett., Vol. 37, pp. L015103, 2010.

[9] Futaana, Y., Barabash, S., Holmström, M., Bhardwaj, A.: Low energy neutral atoms imaging of the Moon, Planet. Space Sci., Vol. 54, pp. 132–143, 2006.

[10] Skalsky A.A., Sadovski A.M.: Reflection of solar wind protons from magnetic anomalies of the moon, Cosmic Research, Vol. 53, pp. 70–73, 2015.

[11] Sadovski A.M., Skalsky A.A.: Coupling of earth's magnetosphere, solar wind and lunar plasma environment, Adv. Space Res., Vol. 54, pp. 2017—2020, 2014.

[12] Kellogg P.J., Goetz K., Monson S.J. et al.: Observations of plasma waves during a traversal of the Moon's wake, Geophys. Res. Lett., Vol. 23, pp. 1267–1270, 1996.

[13] Kuncic Z., Cairns I.H.: Radio emission from mini magnetospheres on the Moon. Geophys. Res. Lett., Vol. 31, pp 11, 2004.

[14] Tsugawa Y., Terada N., Katoh Y. et al.: Statistical analysis of monochromatic whistler waves near the Moon detected by Kaguya, Annales Geophysicae, Vol. 29, pp. 889–893, 2011.

[15] Halekas J.S., Brain D.A., Mitchell D.L., Lin R.P.: Whistler waves observed near lunar crustal magnetic sources, Geophys. Res. Lett., Vol. 33, pp. L22104, 2006.

[16] Nakagawa T., Nakayama A., Takahashi F. et al.: Large-amplitude monochromatic ULF waves detected by Kaguya at the Moon, J. Geophys. Res., Vol. 117, pp. A04101, 2012.

[17] Nakagawa T., Takahashi F., Tsunakawa H. et al.: Non-monochromatic whistler waves detected by Kaguya on the dayside surface of the moon, Earth, Planets and Space, Vol. 63, pp. 37–46, 2011.

EPSC Abstracts
Vol. 10, EPSC2015-325, 2015
European Planetary Science Congress 2015

IN SITU PYRO-GC-MS CHEMICAL ANALYSIS OF LUNAR SOIL : A GROUND TRUTH TO INTERPRET THE ANALYSES OF THE SAMPLES RETURNED FROM THE MOON

C. Szopa[1], M. Gerasimov[2], P. Wurz[3], L. Hofer[3], M. Cabane[1], P. Coll[4], A. Buch[5], A.G. Sapgir[2], S.A. Aseev[2], M.A. Zaitsev[2], D. Coscia[1] and the GAC team
[1]LATMOS, Univ. Pierre et Marie Curie, Univ. Versailles Saint-Quentin & CNRS, 75005 Paris, France, [2]IKI, 84/32 Profsoyuznaya, 117997, Moscow, Russia , [3] Physikalisches Institut, University of Bern, Sidlerstrasse 5, CH-3012, Bern, Switzerland, [4]LISA, Univ. Paris-Est Créteil, Univ. Denis Diderot & CNRS 94010 Créteil, France, [5]Ecole Centrale Paris, 92295 Chatenay-Malabry, France.
Corresponding author : Cyril SZOPA / cyril.szopa@latmos.ipsl.fr / 33 1 80 28 52 89

Abstract

Volatiles were recently discovered to be present at the Lunar pole. These volatiles probably comes from meteorites and micrometeorites which continue to deliver their material at the surface of the satellite. Thus, their characterisation would enable to better constrain the nature of the species brought by the meteorites to the solar system bodies, evaluate their evolution under Moon surface conditions. Thus is what we expect to be able to do within a few years with the Gas Analytical Package experiment onboard the Louna Globe mission.

1. Introduction

The chemical characterization of lunar samples will be of primary importance to assess their content in volatile species. These volatiles could reveal, for instance, part of the nature of : materials delivered to Earth from exogenous sources, minerals present in the Lunar regolith and surface rocks, and Lunar organic material. Even if the accuracy and sensitivity of the analytical instrumentation used in laboratory are very high to allow to thoroughly analyze the content of samples brought from the Moon, the journey of these samples in space, as well as their transportation to Earth environment, could change the nature of the sample volatiles (e.g. loss of chemical species, possible chemical reactions or contaminations). For these reasons, an in situ chemical characterization of the samples could be of precious help for the interpretation of the results obtained in laboratory, and their transposition to the Moon surface environment.

2. The GAC experiment

This is the reason why our team proposes an instrumentation to characterize in situ the content of volatiles in the lunar soil and rocks. This instrumentation would provide important reference data about the samples collected and returned to Earth. It is based on pyrolysis coupled with gas chromatography and mass spectrometry, and could have the capability to: extract volatile materials (either condensed or present in the minerals) from the solid samples, separate the volatile and analyze their structure for identification and quantification, and analyze isotopic ratios in a certain extent. This instrumentation is based on an inheritance of the GAP instrument that was present onboard the late Phobos-Grunt probe. The instrumentation would be composed of : i. a pyrolyzer capable to heat the samples up to about 1000°C, and developed by IKI (Rus), which is also in charge to the whole instrument (PI M. Gerasimov); ii. a gas chromatograph devoted to separate and detect the volatile species released from the samples, developed by LATMOS and LISA (Fra.) (CoI C. Szopa & P. Coll); iii. a time of flight mass spectrometer for the structural identification of the molecules, developed by the University of Bern (Swi.) (CoI P. Wurz). This instrumentation should allow the identification of inorganic volatile molecules and small organic molecules (up to about benzene). This communication aims at presenting this instrumentation that should be onboard the Luna Resource probe to the Lunar South pole, and it could be used for a return sample mission to get ground truth data about the returned samples.

EPSC Abstracts
Vol. 10, EPSC2015-371, 2015
European Planetary Science Congress 2015

The Search for Water in the Lunar Crust

D. E. Smith and M. T. Zuber
Dept of Earth, Atmospheric and Planetary Sciences, Massachusetts Institute of Technology, Cambridge, MA 02139, USA (smithde@mit.edu)

Abstract

There is evidence from several sources that water ice is present at a number of locations on the surface at the lunar poles. But there seems little agreement on the source of the ice with most suggestions being of external nature, such as impacts by ice-rich comets. Here we discuss the lunar crust as a possible source of the water ice and investigate whether there is any evidence from the recent GRAIL [1,2] and Lunar Reconnaissance Orbiter (LRO) [3] missions to support this possibility.

1. Introduction

GRAIL and the laser altimeter (LOLA) [4,5] on LRO have provided high resolution and high accuracy gravity and topography models of the Moon from which we have derived the Bouguer gravity anomaly field. These anomalies represent density contrasts within the Moon that provide information about its interior structure and composition. When Bouguer gravity is represented as a spherical harmonic series it can be analyzed by wavelength with the longer wavelengths representing deeper anomalies and the short wavelengths shallower features. In our analysis we focus on those wavelengths that represent the Bouguer gravity in the top 45 km, corresponding to the crust. Although gravity cannot be uniquely inverted to provide density it can provide some constraints on structure and composition.

2. Water ice signal

Water ice in the lunar crust can be manifest as either a positive or a negative Bouguer anomaly depending on how the ice is mixed in with the regolith. If the ice fills the pore space between the grains then there will be a small mass excess relative to surroundings that will produce a positive gravity signal. If the ice has displaced the grains of the regolith then because water ice is less dense than than compacted regolith we can expect a decrease in local density compared to the surrounding area, leading to a negative gravity anomaly. Our study indicates that the range of Bouguer gravity at the lunar south pole from latitude in a 10-degree radius cap centered on the pole is less than ± 50 mGal, which limits the mass of the material that is producing the density contrast that is causing the gravity anomaly.

One of the larger Bouguer anomalies coincides with the location of the Shoemaker crater at latitude 88S, which is also one of the locations that the LEND instrument [6] on LRO measures a significant decrease in neutrons that is interpreted to be caused by the presence of water ice in the top 1-meter of the surface of the crater floor. A simple model of this anomaly indicates it can be represented (though not uniquely) by a mass deficiency of ~ 10^{15} kg at a depth of about 25 km. If we assume the mass occupies a volume comparable to the size of the central region of the crater floor with similar thickness, then the required density contrast at 25 km mean depth is <200 kg/m^3, or ~8% of the estimated density of the crust. Further, since we can exchange depth for mass the equivalent mass required at 10 km depth is only ~25 kg/m^3, or ~1.5% density contrast. Thus, the Shoemaker Bouguer gravity anomaly could be explained by a few percent of water ice in an ice-rich layer below the surface of the crater, which incidentally is consistent with the indication from LEND of a few percent water in the top 1 meter.

Further, it is at least in principle possible to explain most of the gravity anomalies in the region of the south pole as being due to the presence of water ice in the upper crust. We do not suggest that this is the case but rather that the presence of water in the crust, instead of or in addition to chemical differences, could be at least part of the explanation of the observed Bouguer gravity signal, and might also explain the presence of surface ice seen by other instruments.

3. Conclusions

Analysis of the Bouguer gravity of the lunar south pole region indicates that the component that originates in the crust requires a density contrast of order 1 to 8%, depending on depth, which could, at east in part, be explained by the presence of water ice in the upper crust thereby bounding the amount of possible crustal ice.

Acknowledgements

We wish to acknowledge the help of colleagues at the NASA Goddard Space Flight Center, the Jet Propulsion Laboratory, and the GRAIL and LRO Projects.

References

[1] Zuber, M. T., et al.: Gravity Recovery and Interior Laboratory (GRAIL): Mapping the Lunar Interior from Crust to Core, Space Sci Rev, doi: 10.1007/s11214-012-9952-7

[2] Zuber, M. T., et al,; Gravity Field of the Moon from the Gravity Recovery and Interior Laboratory (GRAIL) Mission, ScienceExpress, 10.1126/science.12315075 December 2012

[3] Tooley, C. R., et al,: Lunar Reconnaissance Orbiter Mission and Spacecraft Design, Space Sci Rev (2010) 150: 23–62, doi: 10.1007/s11214-009-9624-4

[4] Smith, D. E., et al.: Initial Observations from the Lunar Orbiter Laser Altimeter (LOLA), Geophys Res Ltrs, doi:10.1029/2010GL0437511

[5] Smith, D. E., et al,: The Lunar Orbiter Laser Altimeter Investigation on the Lunar Reconnaissance Orbiter Mission, Space Sci Rev (2010) 150: 209–241, doi: 10.1007/s11214-009-9512-y

[6] Mitrofanov, I. G., et al,: Lunar Exploration Neutron Detector for the NASA Lunar Reconnaissance Orbiter, Space Sci Rev (2010) 150: 183–207, doi 10.1007/s11214-009-9608-4

EPSC Abstracts
Vol. 10, EPSC2015-380, 2015
European Planetary Science Congress 2015

LRO Diviner: Viewing the Moon in a Different Light

B.T. Greenhagen (1), D.A. Paige (2) and the Diviner Lunar Radiometer Science Team
(1) Johns Hopkins University Applied Physics Laboratory, Laurel, MD USA, (2) University of California, Los Angeles, CA USA (benjamin.greenhagen@jhuapl.edu)

Abstract

After six years in operation, and well into its second extended science mission, the Diviner Lunar Radiometer continues to reveal the extreme nature of the Moon's thermal environments, thermophysical properties, and surface composition. This presentation will focus on new observations and recent results and will highlight contributions from members of the Diviner Science Team addressing a diverse range of scientific questions.

1. Diviner Lunar Radiometer

Diviner is the first multispectral thermal infrared instrument to globally map the surface of the Moon. To date, Diviner has acquired observations over twelve complete diurnal cycles and six partial seasonal cycles. Diviner daytime and nighttime observations (12 hour time bins) have essentially global coverage, and more than 80% of the surface has been measured with at least 7 different local times. The spatial resolution during the mapping orbit was ~200 m and now ranges from 150 m to 1300 m in the current elliptical "frozen" orbit. Calibrated Diviner data and global maps of visible brightness temperature, bolometric temperature, rock abundance, nighttime soil temperature, and silicate mineralogy are available through the Planetary Data System (PDS) Geosciences Node.

2. Results

Diviner was designed to accurately measure temperatures across a broad range from midday equatorial regions such as the Apollo landing sites (around 400K), typical nighttime temperatures of less than 100K, and extreme permanent shadowed regions colder than 50K. The coldest multiply-shadowed polar craters may have temperatures low enough to put constraints on lunar heat flow. Diviner data have

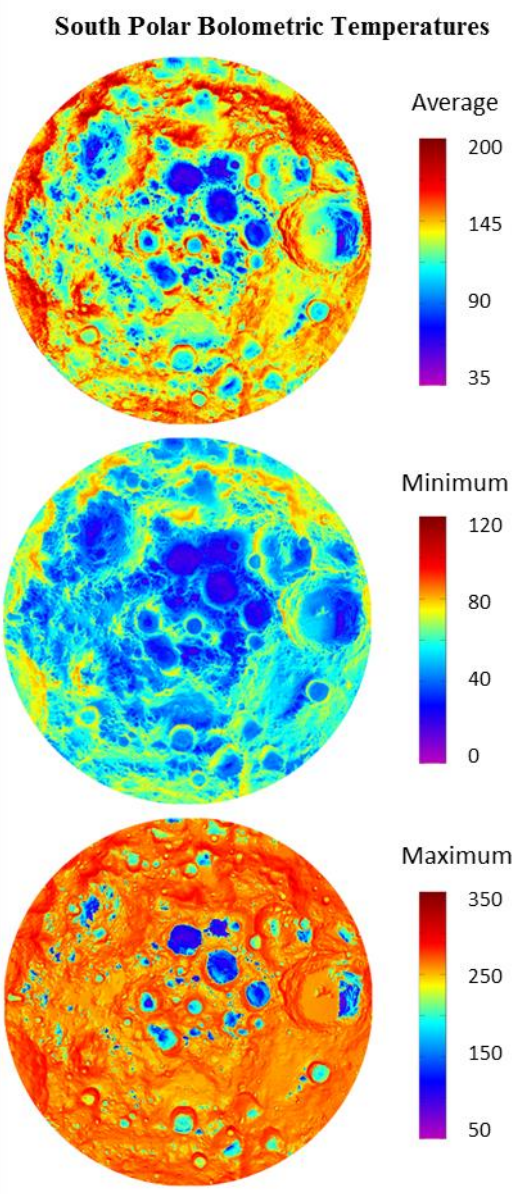

Figure 1: The temperature maps above (pole to 82°) demonstrate the extreme thermal environment of the Moon observed by the Diviner Lunar Radiometer.

also been used to estimate the thermal properties of non-polar permanently shadowed regions.

Diviner is directly sensitive to the thermophysical properties of the lunar surface including nighttime soil temperature, rock abundance, and surface roughness. During the extended science mission we have produced higher fidelity maps of these properties and used them to investigate anomalous rock abundances, "cold spots" with fluffier surface layers, regolith formation and evolution, and surface roughness.

Diviner was designed to characterize the Christiansen Feature (CF) and constrain lunar silicate mineralogy. Recent efforts in this area have focused on improving the quality of Diviner's mid-infrared "photometric" correction, groundtruthing Diviner observations to Apollo soils, using Diviner's longer wavelength channels to improve constraints on olivine abundances, and combining Diviner with visible and near-infared datasets to enhance interpretations of pyroclastic deposits, plagioclase-rich regions, high silica regions, and space weathering.

During its second extended science mission, Diviner has acquired new data to compliment the existing dataset. Diviner has observed three total lunar eclipses with geometry that enables new investigations into the top 2 cm of the regolith. Diviner has begun a systematic campaign to globally maps the Moon viewed at high emission angles, which will provide leverage on surface roughness. And Diviner has performed large quantities of targeted observations to enhance temporal coverage at critical local times for specific investigations.

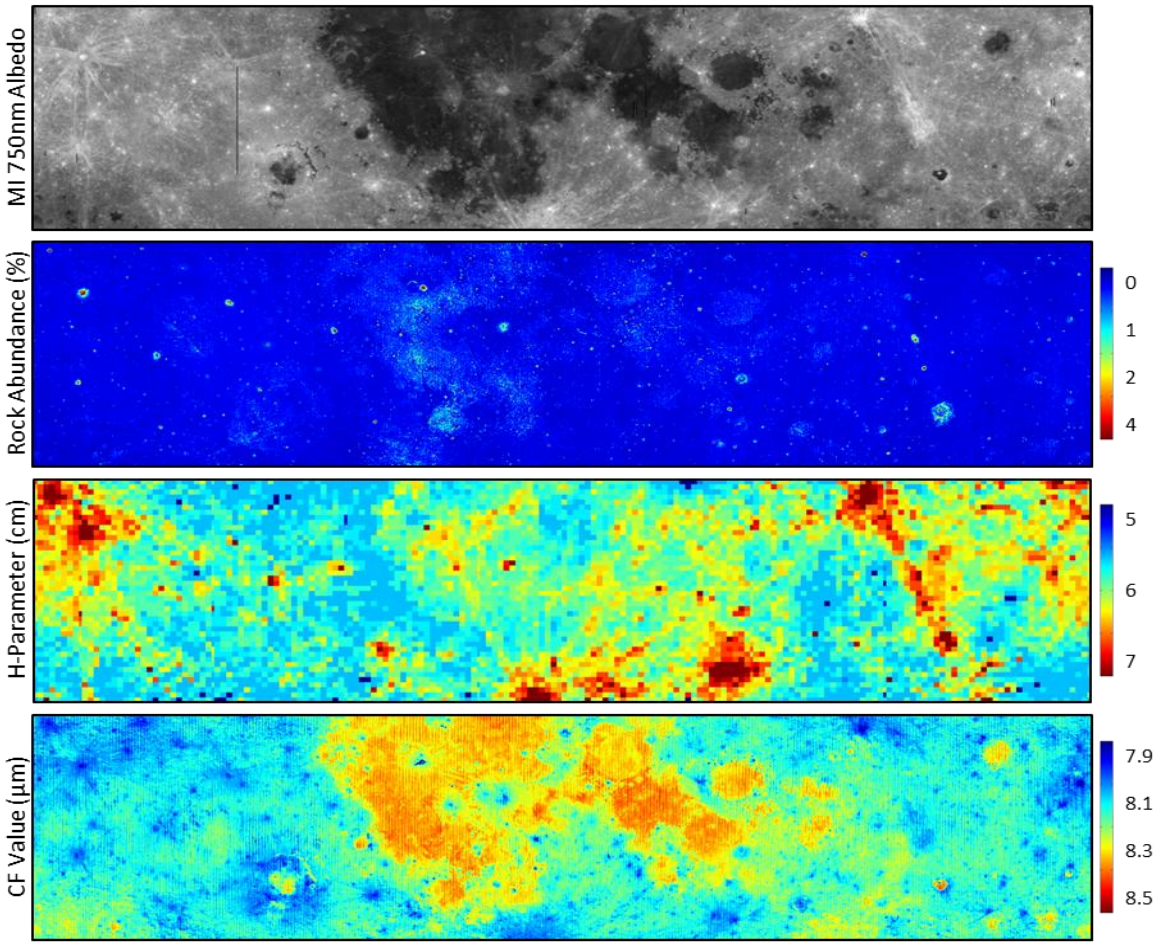

Figure 2: Diviner maps of rock abundance (RA), H-parameter (regolith insulating layer), and Christiansen Feature (CF). RA and CF maps from PDS. SELENE Multiband Imager 750 nm albedo map for context.

EPSC Abstracts
Vol. 10, EPSC2015-393, 2015
European Planetary Science Congress 2015

Explore Chang 'E Lunar dataset by Interactive Integration of Multiple Imagery Maps with Visual Variables

Xingguo Zeng , Lingli Mu , Wei Yan and Xingye Gao

Key Laboratory of Lunar and Deep Space Exploration, National Astronomical Observatories, Chinese Academy of Sciences, China (zengxg@nao.cas.cn / Fax: +86-010-64888703)

Abstract

In the Chang' E lunar exploration program of China, a lot of lunar exploration dataset were captured. Explore the dataset to find out specific topographic and geologic features would be useful for the lunar scientific research. In this approach, a new method for lunar dataset exploration was developed and applied in the Data Management System of China Lunar exploration Program. The method was taken measure by interactive integration of the lunar imagery maps with map visual variables such as color, brightness, and pattern et.al. With this method, topographic or geologic information would be enhanced and could be detected more convenient for the lunar research scientist.

1. Introduction

Discovering the lunar topographic, geological tectonic such as boundary or layer information is of great value to lunar research. However, there are still many difficulties in extracting the complex lunar tectonic information with available lunar data exploration method. Lunar imagery map is one of the major visualization media for the lunar scientist to acknowledge the lunar dataset to fetch the information, and map visual variables defined by Bertin in reference [1] are the vital elements of the imagery map for representing the lunar information.

In this approach, firstly, the general information about the Chang' E lunar data is discussed, after that, a lunar data exploration method by interactive integration of visual variables in imagery map based on multi-source lunar data mainly from Chang 'E(CE) dataset is introduced, the following paragraph is about the application of the method, and the last part is a short summary and conclusion.

2. Data and Method

2.1 CE lunar dataset

China started the Change'E(CE) lunar exploration program in 2007, and until now, there has been 3 missions which include CE1 in 2007, CE2 in 2009 and CE3 in 2013, the captured data were used in creating the global topographic map and imagery map of the moon. Tab. 1 shows some detail information about the captured exploration data.

Table 1: CE dataset

Space craft	Date	Dataset
CE1	2007.11	Global 120m DOM, 500m DEM
CE2	2010.10	Global 7m DOM,7m DEM
CE3	2013.12	High resolution images, geologic radar data of the CE3 landing site

Besides the CE lunar data, we also collected other lunar exploration data originated from NASA and ESA, such as the global lunar geologic map et.al.

2.2 Method

The method generally takes 3 steps to explore the lunar dataset.

First, get the multi-sources data and create to different imagery map such as shaded relief map, DOM map et.al;

Second, change the imagery maps into different channels in RGB, CMYK, or CIELab, overlay and integrate the channels into a new map;

Third, adapt the weight of each channel from different maps, interactive change the map visual variables such as color, brightness, pattern, transparency et.al, to enhance the hidden topographic or geologic features.

3. Application

The method was implemented in the detection of the complex crater edge of the CE3 landing area, by interactive integration of Shaded Relief Map, DOM map, the shape of the complex crater was extracted, see Fig. 1.

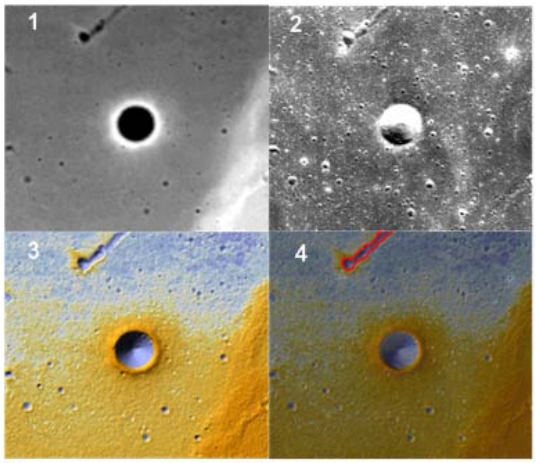

Figure 1: Complex crater edge detection.

4. Summary and Conclusions

An initial method by interactive integration of the lunar maps with map visual variables for exploring the CE lunar dataset to detect the topographic or geologic data was discussed in this approach. The method was implemented in the work of detect the complex shape of the crater and some other work and the experiment result show that the method was applicable. In the future study, we would pay more attention to find more visual variables and get the parameters for integration.

Acknowledgements

This approached was Supported by the Young Researcher Grant of National Astronomical Observatories, Chinese Academy of Sciences, the Lunar dataset for experiment were provided by Laboratory of Lunar and Deep Space Exploration of China, thanks for the scientist and engineer of the lab.

References

[1] BERTIN J. Sémiologie graphique. Les diagrammes, les réseaux, les cartes [M]. Paris: Mouton, 1967.

[2] Li C L, Liu J J, Ren X, et al. The global image of the moon by the Chang'E-1:Data processing and lunar cartography[J], Sci China Earth Sci, 2010 (3): 294-306.

[3] Mu L, Li C, Liu J, et al. A New Mapping Method for the Moon With the Chang'E-1 Data.The 26 INTERNATIONAL CARTOGRAPHIC CONFERENCE, Germany,2013

EPSC Abstracts
Vol. 10, EPSC2015-394, 2015
European Planetary Science Congress 2015

Far-Ultraviolet Characteristics of Lunar Swirls

A. R. Hendrix(1), T. K. Greathouse(2), K, D. Retherford(2), K. E. Mandt(2), G. R. Gladstone(2), D. E. Kaufmann(3), D. M. Hurley(4), P. D. Feldman(5), W. R. Pryor(6), M. A. Bullock(3), S. A. Stern(3); (1)Planetary Science Institute, Tucson, AZ; (2)Southwest Research Institute, San Antonio, TX; (3)Southwest Research Institute, Boulder, CO; (4)Applied Physics Laboratory, Johns Hopkins University, Laurel, MD; (5)Johns Hopkins University, Baltimore, MD; (6)Central Arizona College, AZ (arh@psi.edu)

1. Introduction & Background

Lunar swirls are often described as bright sinuous regions of the Moon that appear to be relatively immature – i.e. less space-weathered than surrounding regions. Swirls are mysterious but seem to be linked to the interaction between the solar wind and the lunar magnetic anomalies (e.g., [1]). Commonly-studied swirls include Mare Ingenii (in a mare-highlands boundary region), Reiner Gamma (in a mare region), and Gerasimovich (in a highlands region). Swirls are known to be surface features: they have no expression at radar depths [2], exhibit no topography, and craters on swirls that penetrate the bright surface terrain reveal underlying dark material [3].

Using Clementine and Lunar Prospector data, it was found [4] that all swirls are associated with areas of magnetized crust, and that swirls exhibit spectral characteristics similar to immature material and generally have slightly lower FeO values compared with their surroundings.

Lunar swirls exhibit VNIR characteristics consistent with a reduced amount of space weathering compared to surrounding regions, which suggests a reduction in solar wind interaction at those locations. Nanophase iron, responsible for the spectral characteristics attributed to space weathering, is created by vaporization/deposition by micrometeorite impacts and sputtering/reduction by solar wind ions. On the swirls, the decreased proton flux (deflected by the magnetic anomalies) slows the spectral effects of space weathering (relative to nonswirl regions) by limiting the nanophase iron production to micrometeoroid impact vaporization/deposition (e.g., [5]). Analysis of Clementine spectra [6] of lunar swirls indicates that swirls are regions of retarded weathering, and that the production of larger-grained (>40 nm) nanophase iron dominates in these locations as a result of charged particle sorting by the magnetic field. In a study of M^3 data of the 2.82 μm feature indicative of OH abundance within and near swirls, [5] found that swirls are depleted in OH relative to their surroundings, consistent with the idea of a divergence of solar wind in these zones.

An electrostatic dust transport mechanism may be at play [7], where charged fine feldspathic dust is attracted into bright areas of swirls, and repelled from dark lanes within swirls. The authors point out that lunar swirls do not exhibit VNIR spectral trends typical of immature lunar soils, using Clementine data.

In the ultraviolet, lunar space weathering effects are the reverse of those at VNIR wavelengths: more weathered regions are bluer than less weathered regions [9], due to a weathering-related degradation of the UV absorption edge in iron-bearing silicates. Indeed, LROC color results of the Reiner Gamma swirl [10] show a low 321/415 nm ratio (i.e., steep UV slope), consistent with a lack of space weathering compared to the surrounding mature mare terrain. For the Gerasimovich swirl, located in low-iron (<5wt% FeO) highlands, regions within the swirl have higher 321/415nm ratio values than the mature background (consistent with the exposure of fresh plagioclase-rich soil). The 321/415nm ratio values for the Gerasimovich swirl are similar to those of the rays of Tycho, Jackson, and Necho [10].

In this work, we investigate the far-ultraviolet (FUV) characteristics of swirl regions to broaden the spectral coverage of these mysterious regions and further illuminate their possible origins.

As pointed out [7], lunar swirls could represent regions on the Moon where both solar wind and micrometeoroid bombardment are important: where solar wind bombardment produces nanophase iron (and the lack of this nanophase iron in swirl regions makes them visibly bright and UV dark) but maturation via micrometeoroid bombardment is important for producing glass-welded aggregates and fine-grained soils that can enhance weathering effects

at VNIR wavelengths. It is also likely (e.g. [5]) that sputtering/vapor deposition, implanted solar wind hydrogen, and agglutination share responsibility for creating the range in nanophase iron particle sizes that produce the spectral effects of space weathering. The study of the shorter wavelengths probed by LAMP allows for further constraints to be placed on grain size and weathering effects.

2. LRO/LAMP Data

The Lunar Reconnaissance Orbiter (LRO) is currently in orbit at the Moon. The Lyman Alpha Mapping Project (LAMP) onboard LRO has been making measurements of the lunar nightside, dayside and atmosphere since September 2009. The LAMP instrument [11] is a photon-counting imaging spectrograph. The entire passband is 57–196 nm, in the far-UV (FUV) spectral region. For dayside measurements, the instrument is operated in "pinhole" mode, with the entrance aperture reduced by a factor of 736. The instrument was usually nadir-pointed in LRO's characteristic 50-km lunar orbit of the prime mission and provided ~500 m resolution. In LRO's extended mission the orbit has been modified to an elliptical frozen orbit that saves fuel and results in up to ~2 km resolution when at the North pole.

To determine the lunar FUV reflectance, we divide the LAMP data by the full-disk solar spectrum from SORCE SOLSTICE [12], taken for the day of each observation and convolved to agree with the LAMP resolution and line spread function. Past analyses of LAMP dayside data (e.g. [13]) have shown that spectral slopes in the 175-190 nm region are good indicators of weathering and composition.

2. LAMP Results

In general, we find that nearly all regions of the Moon are spectrally blue (i.e. increasing in albedo with decreasing wavelength) in the LAMP bandpass, due to the surface-scattering nature of the light interaction with the grains combined with the optical constants of the compositional materials. Mare regions are bluer than highlands regions due to their higher concentrations of opaques. Also, more weathered regions become spectrally bluer in the FUV due to the spectral contributions of nanophase iron [9], while less weathered regions are less spectrally blue, or are spectrally relatively red.

We find that swirls are spectrally red (i.e. less spectrally blue, see Fig. 1) compared to surrounding terrain, and appear to be less mature than other "immature" regions, consistent with a lack of weathering in these zones. Because UV wavelengths sense primarily the weather-produced rims on grains, this result is consistent with a lack of (weathering-produced) opaque rims, not consistent with micrometeoroid production of rims. The LAMP results are also consistent with accumulated fine-grained feldspathic material. Because weathering effects are expected to appear in the UV faster than in the VNIR [9], the lack of weathering effects in the FUV in the swirls regions tells us about timescales of processing.

References

[1] Kramer, G. et al. (2011), *EOS*, 92, 413. [2] Neish, C. et al. (2011) *Icarus,* 215, 186. [3] Lawrence, S. (2011) *Lunar Swirls Workshop without Walls* [4] Blewett, D. et al. (2011) *JGR,* 116, E02002, doi:10.1029/2010JE003656. [5] Kramer, G. et al. (2011b), *JGR,* 116, E00G18, doi:10.1029/2010JE003729. [6] Kramer, G et al. (2011a), *JGR,* 116, E04008, doi:10.1029/2010JE003669. [7] Garrick-Bethell, I. et al. (2011) *Icarus,* 212, 480. [9] Hendrix. A. R. & F. Vilas (2006) *A.J., 132,* 1396-1404. [10] Denevi, B. et al. (2014) *JGR,* 119, doi:10.1002/2013JE004527. [11] Gladstone, G. R. et al. (2010) *SSR, 150,* 161-181. [12] McClintock et al. (2000) P*roc. SPIE Earth Obs. Syst., 4135,* 225–234. [13] Hendrix et al. (2012) *JGR, 117,* E12001, doi:10.1029/2012JE004252.

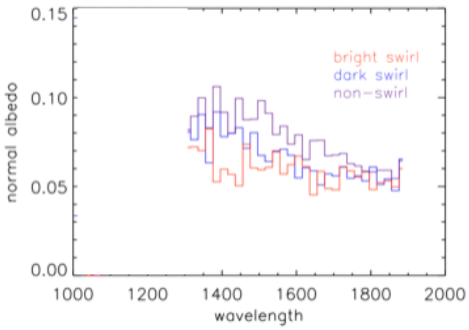

Figure 1. Sample LAMP spectra from the Reiner Gamma swirl bright region, dark region and off-swirl region. The visibly-bright swirl region is significantly less spectrally blue in the FUV than the dark swirl region and off-swirl region.

EPSC Abstracts
Vol. 10, EPSC2015-395, 2015
European Planetary Science Congress 2015

Extending the Lunar Mapping and Modeling Portal – New Capabilities and New Worlds

B. Day (1), E. Law (2), E. Arevalo (2), B. Bui (2), G. Chang (2), K. Dodge (2), R. Kim (2), S. Malhotra (2), S. Sadaqathullah (2), G. Schmidt (1), B. Bailey (1)
(1) NASA Solar System Exploration Research Virtual Institute. NASA Ames Research Center. M/S 17-1. Moffett Field, CA, USA. 94035. (Brian.H.Day@nasa.gov, +01-650-604-2605
(2) Jet Propulsion Laboratory, California Institute of Technology. M/S 168-200. 4800 Oak Grove Dr. Pasadena, CA, USA 91109. (Emily.S.Law@jpl.nasa.gov, +01-818-354-6208)

Abstract

NASA's Lunar Mapping and Modeling Portal (LMMP) provides a web-based Portal and a suite of interactive visualization and analysis tools to enable mission planners, lunar scientists, and engineers to access mapped lunar data products from past and current lunar missions (http://lmmp.nasa.gov). During the past year, the capabilities and data served by LMMP have been significantly expanded. New interfaces are providing improved ways to access and visualize data. At the request of NASA's Science Mission Directorate, LMMP's technology and capabilities are now being extended to additional planetary bodies. New portals for Vesta and Mars are the first of these new products to be released.

This presentation will provide an overview of LMMP, Vesta Trek, and Mars Trek, demonstrate their uses and capabilities, highlight new features, and preview coming enhancements.

1. Introduction

LMMP provides a suite of interactive tools that incorporate observations from past and current lunar missions, creating a comprehensive lunar research Web portal. The online Web portal allows anyone with access to a computer to search through and view a vast number of lunar images and other digital products. The portal provides easy-to-use tools for browsing, data layering and feature search, including detailed information on the source of each assembled data product and links to NASA's Planetary Data System. While mission planning is LMMP's primary emphasis, LMMP also addresses the lunar science community, the lunar commercial community, education and outreach, and anyone else interested in accessing or utilizing lunar data. Its visualization and analysis tools allow users to perform analysis such as lighting and local hazard assessments including slope, surface roughness and crater/boulder distribution. LMMP features a generalized suite of tools facilitating a wide range of activities including the planning, design, development, test and operations associated with lunar sortie missions; robotic (and potentially crewed) operations on the surface; planning tasks in the areas of landing site evaluation and selection; design and placement of landers and other stationary assets; design of rovers and other mobile assets; developing terrain-relative navigation (TRN) capabilities; deorbit/impact site visualization; and assessment and planning of science traverses. Significant advantages are afforded by LMMP's features facilitating collaboration among members of distributed teams. Team members can share visualizations and add new data to be shared either with the entire LMMP community or only with members of their own team. Sharing of multi-layered visualizations is made easy with the ability to create and send LMMP bookmarks. LMMP is also a powerful tool for education and outreach, as is exemplified by its mobile clients (Moon Tours for iOS and Android), serving of data to NASA's Eyes on the Solar System, and serving of data to a growing community of digital planetariums.

At the request of NASA's Science Mission Directorate, LMMP's development team has extended the capabilities of LMMP to additional planetary bodies. Two new web-based portals, Vesta Trek and Mars Trek are the first of these new products to be released. The initial releases of these new products are intended primarily for outreach purposes. However, they contain capabilities that make them of interest to a full range of users. These products make use of a new, fuller-featured interface that will become the standard across the LMMP line of web portals.

2. LMMP Enhancements

Over the past year, LMMP has been significantly enhanced with additional data products, improved data analysis tools, the integration of its touch table client in mission site selection and analysis, new interfaces to external devices including 3D printers, and improved serving of data to external clients. Many of the recent enhancements to LMMP have been specifically in response to the requirements of the proposed Resource Prospector mission, and as such, provide an excellent example of the application of LMMP to mission planning. As the EPSC community looks forward to new lunar decade of surface activities working towards a lunar robotic village with strong opportunities for science and exploration, as well as preparation for human return to the Moon, tools such as LMMP will become increasingly essential.

LMMP is currently working with the Astromaterials Office at NASA's Johnson Space Center to integrate their database of the returned Apollo lunar samples into LMMP. For a given sample, LMMP will display images and information about the sample, and allow the user to put the sample into context by providing visualizations of the location on the lunar surface from which it was retrieved.

3. Vesta Trek

On March 31, 2015, the LMMP team released Vesta Trek (http://vestatrek.jpl.nasa.gov), a web-based application applying LMMP technology to visualizations of the asteroid Vesta. Data gathered from multiple instruments aboard Dawn have been compiled into Vesta Trek's user-friendly set of tools, enabling users to study the asteroid's features. The application includes:

— Interactive maps, including the ability to overlay a growing range of data sets including topography, mineralogy, abundance of elements and geology, as well as analysis tools for measuring the diameters, heights and depths of surface features and more.

— 3-D printer-exportable topography so users can print physical models of Vesta's surface.

— Standard keyboard gaming controls to maneuver a first-person visualization of "flying" across the surface of the asteroid.

4. Mars Trek

With an initial release in June, 2015, Mars Trek replicates the functionality of Vesta Trek for the surface of Mars. While the entire surface of Mars is covered, higher levels of resolution and greater numbers of data products are provided for special areas of interest. Early releases focus on past, current, and future robotic sites of operation. Future releases will focus on potential human exploration areas of interest as they are identified.

5. Summary and Conclusions

NASA's Lunar Mapping and Modeling Portal has grown considerably from its origins as a mission planning tool for the Constellation Program. Its new features make it especially useful for the planning of a new generation of lunar exploration missions, conducting a wide range of lunar science research, and facilitating exciting visualizations and exploration in the realms of education and outreach. LMMP is currently being used in lunar mission site selection and analysis activities. Two new web-based applications, Vesta Trek and Mars Trek, extend the capabilities of LMMP to new destination worlds. Other destinations will follow soon. The user community is invited to provide suggestions and requests as the development team continues to expand the capabilities of LMMP, its related products, and the range of data and tools that they provide.

Acknowledgements

The authors would like to thank the Advanced Explorations Systems Program of NASA's Human Exploration Operations Directorate and the Planetary Science Division of NASA's Science Mission Directorate for their support and guidance in the continuing development of LMMP.

EPSC Abstracts
Vol. 10, EPSC2015-446, 2015
European Planetary Science Congress 2015

Mapping the crust/mantle boundary with the Moon Mineralogy Mapper instrument data

M. Martinot (1), S. Besse (2), J. Flahaut (1), J.-F. Blanchette-Guertin (3), P. Isaacson (4) and W. van Westrenen (1)
(1) Faculty of Earth and Life Science, VU University Amsterdam, The Netherlands (m.martinot@vu.nl)
(2) ESA/ESTEC, 2201 AZ Noordwijk, The Netherlands
(3) IPGP, 75013 Paris, France
(4) Hawaii Institute of Geophysics and Planetology, University of Hawaii, Manoa, Honolulu, HI, 96822

1. Introduction

Determining the composition and structure of the lunar crust is crucial to study its origin and evolution [5]. Several space missions were sent to the Moon in order to study its gravity field, which can be used to derive information about its crustal thickness [9]. Results from the Clementine mission (1990s) suggested a lunar crustal thickness varying between 20 and 120 km [6], and enabled studies of the mineralogy of the lunar crust [8]. From September 2011 to December 2012, the Gravity Recovery and Interior Laboratory (GRAIL) mission acquired more precise gravimetric data from the Moon. GRAIL data suggest a significantly smaller average lunar crustal thickness between 34 and 43 km depending on the model considered [9]. This survey aims to study the crust/mantle boundary region, and evaluate the lunar crustal thickness using impact craters as natural drill holes. To this end, the proximity to the mantle was calculated for all craters in the lunar crater database, using the method described in [4]. Craters that fall within a specific proximity range, diagnostic of the crust/mantle boundary region, and with preserved central peaks are selected for further investigations. The mineralogy of the selected craters central peaks is derived from the Moon Mineralogy Mapper (M^3) data [7] to evaluate the presence or absence of mantle material. One ultimate goal is to place constraints on the crust/mantle boundary depth and mineralogy, and assess which GRAIL model(s) best describe the Moon crust.

2. Approach

2.1 Proximity value

New crustal models were derived from the gravity measurement of the recent GRAIL mission to the Moon [9]. A set of 4 models is available making variable assumptions (crustal porosity, crustal thickness, mantle density, ...). For each model, pre-impact crustal thicknesses (calculated as in [4]) were compared to the estimated depth of origin of the central peak material. The proximity to the mantle is defined as the difference between the pre-impact crustal thickness, and the depth of origin of the material [1, 4]. In this study, the maximum depth of melting is assumed to be equal to the minimum depth of origin of the central peak material, as suggested by [3]. If the proximity has a negative value, the impact potentially exposed material from below the crust/mantle boundary in the central peak of the resulting crater. On the contrary, if the proximity value is positive, the mantle material should not have been excavated by the impact [4]. Therefore, the proximity value gives the original distance between the material of the central peak and the crust/mantle boundary, before the original layer was disturbed and uplifted by the impact.

2.2 Data

In order to map the crust/mantle boundary depth, a subset of craters with proximity values ranging between – 10 and + 10 km on the various GRAIL models was selected. For each crater, a combination of Lunar Orbiter Laser Altimeter (LOLA) and Lunar Reconnaissance Orbiter Camera (LROC) observations were used to verify the presence of a preserved central peak. The composition of the central peaks of these craters is being investigated with M^3 data.
M^3 is a hyperspectral imager onboard Chandrayaan-1 which acquired visible and near infrared (VNIR) reflectance data in 85 spectral channels spanning from 430 to 3000 nm. M^3 data are available over most craters of our selection with a spatial resolution of 140 or 280 m/pixel. The data used in this study are the Level 2 delivery from the Planetary Data System (PDS).

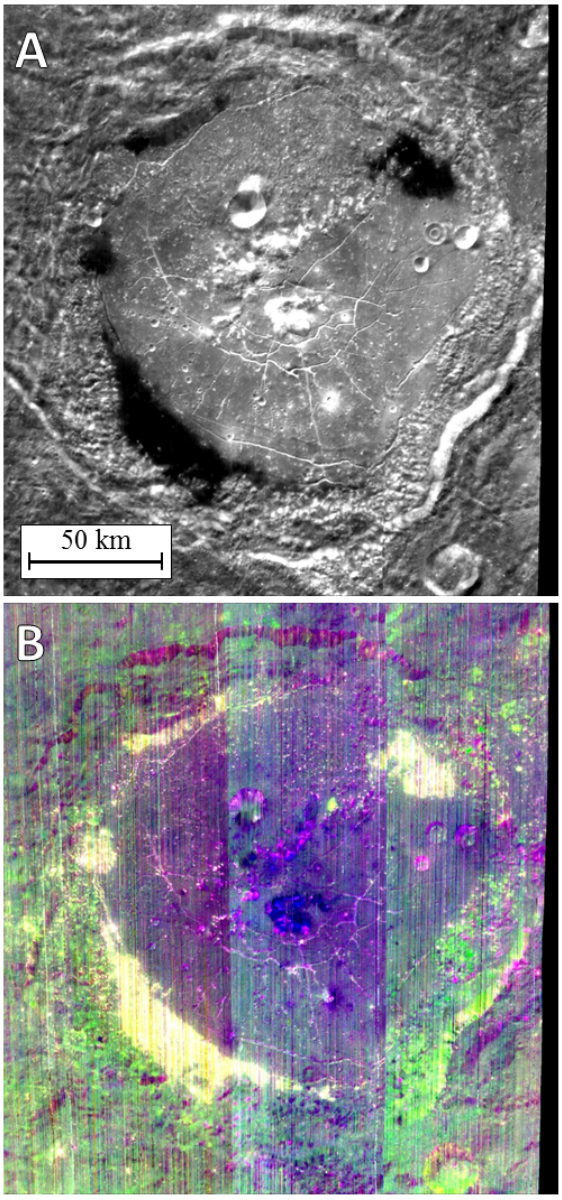

Figure 1: Humboldt crater M^3 mosaic. **A**: 1508 nm band; **B**: RGB colour composite of spectral parameters: R = integrated 1000 nm band depth, G = integrated 2000 nm band depth, B = 1250 nm band depth.

3. Preliminary Results

Figure 1 shows a M^3 frame (**A**) and a colour composite mosaic (**B**) of Humboldt crater. The selected colour composite displays parameters that should highlight olivine-rich outcrops in red, and plagioclase-rich outcrops in blue. Figure 1 shows a blue-coloured central peak, where the detection of plagioclase is confirmed by a diagnostic 1250 nm absorption band on the associated spectra [2]. Olivine has not been detected in Humboldt crater; therefore, mantle rocks have not yet been identified in this crater. Humboldt crater proximity value is slightly negative with GRAIL model 1 (M1) and 2 (M2), but within the error bar, and positive with GRAIL model 3 (M3) and 4 (M4). Therefore, it seems likely that the Humboldt impact did not reach the crust/mantle boundary.

Further work will extend the study with a larger amount of craters, and could first focus on craters in the vicinity that display lower proximity values than Humboldt crater.

References

[1] Cahill, J.T.S., Lucey, P.G., and Wieczorek, M. A.: Compositional variations of the lunar crust: Results from radiative transfer modeling of central peak spectra, J. Geophys. Res. E Planets. 114 (2009) 1–17.

[2] Cheek, L.C., Donaldson Hanna, K.L., Pieters, C.M., Head, J.W., Whitten, J.L.: The distribution and purity of anorthosite across the Orientale basin: New perspectives from Moon Mineralogy Mapper data, J. Geophys. Res. Planets. 118 (2013) 1805–1820.

[3] Cintala, M.J. and Grieve, R. A. F.: Scaling impact melting and crater dimensions: Implications for the lunar cratering record, Meteorit. Planet. Sci. 33 (1998) 889–912.

[4] Flahaut, J., Blanchette-Guertin, J.F., Jilly, C., Sharma, P., Souchon, A., Van Westrenen, W., Kring, D.A.: Identification and characterization of science-rich landing sites for lunar lander missions using integrated remote sensing observations, Adv. Sp. Res. 50 (2012) 1647–1665.

[5] Jaumann, R. and 20 co-authors: Geology, geochemistry, and geophysics of the Moon: Status of current understanding, Planet. Space Sci. 74 (2012) 15–41.

[6] Neumann,G. A., Zuber, M.T., Smith, D.E., Lemoine, F.G.: The Lunar Crust: Global Structure and Signature of Major Basins, 101 (1996).

[7] Pieters, C.M. and 19 co-authors: The Moon Mineralogy Mapper (M^3) on Chandrayaan-1, Current. 96 (2009) 1–6.

[8] Tompkins, S. and Pieters, C.M.: Mineralogy of the Lunar Crust - Results From Clementine, Meteorit. Planet. Sci. 34 (1999) 25–41.

[9] Wieczorek, M.A. and 15 co-authors: The crust of the Moon as seen by GRAIL., Science. 339 (2013) 671–5.

EPSC Abstracts
Vol. 10, EPSC2015-468, 2015
European Planetary Science Congress 2015

A Web-GIS for the Kaguya/Spectral Profiler data, "GEKKO" (moonlight in Japanese): toward comprehensive mapping of the surface minerals on the Moon

Y. Ogawa (1), Y. Hayashi (2), N. Hirata (1), J. Terazono (1), H. Demura (1), T. Matsunaga (3), S. Yamamoto (3), Y. Yokota, M. Ohtake (4), H. Ootake (4)
(1) The University of Aizu, Aizu-Wakamatsu, Japan, (2) Space Development Atelier, Japan, (3) National Institute for Environmental Studies, Tsukuba, Japan, (4) Japan Aerospace Exploration Agency, Sagamihara, Japan.
(yoshiko@u-aizu.ac.jp / Fax: +81-242-372731)

Abstract

The "GEKKO" is a Web-GIS to exhibit the reflectance spectra of the Moon observed by the Spectral Profiler (SP) onboard Kaguya satellite. The client can access the system via a web browser and select any area of the whole Moon. The client can view, plot and download the SP data observed at the corresponding location on the referenced lunar image just by mouse-clicks. The system also provides some basic analysis functions. The operation and service of "GEKKO" started in August 2014 for the Japanese lunar science community. We now plan to cultivate the potential users internationally. We are implementing new functions and extending the system. Our final goal is comprehensive mapping of the surface minerals on the Moon.

1. Introduction

The Kaguya satellite, a Japanese lunar orbiter, observed the whole Moon during 2007-2009. The Spectral Profiler (SP) onboard Kaguya is a visible and near - infrared (VIS-NIR) spectrometer and observed the continuous reflectance spectra of the Moon [1].

The lunar minerals characteristically have their substantial absorption bands in VIS-NIR wavelengths which are fully covered by SP instrumental specifications. By using and analyzing the SP data, we can constrain the characteristic quality of the o observed absorption bands in the observed spectra and then identify the surface minerals on the Moon [e.g. 2].

The SP observation spots (footprints) distribute on the lunar surface globally. The total number of the footprints amounts to about 70 million. Each single SP spectrum consists of 296 reflectance components.

Our aim is to comprehensively understand the mineral distribution on the Moon by using the Kaguya/SP data. This study introduces the "GEKKO" which is positioned as a preliminary step for that. The GEKKO system handles all the observed SP data extensively, simply and conveniently. The system is a Web-GIS, therefore, all the client needs is an internet access via a web browser. "GEKKO" is a Japanese term meaning moonlight.

2. Data

We installed the complete data set of SP Level 2C (SP L2C) data product in the GEKKO system. SP L2C data is currently the highest level in the processing phase. SP L2C data includes the latest version of the calibrated SP spectral data [3], ancillary data and the simultaneously observed image data from Multi-band Imager or Terrain Camera both onboard Kaguya satellite. Such simultaneously observed image is indispensable for confining and finding the exact spots of SP observation.

The GEKKO prepares more than10 kinds of base maps of the Moon. The default base map is MI mosaic image [4] and the data is installed in the system as well as SPL2C data set. The other base maps supported in the GEKKO system are the shaded relief map based on the Clementine/UVVIS image [5], the topography map from LRO/LOLA, and the image mosaic from LRO/LROC-WAC which are referred to the Planetary WMS service [6].

3. How to Use this System; Equipped Functions

The client accesses the system by via a web browser and logs-in. The base map of the Moon appears. The client can choose and change the base

map among more than 10 options. The client selects any area on the preferred base map of the Moon controlling zooming-in or -out. Then the footprints of SP observation in that area are marked on the lunar base map image. The clients select a particular SP footprint and then the SP spectrum observed exactly at the corresponding spot is plotted with the graph. At the same time, the text table is shown too, which describes the ancillary data at the time of the observation. The client can register the plotted spectral graph with the observation footprints so that he/she could compare the spectrum observed on the other spots. Every step of the procedure is very simple and completed just with mouse-control.

In addition, the GEKKO supports optional functions. First are the basic analysis functions commonly used for the general spectral analysis, such as running-average and stacking procedure. Second is the continuum-removal function which is useful for detecting the absorption band feature. The system also prepares a function peculiar for the lunar VIS-NIR spectral analysis, which is to multiply coefficients to SP reflectance. By using this last function, the matching of the reflectance of SP at the Apollo 16 site with that of Lunar sample No. 62231 [7] is assured, which means that the direct comparison of SP data with other mission data is possible.

The GEKKO provides download function, too. The clients can download the SP spectral data and also the data after the analyses.

The system configuration and technical details are described in [8].

5. Service Plan

We started the service and operation of GEKKO in August 2014 first for the Japanese lunar science community. We ask the clients to accept the general agreements and keep a single account for one client.

We now plan to extend the service to international use. We are preparing English descriptions and plan to release it this fall. We would like to cultivate the potential users.

6. Summary and Future Works

The “GEKKO” is a Web-GIS to view and analyze the SP data. The client accesses the system via a web browser, and can view and download the SP spectra in very simple steps.

We plan to apply Modified Gaussian Model analysis (MGM) [9] extensively to SP data and archive all the output data in the GEKKO system. The deconvolutioned parameters resulting from MGM-analysis describe the absorption features of the observed spectra which directly link to the uniqueness of the each mineral. We also plan to extend the GEKKO system by implementing a new framework where the client would be able to perform the spectral analysis dynamically, not in a predetermined manner [10].

Acknowledgements

We thank the SELENE (KAGUYA) SP team and the SELENE Data Archive for providing the SELENE (KAGUYA) data. SELENE is a Japanese mission developed and operated by JAXA.

References

[1] Matsunaga, T. et al.: Discoveries on the lithology of lunar crater central peaks by SELENE Spectral Profiler, Geophys. Res. Lett., 35, doi:10.1029/2008GL035868, 2008.

[2] Ogawa, Y. et al.: The widespread occurrence of high-calcium pyroxene in bright-ray craters on the Moon and implications for lunar crust composition, Geophys. Res. Lett., 38, doi:10.1029/2011GL048569, 2011.

[3] Yamamoto, S. et al.: Calibration of NIR 2 of Spectral Profiler onboard Kaguya/SELENE, IEEE Trans. Geosci. Remote Sens., 52, 6882-6898, doi:10.1109/TGRS.2014. 2304581, 2014.

[4] Ohtake, M. et al.: The global distribution of pure anorthosite on the Moon, Nature, 461, 236–240, doi:10.1038/nature08317, 2009.

[5] USGS, Planetary GIS Web Server. http://webgis.wr.usgs.gov/pigwad/down/moon_airbrushed_shadedrelief_warp . htm (accessed on April 30, 2015).

[6] USGS, Astrogeology WMS Map Layers. http://astrowebmaps.wr.usgs.gov/webmapatlas/Layers/maps.html (accessed on April 30, 2015).

[7] Tompkins, S. and Pieters, C. M.: Mineralogy of the lunar crust: Results from Clementine, Meteorit. Planet. Sci., 34, 25–41, 1999.

[8] Hayashi, Y. et al.: Web GIS system "Gekko" for data analysis of Kaguya's Spectral Profiler, Journal of Space Science Informatics Japan, 4, 91-103, 2015.

[9] Sunshine, J. M., Pieters, C. M. and Pratt, S. F.: Deconvolution of mineral absorption bands: an improved approach, J. Geophys. Res., 95, 6955–6966, doi:10.1029/JB095iB05p06955, 1990.

[10] Sugimoto, K. et al., Development of a web application for dynamic analysis of the Kaguya Spectral Profiler data, Japan Geosci. Union Meeting, 28April–2May, Yokohama, Japan, 2014.

EPSC Abstracts
Vol. 10, EPSC2015-531, 2015
European Planetary Science Congress 2015

Thicknesses of Mare Basalts from Gravity and Topograhy

S. Gong (1,2,3), M. A. Wieczorek (2), F. Nimmo (4), W. S. Kiefer (5), J. W. Head (6), D. E. Smith (7) and M. T. Zuber (7)
(1) Key Laboratory of Planetary Sciences, Shanghai Astronomical Observatory, Chinese Academy of Sciences, Shanghai 200030, China, (2) Insitut de Physique du Globe de Paris, Sorbonne Paris Cité, Université Paris Diderot, 75013 Paris, France, (3)University of Chinese Academy of Sciences, Beijing 100049, China, (4) Department of Earth and Planetary Sciences, University of California Santa Cruz, Santa Cruz, CA 95064, USA, (5) Lunar and Planetary Institute, Houston, TX 77058, USA, (6) Department of Earth, Environmental and Planetary Sciences, Brown University, Providence, RI 02912, USA, (7) Department of Earth, Atmospheric, and Planetary Sciences, Massachusetts Institute of Technology, Cambridge, MA 02139, USA. (sxgong@shao.ac.cn)

1. Introduction

Mare basalts are derived from partial melting of the lunar interior and are mostly located on the near side of the Moon [1, 2]. Their iron-rich composition gives rise to their dark color, but also causes their density to be substantially higher than normal crustal rocks.

The total volume of mare basalts can provide crucial information about the Moon's thermal evolution and volcanic activity. Unfortunately, the thicknesses of the mare are only poorly constrained. Here we use gravity data from NASA's GRAIL mission to investigate the thickness of mare basalts.

2. Method

Besserer et al. [3] have developed a method for constraining the depth dependence of density below the surface by use of an "effective density" spectrum, which relates the free-air gravity and the gravity predicted from unit-density topography:

$$g_{lm} = \rho_{eff}(l) b_{lm} + \nu_{lm}$$

Here g and b refer to the observed (free-air) gravity and Bouguer correction of unit density topography [4], respectively, and ν is the noise which is assumed to be uncorrelated with topography. From this equation an unbiassed estimate of the effective density spectra can be calculated as,

$$\rho_{eff}(l) = \frac{S_{gb}(l)}{S_{bb}(l)}$$

Localized estimates of the effective density spectrum, obtained from a multitaper spectral analysis [5], are then compared to an analytical model that depends on the subsurface density model.

2.1 Subsurface density model

We construct a theoretical subsurface density model which contains a constant density mare basalt layer of thickness t_b, and an underlying highland crust whose density increases with depth. For the basalt density, we use the pore-free grain density predicted from remote sensing data [6] with a porosity of 12%, while for the density gradient in the underlying highlands crust we use the average value from the work of Besserer [3]. The basalt thickness t_b, density and the uppermost density of the highlands crust ρ_o are free parameters.

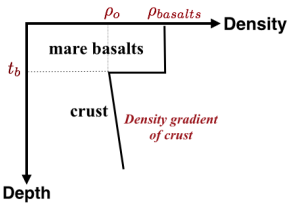

Figure 1: Theoretical density model that contains a constant density mare basalt layer overlying the highlands crust.

2.2 Localized multitaper spectral analysis

When calculating the localized effective density spectrum, we used 30 orthogonal windows localized to a spherical cap with an angular radius of 15 degrees and a spectral bandwidth of $L_w = 58$. These are the same windows used by Besserer et al. [3], and only the spherical harmonic degree range of 250-550, was considerer in order to neglect the effects of lithospheric flexure and lateral variations in crustal thickness. Example effective density spectra in Fig. 3 show that this function is sensitive to both the mare thickness and

density of the upper crust.

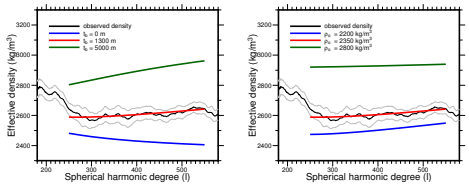

Figure 2: Theoretical effective density spectra for various basalt thicknesses (left) and various upper crustal densities beneath the basalts (right). In the first case, the upper crustal density and density gradient were set to 2340 kg m^{-3} and 21 kg m^{-3} km^{-1}, respectively, and in the second case the mare basalt thickness was set to 1300 m. The example spectra corresponds to 26^{o}N 129^{o}W. Gray lines denote the 1-σ uncertainty from the multitaper spectrum analysis.

3. Results

As the presence of highland materials with the localization windows would bias the calculated effective densities, only those locations where 75% of the window is covered by mare basalts are shown in our results.

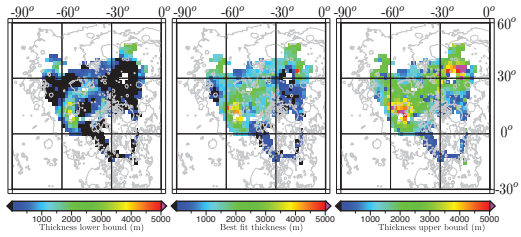

Figure 3: 1-σ lower bound (left), best fit (middle) and 1-σ upper bound (right) of the mare basalt thickness. The lower and upper bounds are determined by use of the possible distribution of reduced χ^2 from 1000 Monte carlo simulations.

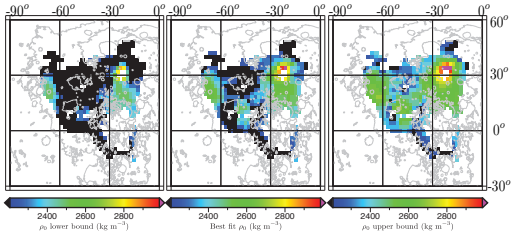

Figure 4: 1-σ lower bound (left), best fit (middle) and 1-σ upper bound (right) of uppermost highlands crustal density.

4. Summary and Conclusions

Our results show that mare basalts are thickest near Marius Hills, which is a prominent, long-lived volcanic complext in Oceanus Procellarum. In general, our basalt thicknesses are somewhat larger than those obtained using the techniques of flooded craters, the composition of impact crater ejecta, and radar sounding. [7, 8, 9]

Acknowledgements

This work is supported by a CSC (China Scholarship Council) doctoral fellowship.

References

[1] Wieczorek, M. A. and Phillips, R.: The "Procellarum KREEP Terrane": Implications for mare volcanism and lunar evolution, J. Geophys. Res., Vol. 105(E8), pp. 20417-20430, 2000.

[2] Head, J.: Lunar Volcanism in Space and Time, Rev. Geophys. Space Phys., Vol. 14, pp. 265-300, 1976.

[3] Besserer, J., et al.: GRAIL gravity constraints on the vertical and lateral density structure of the lunar crust, Geophys. Res. Lett., Vol. 41, pp. 5771–5777, 2014.

[4] Wieczorek, M. A., et al.: The crust of the Moon as seen by GRAIL, Science, Vol. 339.6120, pp. 671-675, 2013

[5] Wieczorek, M. A. and Simons, F. J.: Minimum-variance multitaper spectral estimation on the sphere, J. of Fourier Anal. Appl., Vol. 13.6, pp. 665-692, 2007

[6] Huang, Q., and Wieczorek, M. A.: Density and porosity of the lunar crust from gravity and topography, J. Geophys. Res., Vol. 117, pp. E5003, 2012.

[7] De Hon, R. A.: Thickness of the western mare basalt, Proc. Lunar Sci. Conf., pp. 274-276, 1979.

[8] Thomson, B. J., et al.: A new technique for estimating the thickness of mare basalts in imbrium basin, Geophys. Res. Lett., Vol. 36, pp. L12201, 2009

[9] Cooper, B. L. et al.: New evidence for graben origin of Oceanus Procellarum from lunar sounder optical imagery, J. Geophys. Res., Vol. 99, pp. 3977-3812.

EPSC Abstracts
Vol. 10, EPSC2015-532, 2015
European Planetary Science Congress 2015

Lunar rovers and archive panoramas: Past for the Future

N. **Kozlova** (1), A. Zubarev (1), A. Solodovnikova (1), Yu. Rybakin (1), A. Garov (1), A. Abdrakhimov (1,2), I. Karachevtseva (1)
(1) Moscow State University of Geodesy and Cartography (MIIGAiK), MIIGAiK Exraterrestrial Laboratory (MExLab), Moscow, Russia (natally.ko@gmail.com); (2) Vernadsky Institute of Geochemistry and Analytical Chemistry of Russian Academy of Sciences, Moscow, Russia

Abstract

At MIIGAiK Exraterrestrial Laboratory (MExLab) we have carried out modern processing of lunar panoramic images obtained by Soviet Lunar missions (1966-1973) in the frame of PRoViDE project (www.provide-space.eu/). We have found and collected old schemes, maps, images, documentation and used these data at the beginning of the study. Then we gathered and processed data collected by recent and ongoing missions. These data helped to refine the Lunokhod route, prepare different detailed and thematic maps of the landing sites, and carry out GIS-analysis of the routes and areas.

1. Study of Lunokhod archive data

We have obtained from Russian State Archive lunar panoramic images collected during five Soviet Lunar missions Luna-9,-13,-17,-20,-21 (1966-1973). A special technique has been developed to assemble and process the archive image fragments and prepare them for further scientific use [1]. Based on this technique all Lunokhod-2 panoramas have been processed as well as several Lunokhod-1 panoramas on regions of interest (ROI). Also supplementary information was found or recovered (recalculated) to create metadata for the panoramas.

2. Study of modern data for the Lunokhod areas

Modern LRO data made it possible to study Lunokhod routes and landing sites in more details. So, by means of stereo photogrammetric processing of LRO NAC images we have created high-resolution DEMs and orthoimages with best visibility of rover tracks. Based on these data we have digitized Lunokhod-1,2 routes and verified the covered distances, studied craters along the route, etc. [2]. We also have developed software for artificial modeling of lunar surface images based on orthomosaic and DEM [1].

3. Results

Combination with LRO orbital data helped to determine coordinates of observation points for the Lunokhod archive panoramas. The developed technique for lunar surface image processing helped to perform comprehensive morphologic analyses of the panoramic images and create a descriptive catalog including size and structure of various types of objects (craters, blocks, boulders). All the obtained data were unified and uploaded into Lunar Database, which is available via MExLab Geoportal (http://cartsrv.mexlab.ru/geoportal/). To sum up, main results of the study are the following:

- catalogue of lunar panoramic images collected by 5 Soviet spacecraft (Luna-9, -13, -17, -20, -21), which includes more than 300 assembled panoramas with new or updated archive metadata;
- detailed morphologic description of all panoramas obtained by Lunokhod-2;
- set of fully-processed panoramas on ROI (such as landing sites; areas of old Lunokhod-1topographic plans, published soon after Luna-17 mission; Lunokhod-2 panoramas obtained near the groove Fossa Recta, etc.);
- set of processed orbital data (DEMs, orthoimages, for Lunokhod's landing sites;
- morphologic and geologic assessment of the Lunokhods landing sites [3];
- basic and thematic maps of the landing sites;
- set of layers which include supplementary data (Lunokhod traverses, panoramas points, stops where Lunokhods slept over the lunar nights, etc.);
- techniques and software: for lunar surface image processing and for artificial lunar surface image modeling;
- Lunar database with web-access.

4. Summary and Conclusions

The project helped to bring together old archive and modern Lunar data. Developed techniques can be useful for preparation of future Lunar lander and rover missions, e.g. Luna-Glob and Luna-Resource.

Acknowledgements

The research leading to these results has partly received funding from the European Community's Seventh Framework Programme (FP7/2007-2013) under grant agreement № 312377 PRoViDE.

Studies of the suitability of images obtained by planetary rovers for coordinate and navigation support of rover missions (Kozlova N.A.) are supported by a grant from Russian Foundation for Basic Research (RFBR) #15-35-50509.

References

[1] Kozlova N., Zubarev A., Karachevtseva I., et al. Some aspects of modern photogrammetric image processing of Soviet Lunokhod panoramas and their implementation for new studies of lunar surface. ISPRS TC IV Symposium China (Suzhou) 14-16 May, 2014.

[2] Karachevtseva I., Oberst J., Scholten F., et al. Cartography of the Lunokhod-1 Landing Site and Traverse from LRO Image and Stereo Topographic Data // Planetary and Space Science, Vol.85, p. 175-187, 2013, http://dx.doi.org/10.1016/j.pss.2013.06.002.

[3] Abdrakhimov A., Basilevsky A., Karachevtseva I. Geological review of Lunokhod-1 area // 4M-S3, IKI RAS, Moscow, Russia, 14-18 October 2013.

EPSC Abstracts
Vol. 10, EPSC2015-550, 2015
European Planetary Science Congress 2015

MINERALOGICAL AND MORPHOLOGICAL ANALYSIS OF LUNAR FLOOR-FRACTURED CRATER ATLAS USING HIGH-RESOLUTION REMOTE SENSING DATA.

Sumit Pathak, Aurobindo Kumar Basantaray, Mamta Chauhan, Satadru Bhattacharya and Prakash Chauhan
Planetary Sciences Division, Biology, Planetary Sciences and Applications Group, Space Applications Centre, ISRO, Ahmedabad-380015 (INDIA). (geologymamta@gmail.com, satadru@sac.isro.gov.in)

Abstract

Crater Atlas is a floor-fractured crater characterized by mineral diversity associated with impact cratering and modified by later magmatic activity in the form of lava flows and pyroclasts. Here, we report occurrence of mafic lithology in form of spinel troctolites and norites detected from the central peak and rim of the crater Atlas. Localized concentration of dark deposits of pyroclastic origin is present towards the inner rim in the N and S part of the crater that are characteristically showing high-Ti content (~14 wt %).

1. Introduction

Crater Atlas (46.7°N, 44.4°E) is a ~100-km diameter crater present near to the southern edge of Mare Frigoris towards its east. It is a floor-fractured crater with a few small and highly degraded peaks arranged in semicircular pattern and a visible fracture systems exposed over its floor. Its age is upper Imbrian [1] with lava flows belonging to later period. It is characterized by basalt filled flat-floor with two prominent low-albedo pyroclast deposits localized at the terminal edges of the most prominent linear rille slightly offset from the centre that cross the crater in N-S direction (Fig.1). Present study is the mineralogical and morphological analysis of the crater Atlas through high-resolution remote sensing data.

2. Datasets and Methodology

For mineralogical analysis photometrically and thermally corrected Level-2 data products from Chandrayaan-1 Moon Mineralogy Mapper (M^3) having spectral range from ~460-3000-nm [2] has been used. Minerals are identified on the basis of their individual diagnostic absorption features at specific wavelengths [3]. For morphological analysis high-resolution data (~1.7m/px) from Lunar Reconnaissance Orbiter–Narrow Angle Camera (LRO-NAC) and for topographical analysis LOLA data have been used [4, 5]. Empirical data of wide angle camera (WAC-EMP) from the same mission

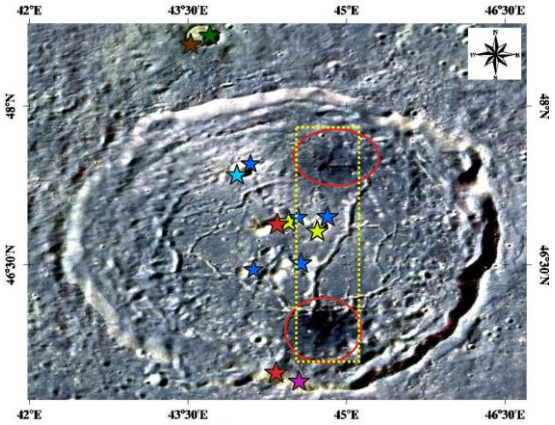

Figure 1: FCC Mosaic from M^3 datasets of Crater Atlas marked by circles and stars indicating the area of pyroclast concentration and spectra extraction location, respectively.

(LRO) with 7 bands (321 to 689 nm) have been used to study the TiO_2 concentration in the study area as the spectral slope from UV to visible wavelengths is known to be affected by variation in Illmenite concentration [6]. The TiO_2 concentration (wt%) was estimated from bands (321 and 415 nm) using the relation [7]. We have also used LRO Mini-RF datasets of S-band Radar at resolution of 29.6 m/deg. to understand the physical characteristics of pyroclasts [8].

3. Results

To record the mineral diversity occurring if any within and around the crater, a false colour composite (FCC) of M^3 mosaic of the area has been generated using bands 930-nm (Red), 1249-nm (Green) and 2137-nm (Blue). In this image (Fig.1) few patches of mafic exposures in the shades of yellow and brown (marked by red star) could be seen over the central peak area. Their representative spectra (red coloured, Fig.2) indicate the presence of olivine, plagioclase and spinel noted by their respective absorption features near 1100-nm, 1250-nm and 2000-nm. In the area adjacent to the central peak green and light green patches (blue stars) represent the mineral low-Ca pyroxenes (LCP) (Fig.2) with absorption peak near 940-nm and 1800-nm for band I and II, respectively.

On the floor of crater Atlas localized concentration of dark pyroclasts (red circles) are present and are spectrally featureless (Fig. 2). A small crater (Atlas E) towards the North of Atlas is showing signatures of olivine and spinel (brown stars) as well as LCP (olive green stars) in and along its rim. The WAC derived TiO_2 concentration map (Fig. 3) for the crater is showing strong positive values (~14 wt%) within these pyroclastic regions. Excluding the area where prominent pyroclasts are concentrated, at other areas also (marked in Fig. 1 and shown in Fig. 4) their presence has been detected in radar images. Here the pyroclastic deposits are showing low backscattered as well as very low CPR (avg.=0.3) value at S band wavelength compared to surrounding areas (Fig. 4). Changes in CPR across some of the pyroclastic deposits show areas with increased rock abundance. The CPR changes may be caused by mixing of blocky crater ejecta with the pyroclast due the gradual thinning of the pyroclastic material when it moves away from the source [9]. No well developed vents could be seen in these low albedo deposits region, however a slight depression in topography could be inferred from the profile drawn using LOLA DEM. In the high-resolution image (NAC), the crater Atlas is showing highly fractured floor characterized by large to medium sized fractures.

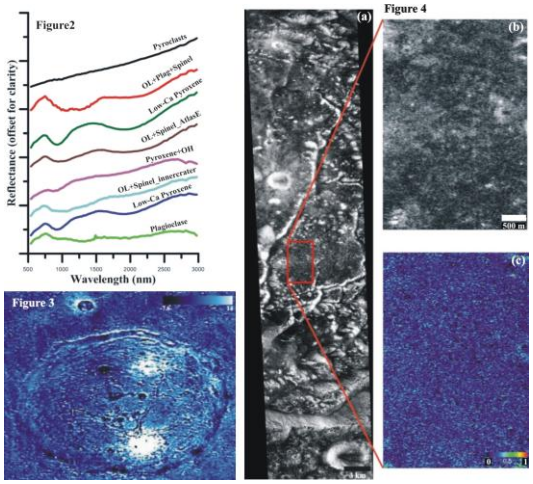

Figure 2: Representative mineral spectra extracted from the area marked by stars in Fig. 1
Figure 3: TiO_2 concentration (wt %) map for crater Atlas derived from WAC.
Figure 4: LRO-Mini RF radar backscattering image (a) of portion marked by yellow box in Fig. 1. Subset of portion (marked by red box) showing (b) backscattering and (c) CPR image.

The pyroclasts are characterized by their dark and smooth textured nature and are mantling the underlying flows/lithology (Fig. 5). The central part of the crater floor is dominated by basaltic lava flows.

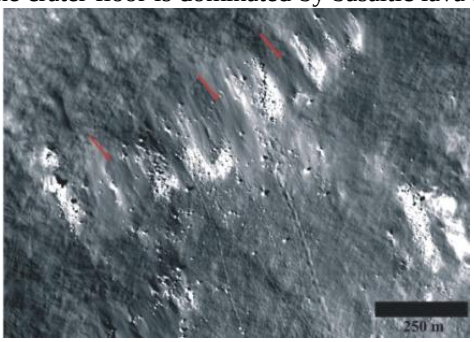

Figure 5: Subset of LROC-NAC image showing fine pyroclasts (indicated by red arrows) showing low albedo and smooth texture.

4. Discussion and Conclusions

The crater Atlas characterized by central peak complexes, lava flows, pyroclasts and fractures belongs to Class 1 type floor-fractured crater [10, 11]. The mineralogy identified through M^3 data indicates the presence of olivine, low-Ca pyroxene, spinel and plagioclase. Their association with central peak, crater rim or ejecta of small craters generally represent exposures of subsurface lithology due to cratering event. The distribution pattern of the fractures present as well as the presence of pyroclast deposits suggests that their formation occurred through magmatic intrusion. Later pyroclasts eruption probably occurred as a result of passive volatile leakage and degassing followed by localized subsidence due to the drainage of overlying material [1].

Acknowledgements

We express our sincere thanks to Tapan Mishra, Director and Dr. P. K. Pal, Deputy Director (EPSA), Space Applications Centre, ISRO for their valuable guidance and support. We are grateful to the entire team members of Chandrayaan-1 and LRO mission.

References

[1] Jozwiak et al. 2015, ICARUS 248, 424-447.
[2] Green et al. 2011, JGR, Vol. 116, E00G19.
[3] Burns 1993, Mineral App. Crystal Field Theory, CUP, 551p.
[4] Robinson et al. 2010, Space Sci. Rev., Vol. 150, 81-124.
[5] Smith et al., 2010, GRL, Vol. 37, L18204.
[6] Cloutis et al. 2008, ICARUS, Vol. 197, 321-347.
[7] Sato et al. 2015, LPSC XXXXVI, 1111.
[8] Nozette et al. 2010, Space Sci. Rev., Vol. 150, 285-302.
[9] Carter et al., 2009, JGR, Vol. 114, E11004.
[10] Schultz 1976, The Moon, Vol. 15, 241-273.
[11] Jozwiak et al. 2012, JGR, Vol. 117, E11005.

EPSC Abstracts
Vol. 10, EPSC2015-558, 2015
European Planetary Science Congress 2015

A new model of the lunar ejecta cloud: implications for *in situ* dust measurements

A. A. Christou
Armagh Observatory, Armagh, UK (aac@arm.ac.uk / Fax: +44-2837-527174)

Abstract

We apply a recent model of the cloud of ballistic impact ejecta surrounding an airless body [1] to the lunar case. For power-law-distributed ejection speeds [2, 3, 4], we identify regimes where the height and the speed distribution of ejecta are approximately power-law functions that directly depend on the exponent of the ejection law. Likewise, key features of the distribution of a particle's speed with respect to an orbiting spacecraft depend sensitively on the ejection zenith angle. Measurements at those regimes can therefore constrain the ejection physics.

Introduction

Every airless body in the solar system is surrounded by a cloud of ejecta produced by the impact of interplanetary meteoroids on its surface [5]. Such "dust exospheres" have been observed around the Galilean satellites of Jupiter [6, 7]. The prospect of long-term robotic and human operations on the Moon by the US and other countries has rekindled interest on the subject [8]. This interest has culminated with the recent investigation of the Moon's dust exosphere by NASA's *LADEE* spacecraft [9].

The most detailed models to-date [3, 4] have focused on measurements at relatively high altitudes ($\geq$ a few tenths of a satellite radius $-$ R_S). Exploiting new datasets requires models that focus on the low-altitude ($\lesssim 0.1 R_S$) regime.

Model Predictions

A new model of a ballistic, collisionless, steady state population of impact ejecta was presented in [1]. For grains launched vertically with speed v_L distributed according to the law

$$p(>\mathrm{v}_L) = (\mathrm{v}_L/\mathrm{v}_0)^{-\gamma}, \mathrm{v}_L > \mathrm{v}_0 \qquad (1)$$

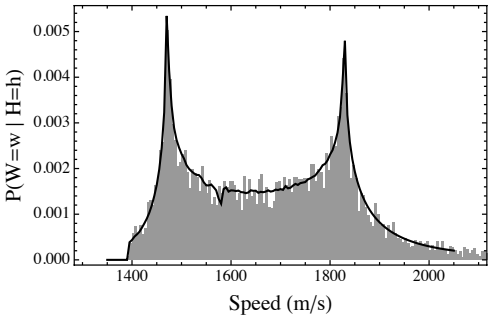

Figure 1: Probability density function of grain impact speed on a low-altitude lunar orbiter. See text for details.

where v_0 & γ are model parameters [2, 3, 4], the model furnishes closed-form expressions for the probability density functions (pdfs) of grain altitude $p(h)$ and grain speed at a given altitude $p(\mathrm{v}|h)$. The functional forms of these pdfs show that both (a) the *altitude* distribution of grains, and (b) the grain *speed* distribution near the surface, follow a power-law with an exponent that depends on γ. The result holds even if non-vertical ejection is imposed.

The model also treats the statistics of grain motion relative to a moving platform such as an orbiting spacecraft. Fig. 1 shows the pdf (bold curve) of the grain impact speed w on a platform moving horizontally at a speed and altitude typical of a low-altitude lunar orbiter: $u = 1650$ m sec^{-1} and $h = 30$ km. The ejection zenith angle z has been set to 30 degrees. The grey bars represent a snapshot of the w-statistics of 10^7 particles ejected with randomly-distributed speeds following the pdf in Eq. 1. The two-pronged shape is due to the non-vertical ejection (i.e. $z \neq 0$) with the two peaks merging into one as $z \rightarrow 0$.

Implications and Future Work

The raison d'être of any model is to interpret measurements and understand the physical processes at work. The model presented here is probabilistic (i.e. normalised to integrate to unity) therefore verifying its predictions does not require absolute measurements.

If a power-law ejection speed distribution is physically realistic, the model predicts that the steady state distribution of grain altitudes in the first instance, and that for the speeds of near-surface grains in the second, are related to each other and to the exponent of this power law. Future measurements from landers combined with data from *LADEE* would therefore form a strong observational test of Eq. 1. Moreover, accurate orbital measurements of grain speed within the ejecta cloud combined with models such as that in Fig. 1 can constrain the ejection zenith angle of grains.

Future improvements to the model will include a dependency of the ejection speed on grain size and a probabilistic distribution of ejection angles. This will increase its predictive power and allow to place additional constraints on the dust population.

Acknowledgements

Astronomical research at the Armagh Observatory is funded by the Northern Ireland Department of Culture, Arts and Leisure (DCAL).

References

[1] Christou, A.A.: Modelling circumplanetary ejecta clouds at low altitudes: A probabilistic approach, Icarus, 250, 268, 2015.

[2] Krüger, H., Krivov, A.V., Grün, E.: A dust cloud of Ganymede maintained by hypervelocity impacts of interplanetary micrometeoroids, Planetary and Space Science, 48, 1457, 2000.

[3] Krivov, A.V., Sremčevic, M., Spahn, F., Dikarev, V.V., Kholshevnikov, K.V.: Impact-generated dust clouds around planetary satellites: spherically symmetric case, Planetary and Space Science, 51, 251, 2003.

[4] Sremčevic, M., Krivov, A.V., Spahn, F.: Impact-generated dust clouds around planetary satellites: asymmetry effects, Planetary and Space Science, 51, 455, 2003.

[5] Gault, D. Shoemaker, E.M., Moore, H.J.: Spray ejected from the lunar surface by meteoroid impact, NASA TN-D 1767, 1963.

[6] Krüger, H., Krivov, A.V., Hamilton, D.P., Grün, E.: Detection of an impact-generated dust cloud around Ganymede, Nature, 399, 558, 1999.

[7] Krüger, H., Krivov, A.V., Sremčević, M., Grün, E.: Impact-generated dust clouds surrounding the Galilean moons, Icarus, 164, 170, 2003.

[8] Grün, E., Horányi, M., Sternovsky, Z.: The lunar dust environment, Planetary and Space Science, 59, 1672, 2011.

[9] Elphic, R.C., Hine, B., Delory, G.T., Salute, J.S., Noble, S., Colaprete, A., Horányi, M., Mahaffy, P., and the LADEE Science Team: The Lunar Atmosphere and Dust Environment Explorer (LADEE): Initial science results, LPSC XLV, LPI Contr. 1777, 2677, 2014.

EPSC Abstracts
Vol. 10, EPSC2015-559, 2015
European Planetary Science Congress 2015

REMOTE OBSERVATION OF LUNAR CRATER HAYN FOR MINERALOGICAL ANALYSIS USING DATASETS FROM RECENT LUNAR MISSIONS

Sumit Pathak, Ramdayal Singh, Mamta Chauhan, Satadru Bhattacharya and Prakash Chauhan.
Planetary Sciences Division, Biology, Planetary Sciences and Applications Group, Space Applications Centre, ISRO, Ahmedabad-380015 (INDIA). (geologymamta@gmail.com, satadru@sac.isro.gov.in)

Abstract

Crater Hayn situated in the Northern hemisphere of Moon is a complex crater showing diverse lithology in form of norites and troctolites. Mineralogical analysis of this crater reveals the presence of mafic minerals viz. low-ca-pyroxenes, spinel and plagioclase detected mainly from the central peak and rim of the crater. Crystalline plagioclase is also detected from the ejecta. Most of the detected spectra are showing prominent absorption feature near 2800-nm with a band strength of ~2-3% reaching upto 4% in crystalline plagioclase. Presence of localized mafic minerals in an otherwise melt dominated lithology probably indicates them to parts of underlying mafic plutonic body exposed due to cratering.

1. Introduction

Study of complex craters provides significant understanding about mineralogical and compositional diversity of the lunar subsurface. These structures given their better preserved nature on the Moon are important landform for studying crustal diversity as well as the phenomenon of cratering. Hayn (64.58°N and 83.87°E) is one such complex crater of Copernicus period [1] located on the north-western rim of the crater Belkovich towards north-eastern side of Mare Humboldtianum. This ~89 km diameter crater is having a central peak that rises ~1.2 km above the crater floor. Earlier study has reported the Mg-spinel at Hayn [2]. Present study is undertaken to study its mineralogy in order to analyze the compositional diversity occurring if any, so as to understand its subsurface lithology.

2. Datasets and Methodology

Mineralogical analysis was carried using Chandrayaan-I M^3 data having 85 bands with 20-40 nm spectral resolution spanning a spectral range from 430-nm to 3000-nm and a spatial scale of 160 m/pixel [3]. Photometrically and thermally corrected Level 2 data products are used in this study. Moreover for silicic mineralogy LRO Diviner radiometer data have been used to produce Christiansen Feature (CF) [4]. To understand geological setting of exposed mafic lithology we have used data from Lunar Reconnaissance Orbiter – Narrow Angle Camera (LRO-NAC) and Lunar Orbiter Laser Altimeter (LOLA) [5 and 6].

3. Results and Discussion

False colour composite (FCC) is generated from the mosaicked M^3 images of crater Hayn using red, green and blue channel at 930-nm 1249-nm and 2137-nm, respectively, to capture compositional variation in the area (Fig.1). Spectra were collected from various regions of the crater and analyzed for their mineralogy using diagnostic absorption properties of important lunar minerals. Their representative spectra are presented in Figure 2.

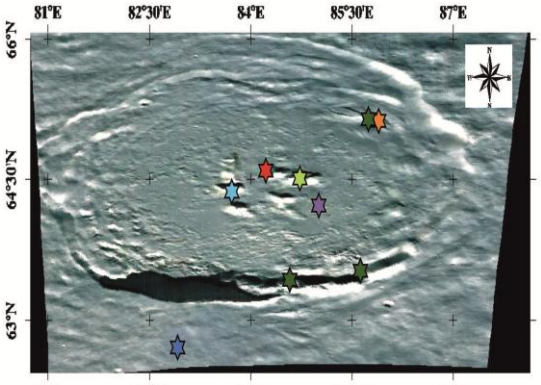

Figure 1: FCC Mosaic from M^3 strips of crater Hayn marked by coloured stars indicating the area from which their respective spectras have been taken.

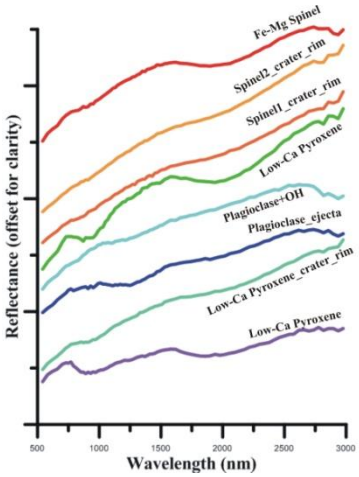

Figure 2: Representative reflectance spectra of minerals extracted from the location marked by their respective coloured stars in Fig. 1.

The locations marked by stars (Fig. 1) indicate the area where pure end-members spectras are detected, while at other places either mixed spectral signatures or melt bearing lithology indicated by more or less featureless spectra have been observed. Spinels (Mg-spinels) are detected from the lower terraced wall near north east rim characterized by their absorption feature near 2000 nm. At central peak the spinel are showing an additional minor absorption feature near 1000-nm indicating Fe-Mg spinel. Low Ca-pyroxenes (LCP) are recorded from the central peak and rim of the crater having absorption features near 940-nm and 1950-nm for Band I and II respectively. Besides, crystalline plagioclase was recorded from the ejecta present at the southern side of the crater showing prominent absorption peak near 1240-nm. This mineral is also detected from near to the crater floor. Most of the detected mineral spectra are showing hydration feature (strength ~2-3%) observed near 2800-nm. Crystalline plagioclase is showing a slight enhanced band strength of ~ 4% for the observed hydration feature. The detected minerals when observed for their geological setting within the crater seems confined to the central peak region and along the crater rim (Fig. 3).

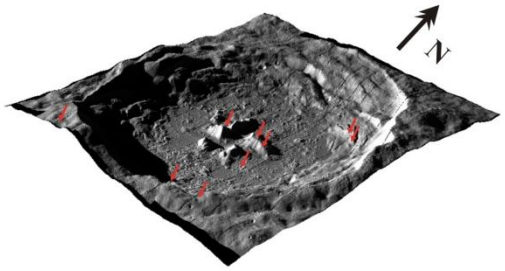

Figure 3: 3D surface view of crater Hayn generated by draping NAC mosaic over LOLA-DEM.

Compositional analysis from Diviner data also characterizes the area with mafic dominated lithology concentrated particularly along the rim and central peak of the crater (Fig. 4). The longer-wavelength CF position indicates mafic lithology. The effective emissivity calculated for a particular pixel is shown in Figure 5.

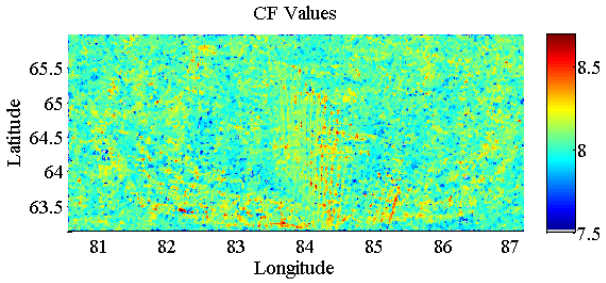

Figure 4: Variations in CF values as observed over the crater Hayn.

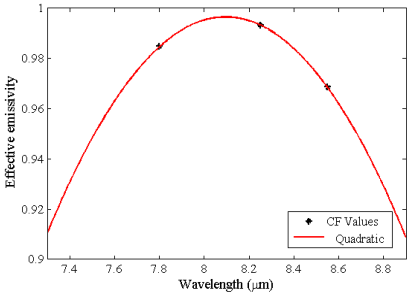

Figure 5: Variation of Diviner emissivity of Diviner channel 3, 4 and 5.

4. Conclusions

The Hayn is a complex impact crater exhibiting mineral diversity occurring in form of various mafic assemblages. Mineralogical analysis using M^3 data reveals presence of spinels, Low-Ca Pyroxenes and crystalline plagioclase indicating noritic and troctolitic affinity. Their mineralogy as well as their geological location being present at central peak and crater rim indicates that they are probably exposures of subsurface mafic body. They could represent samples of Mg-suite present in form of plutonic mafic body that lie beneath the surface that would have been excavated and emplaced by the subsequent impact process. The detection of Fe-Mg spinel indicates that this mineral is widespread on the lunar surface.

Acknowledgements

We express our thanks to Tapan Mishra, Director and Dr. P. K. Pal, Deputy Director (EPSA), Space Applications Centre, ISRO for their valuable guidance and encouragement. We are also grateful to the hard work of the entire team members of Chandrayaan-1 and LRO.

References

[1] Kreslavsky et al., 2013, LPSC, XXXXIV, 1759
[2] Sun et al. 2013, LPSC XXXXIV, 1393.
[3] Green et al. 2011, JGR, Vol 116, E00G19.
[4] Greenhagen B.T. et al. 2010, Science, 329, 1507-1509.
[5] Robinson et al. 2010, Space Sci. Rev., 150, 81-124.
[6] Smith et al., 2010, GRL, Vol. 37, L18204.

EPSC Abstracts
Vol. 10, EPSC2015-601, 2015
European Planetary Science Congress 2015

From Regolith to Shallow Structure of Chang'E-3 Landing Site

W. R. Wang (1,2), J. Q. Feng (1,2), L. L. Mu (1,2), J. J. Liu (1,2), Y. Y. Liu (1,2)
(1) National Astronomical Observatories, Chinese Academy of Sciences, China, (2) Key Laboratory of Lunar and Deep Space Exploration, National Astronomical Observatories, Chinese Academy of Sciences, China, (wangwr@nao.cas.cn)

Abstract

In this paper, a complex calculation and preliminary analysis of geological characteristics of Chang'E-3 landing site, including the regolith thickness and the shallow structure of albedo boundary lying10km away from the Lander were provided, using the detective data both from Chang'E missions and other comtemporary exploration projects.

1. Introduction

Chang'E-3 touched down on the east edge of Mare Imbrium beside a crater with a diameter of 430 m in the east part of Sinus Iridum. Coinciding with DEM and contour lines, its landing site is on the edge of a plateau in the mare, with the large-scale gradient of inclination being in the direction northeast-southwest. The landing site is located in the Eratoshenian basalt stratum and it has a low albedo, with a low density of craters. However, 10 km north of the landing site is a region of Mare Imbrium that has a high albedo and high crater density [1]. In order to get a thorough understanding of this area, we need to look from the surface to the interior structure.

2. Regolith thickness

Oberbeck and Quaide in 1967 have evaluated lunar regolith thickness from crater morphology. Based on four types of craters recognized from LO images, and lots of laboratory simulants, they got the relationship between regolith thickness and crater diameters, differing from $D_A/3.8$ to $D_A/10$, depending on crater types. With these relationships, lunar mare regolith thicknesses were estimated, varying from 1-6m to 1-16m, and mare Iridum is with an average thickness of 8.5m[2]. Besides, Shoemaker [3] and Wilcox [4] developed another method with crater frequencies. In 2005, Wilcox draw the production curve and equilibrium curve of Oceanus Procellarum craters, and got the minimum thickness of 8m[4].

Chang'E-3 landing camera obtained thousands of high-resolution images, with which the small and fresh craters can be delicately recognized. After statistics of large amount craters (Figure 1, Table 1), the morphological method drew an estimated regolith thickness (Equation 1). Also, the crater distribution frequency curve tell an equilibrium diameter of about 60m, which means the maximum regolith thickness will not exceed (60*0.2) m, and the mean value will be (60*0.14) m [4].

$$D_F/D_A = k - (D_A/t)^{-1} 2\cot\alpha \qquad (1)$$

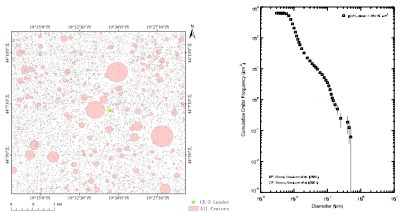

Figure 1: Crater distributions and frequency curve of landing site

Table 1: Part of fresh craters recognized from LRO_NAC and CE3_LCAM images (concentric and flat-bottomed)

Longitude	Latitude	Diameter (m)
-19.5044994	44.1133995	10.940
-19.5135994	44.1058998	10.114
-19.5179996	44.1016006	42.991
-19.5209999	44.1054001	19.398
-19.5151005	44.0905991	19.519
-19.5254002	44.1398010	39.887
-19.5743999	44.1408005	18.490
-19.5673008	44.1128006	19.517
-19.5028000	44.0840988	24.029
-19.5529003	44.0839996	29.106

3. Shallow structure of albedo boundary region

As mentioned above, an albedo boundary is located north of the landing site. It may be caused by differentiations of topography, minerals, and even the large-scale crust-mantle undulations. Figure 3 shows the DOM, DEM, free-air gravity, and mare thickness [5] of enlarged landing area, with the lines marked the albedo boundary. Figure 4 are profiles vertical to the boundaries on DEM and gravity maps.

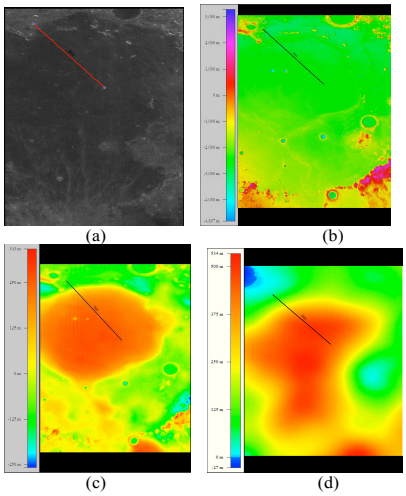

Figure 3: Boundaries in DOM (a), DEM (b), gravity (c) and mare thickness maps (d)

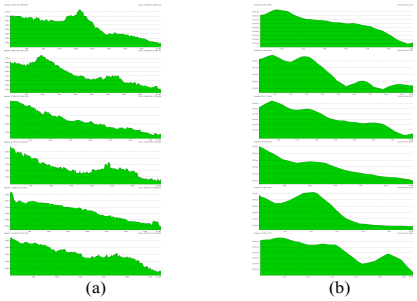

Figure 4: Profiles vertical to the boundaries on DEM (a) and free air gravity maps (b)

The topography and free air gravity show declining trend from southwest to northeast, with difference values of about 50-100m and 150mgal separately. However, we can't find such a trend in crustal thickness by Mark Wieczorek [6]. This provides a hypothesis that the boundary is caused by lunar surface non-homogeneity such as thickness differences, instead of the large-scale undulations or mascons. Referring to Wang's inversion of mare thickness of Imbrium [5], the thickness near boundary varies from about 100mgal to 500mgal. With the six profiles vertical to boundary, we record the thickness differences of two-side values (Table 2). Uunder consideration of uniform mare density, the thickness on the southwest of boundary is tens of meters larger than the northeast, which may be covered by a newer magmatic eruption.

Table 2: Mare thickness differences of six profiles vertical to the boundary

Southwest thickness (m)	Northeast thickness (m)	Thickness difference (m)
490	430	60
400	330	70
470	410	60
500	450	50
505	485	20
509	495	14

4. Summary and Conclusions

With the latest data from Chang'E and LRO missions, the landing site regolith thicknesses were estimated with morphological and crater frequency techniques. The maximum and mean regolith thickness will not exceed 12m and 8.4m. The boundary was studied with multi-source data. We conclude that the boundary was caused by different magmatic eruptions, with the southwest thicker than the northeast, which formed this geological boundary.

References

[1] C. L., Li, et al. Analysis of the geomorphology surrounding the Chang'e-3 landing site, RAA, 2014
[2] Oberbeck, et al. Estimated thickness of a fragmental surface layer of Oceanus Procellarum, JGR, 1967
[3] E. M. Shoemaker, et al., Observations of the lunar regolith and the earth from the television camera on Surveyor 7, 1969
[4] B. B. Wilcox, et al., Constraints on the depth and variability of the lunar regolith, Meteoritics & Planetary Science, 2005
[5] W.R. Wang, Topography and Mare Thickness of Chang'E-3 Landing Area, AOGS, 2014
[6] M.A.Wieczorek, et al. The crust of the Moon as seen by GRAIL, Science, 2012

EPSC Abstracts
Vol. 10, EPSC2015-639, 2015
European Planetary Science Congress 2015

New seismic events identified in the Apollo lunar data by application of a Hidden Markov Model

B. Knapmeyer-Endrun (1) and C. Hammer (2)
(1) Max Planck Institute for Solar System Research, Göttingen, Germany (endrun@mps.mpg.de), (2) Swiss Seismological Service, Zurich, Switzerland

1. Introduction

The Apollo astronauts installed seismic stations on the Moon during Apollo missions 11, 12, 14, 15 and 16. The stations consisted of a three-component long-period seismometer (eigenperiod 15 s) and a vertical short-period sensor (eigenperiod 1 s). Until today, the Apollo seismic network provides the only confirmed recordings of seismic events from any extraterrestrial. The recorded event waveforms differ significantly from what had been expected based on Earth data, mainly by their long duration body wave codas caused by strong near-surface scattering and weak attenuation due to lack of fluids. The main lunar event types are deep moonquakes, impacts, and the rare shallow moonquakes.

Digital data from the Apollo stations posed a huge challenge to the available processing equipment when they first arrived on Earth, and event detection and arrival time reading was orginally done by visual inspection of data at a reduced temporal resolution. Automatic detection schemes were considered too unreliable or time-consuming at that time. Later re-analysis mainly focussed on deep moonquakes, since they are the most abundant events and occur in spatial clusters of high waveform similarity which allows the use of cross-correlation techniques [6, 2].

These techniques might actually not be ideal for the general use in planetary seismology, though, as they require an extensive set of waveform templates, work best for networks, and might encounter problems if waveform similarity between different events is low. In planetary seismology, waveforms and event types are a priori unknown, missions likely consist of a single seismic station that needs to cover a whole planet, and events might be sparse, but detection and classification should start as soon as possible after deployment. Besides, like for NASA's 2016 InSight mission to Mars, continuous seismic data might only be available at a reduced rate, with higher rate data only available by request for a very limited time after the original downlink [1]. Under these circumstances, a recently introduced event detector and classifier based on Hidden Markov Models that works on continuous single-station data with minimum prior information could be an alternative [4, 3]. We test this algorithm on the data of Apollo station 16. Previously, it had only been applied to broad-band, regional terrestrial data, with events of about one minute duration at high sampling rates and recording dynamics. In all of these aspects, the Apollo data are significantly different.

2. Results

We applied the classifier to both long-period and short-period data streams from April, 1972 to June, 1975. In total, 80% of all events of sufficient quality listed in the Long Period Event Catalog (LPEC) [5] are found, and 70% classified correctly. The false alarm rate is about 20%, mainly determined by deep moonquakes that make up the majority of the data set: For impacts, the false alarm rate is only 6%, and for shallow moonquakes, zero. These results are based on just a single prototype event per event class, which is used to learn the characteristic features of this class. We found that the choice of the prototype deep moonquake, which belongs to cluster A20, does not lead to a preferential detection of events from this cluster. Rather, events from other clusters, notable one located on the farside, are detected with an equal reliability.

Previously unclassified events have the lowest detection rate (58%), which is not surprising: If visual comparison had shown their waveforms to be very similar to any of the known event types, they would have been classified accordingly. Still, we are able to newly classify 35 of these events as deep moonquakes, and 15 as impacts. Events which are detected on both short-period and long-period data streams are also classified consistently.

Besides, we find more than 200 new events not listed in the LPEC. 150 of these events are deep moonquakes, and more than half of them belong to clus-

ters newly identified within these data. Fig. 1 shows the largest of these new clusters, containing 8 events. The newly identified deep moonquakes also show the known temporal pattern in their occurence, related to tidal stresses in the Sun-Earth-Moon system. Newly detected deep moonquakes preferential occur in the later part of the data set, 400 days and more after the installation of station Apollo 16. This observation correlates with a drop in the overall number of deep moonquakes listed in the LPEC by a factor of 4 between the first 100 days after the installation of station 16 to a year or more later. The occurence of newly detected impacts, which are mainly small, close events detected on the short-period component, correlate with known meteorite showers as found by [7].

No unambiguous detections of new shallow moonquakes were made. We tested the ability of the classifier to identify shallow moonquakes as a new, unknown event class if they were not included in the training, assuming that rare events might be unknown at the beginning of a recording period. Identification appears possible based on low values for both noise and event probabilities on the short-period channel, similar to the example in [4].

3. Figures

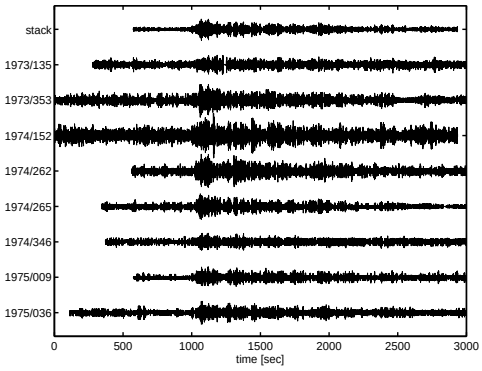

Figure 1: LPY components of a cluster of newly discovered deep moonquakes.

4. Summary and Conclusions

We used a Hidden Markov Model based event detector and classifier on the seismic data of Apollo station 16. It is sufficient to provide a single example waveform of each common event type (deep moonquake, impact, shallow moonquake) for the detector to work, which is a huge advantage over cross-correlation algorithms. The algorithm has proven to work satisfactory and reliably for this rather complex data set, surprisingly also leading to new discoveries in an already well-worked catalog almost 40 years after the end of seismic data transmission from the Moon. It could thus potentially also be useful for future seismometer missions to other planets.

Acknowledgements

We would like to thank Yosio Nakamura and Renee C. Weber for sharing their extensive knowledge about and experience with the Apollo lunar seismic data. Renee C. Weber also kindly provided her waveform stacks for deep moonquake clusters.

References

[1] Banerdt, W. B. et al.: Insight: A Discovery mission to explore the interior of Mars, Proc. 44th Lunar Planet. Sci. Conf., 18–22 March 2013, The Woodlands, Texas, 2013.

[2] Bulow, R. C., C. L. Johnson, and P. M. Shearer: New events discovered in the Apollo lunar seismic data, J. Geophys. Res., Vol. 110, E1003, doi:10.1029/2005JE002414, 2005.

[3] Hammer, C., M. Beyreuther, and M. Ohrnberger, A seismic-event spotting system for volcano fast-response systems, Bull. Seism. Soc. Am., Vol. 102, pp. 948-960, doi:10.1785/0120110167, 2012.

[4] Hammer, C., M. Ohrnberger, and D. Fäh: Classifying seismic waveforms from scratch: a case study in the alpine environment, Geophys. J. Int., Vol. 192, pp. 425-439, doi:10.1093/gji/ggs036, 2013.

[5] Nakamura, Y.: Catalog of lunar seismic data from Apollo passive seismic experiment on 8-mm video cassette (Exabyte) tapes, UTIG Tech. Rep. No. 118, Institute for Geophysics, The University of Texas at Austin, 1992.

[6] Nakamura, Y.: New identification of deep moonquakes in the Apollo lunar seismic data, Physics Earth Planet. Int., Vol. 139, pp. 197-205, doi:10.1016/j.pepi.2003.07.017, 2003.

[7] Oberst, J., and Y. Nakamura: A search for clustering among the meteroid impacts detected by the Apollo lunar seismic network, Icarus, Vol. 91, pp. 315-325, 1991.

EPSC Abstracts
Vol. 10, EPSC2015-675, 2015
European Planetary Science Congress 2015

Morphometric analysis of Linné crater and relations with numerical modelling

V. Vivaldi (1,2), E. Martellato (1), M. Massironi (1,2), A. Ninfo (2), G. Cremonese (1)
(1) INAF-OAPD, Padua, Italy, (2) Dept. of Geosciences, University of Padua, Italy (valerio.vivaldi@studenti.unipd.it).

Abstract

Morphometric analyses, applied to high resolution DTMs, allowed us to enhance the morphologic variations occurring in crater inner scarp. This specific analysis on surface topography, applied to the case study of Linné, was able to emphasize and possibly confirm the presence of different stratigraphic layers at the Linné site.

1. Introduction

Linné is a well preserved impact crater of 2.2 km in diameter, located at 27.7°N 11.8°E, near the western edge of *Mare Serenitatis* on the Moon. The crater was photographed by the Lunar Orbiter and the Apollo space missions, and therefore has served as most striking example of small fresh simple craters with its characteristics bowl shape. However, recent high resolution data of Lunar Reconnaissance Orbiter Camera (LROC) has revealed that Linné is an inverted truncated cone [1].

2. Morphometric analysis

In this study we have applied 3D morphometric analysis on high resolution DTMs, derived from LROC Narrow Angle Camera (NAC) that provide a resolution range from 0.5 to 2 m/pixel. This analysis was carried out by processing the Linné crater DTM, with a cell size of 2m/px. Firstly, we applied a multiscalar approach [2], to reduce DTM building and interpolation errors aiming to find the best compromise of a smoothed DTM without losing the topographic relevance of the smaller landforms. To this regards, we tested different kernel sizes, ranging from 3x3 to 99x99, in order to evaluate the best window size to calculate morphometric variables such as slope (first derivative) and curvatures (second derivative), useful to characterize the different sectors of the crater (rim crest, floor, slopes and related boundaries). From the statistics of expression of multiscale morphometric analysis we were able to establish that the best windows size for this DTM is around 66m.

3. Morphometric signature of Linné crater

The statistical analysis of slope and curvature values allowed us to characterize the morphometric signature of Linné crater.
Firstly we subdivided the crater in four morphologic sectors: floor, inner scarp, rim and external scarp.
The floor presents a mean slope gradient of 0°-3° with a profile curvature of 0.05°; those values are typical of a flat floor, confirming the freshness of Linné. For the inner scarp the mean slope gradient is 31.2°, consistently with the lunar regolith angle of repose (31°), whereas the mean profile curvature is 0.1°, slightly convex (> 0).
The most interesting result derives from the rim sector that presents a mean profile curvature of 0.5° (convex morphology), with a slim top area with about 0° of profile curvature and 0° of slope, revealing the presence of a pristine crest: this kind of feature is characteristic of a very fresh crater.
On the external scarp the mean slope gradient is about 10° and the profile curvature is negative (-0.05°), defining a slightly concave morphology.

4. Analysis of the Linné inner scarp

The slope map classification enhanced a clear cut boundary within the inner scarp of the crater, at a depth of about 200-300 m, also identified on the topographic profile, as a bland morphological step on the inner crater scarp. This feature was firstly hypothesized through numerical investigation [3] and can be explained as the transition between two different geological units, as shown by the numerical model. The model is based on a projectile of 40 m in radius impacting at 18 km/s into a 2-layered target, with the upper layer made of fractured material of

variable thickness. We found that the non-bowl-shape morphology of Linné may be ascribed to the transition from an upper 200 m highly fractured layer to a lower more competent one (FIG-2B) [3].
Moreover from the classification of the profile curvature we detected other two morphologic layers, between the first feature and the rim crest. Those layers are imperceptible on the topographic profile and on the orthoimage, making morphometric analysis a useful and valuable tool to detect and quantify crater morphologic features.

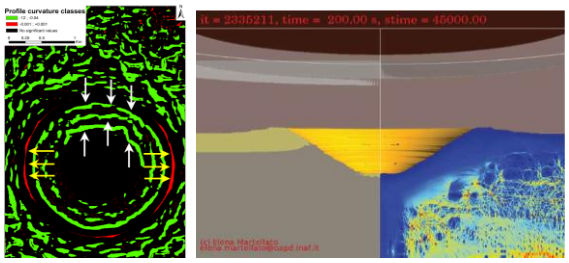

Figure 1: *left*: profile curvature classified to enhance the rim crest (red) and morphological steps in the inner scarp; *right*: numerical modelling of the Linné crater [3].

5. Summary and Conclusions

This research shows how morphometric analysis can be useful to detect and quantify the morphology of impact craters. The extraction of pixel values, from different morphometric variables, enable us to calculate surface statistics, in order to quantify different sectors of an impact crater. Moreover, morphometric analysis allowed us to detect and measure morphological layers within Linné crater, which can be associated to numerical investigations [3]. This analysis is only a part of a more extensive project, aimed to estimate the degradation evolution of simple impact craters. We are extracting morphometric variables from several impact craters in *Mare Serenitatis*, in order to quantify the degradation of the different sectors of craters.

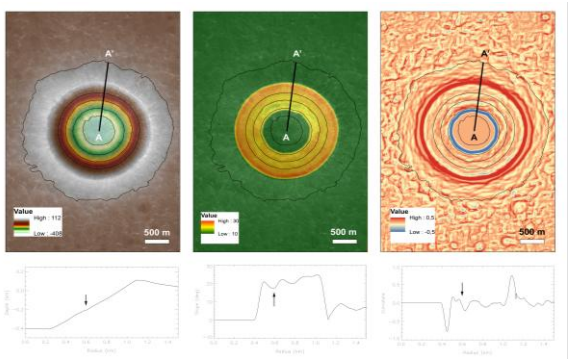

Figure 2: *left*: topographic map of Linné crater, with the relative topographic profile A-A'; *center*: slope map, which enhances the inner scarp and the floor, with the relative slope profile along the A-A' segment; *right*: profile curvature, which enhances the rim (red) and the morphological steps in the crater inner slope. The arrows on each profile indicate the location of the morphological step.

Acknowledgements

This research was supported by the Italian Space Agency (ASI) within the SIMBIOSYS Project (ASI-INAF agreement no. I/022/10/0).

We gratefully acknowledge the developers of iSALE-2D, including Gareth Collins, Kai Wünnemann, Dirk Elbeshausen, Boris Ivanov and Jay Melosh (see www.iSALE-code.de)

References

[1] Garvin, J.B., et al.: Linné: Simple lunar mare crater geometry from LRO observations. LPSC 2011, Abstract # 2063, 2011.

[2] Wood, J.: The geomorphological characterization of digital elevation models. PhD Thesis, University of Leicester, UK, 1996.

[3] Martellato, E., Robinson, M.S., Cremonese, G. and Lucchetti, A.: Numerical modeling of Linné crater. EPSC Abstracts Vol. 8, EPSC2013-649, 2013.

EPSC Abstracts
Vol. 10, EPSC2015-679, 2015
European Planetary Science Congress 2015

GRAIL gravity field determination using the Celestial Mechanics Approach – status report

S. Bertone (1), D. Arnold (1), A. Jäggi (1), G. Beutler (1) and L. Mervart (2)
(1) Astronomical Institute of the University of Bern, Switzerland (stefano.bertone@aiub.unibe.ch), (2) Institute of Advanced Geodesy, Czech Technical University, Prague (CZ)

Abstract

The NASA mission GRAIL (Gravity Recovery And Interior Laboratory [1]) inherits its concept from the GRACE (Gravity Recovery And Climate Experiment) mission to determine the gravity field of the Moon. The use of inter-satellite Ka-band range-rate (KBRR) observations enables data aquisition even when the spacecraft are not tracked from the Earth [2]. The data allows for a highly accurate estimation of the lunar gravity field on both sides of the Moon, which is crucial to improve the understanding of its internal structure and thermal evolution. In this presentation we discuss our latest GRAIL-based lunar gravity fields generated with the Celestial Mechanics Approach using the Bernese Software.

1. Orbit and gravity field

We present our most recent AIUB lunar gravity fields based on the data of GRAIL primary mission (PM) phase, covering the period March to May 2012. Gravity field recovery is realized in the framework of the Celestial Mechanics Approach [3], using a development version of the Bernese GNSS Software [4] along with Ka-band range rate (KBRR) data series as observations and the dynamic GNI1B positions provided by NASA JPL as pseudo-observations.

Apart from normalized spherical harmonic coefficients up to degree $n = 200$, also arc-specific parameters like initial state vectors and appropriately spaced empirical parameters (pseudo-stochastic pulses and empirical accelerations) are set up as common parameters for all measurement types. The latter shall compensate for imperfect models of non-gravitational forces. In this respect, we present our advances towards a more realistic model of solar radiation pressure using empirical accelerations in appropriate directions. We compare our results with the most recent lunar gravity field models released by other groups [5, 6] (see Fig. 1), as well as their consistency with topography induced gravity. We show that the lunar gravity field can be recovered with a high quality by adapting the Celestial Mechanics Approach, even when using pre-GRAIL gravity field models as a priori fields.

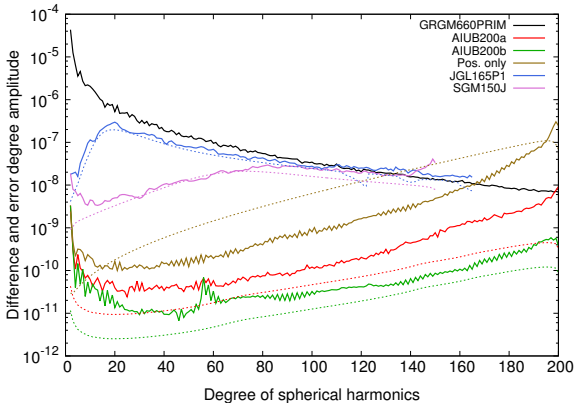

Figure 1: Left: Difference degree amplitudes (solid) and formal errors (dashed) of our preliminary degree-200 solutions based on the a priori field GRGM660PRIM (up to d/o 200, red, and 660, green) compared to pre-GRAIL solutions. The brown curve represents a position-only solution, showing that KBRR observations improve the solution over nearly the full spectral domain.

Fig. 2 shows the free-air gravity anomalies derived from AIUB200a using a Moon reference radius of 1738 km.

2. Doppler data processing

As a further extension of our processing, the GNI1B positions are replaced by the original Doppler observations of the Deep Space Network (DSN) to allow for a completely independent determination of the lunar gravity field using the Celestial Mechanics Approach. Fig. 3 shows the current status of our pre-fit Doppler

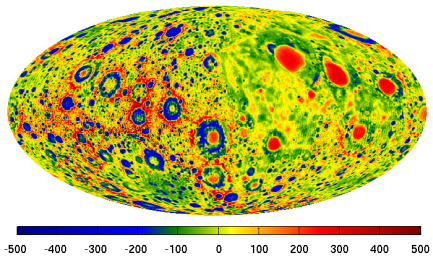

Figure 2: Free-air gravity anomalies on a 0.5° x 0.5° grid (Mollweide projection centered around 270°, with the nearside on the right).

residuals based on GNI1B-derived orbits of GRAIL-A and GRAIL-B and the Doppler data. Observations are screened for outliers by setting a threshold on the residuals and by applying an elevation cutoff at 25°. We present our latest results about DSN data modeling and orbit determination in the Bernese Software.

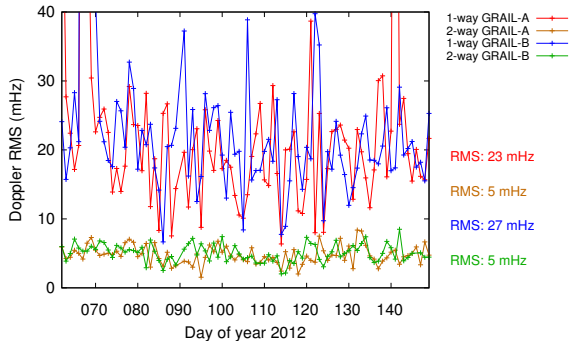

Figure 3: Daily RMS of one-way and two-way Doppler residuals for both GRAIL-A and GRAIL-B over the PM.

3. Summary and Conclusions

In conclusion, AIUB200 already represents an alternative solution for the lunar gravity field from GRAIL data obtained using an independent software. We have compared our solution to the first official NASA GRAIL solution GRGM660PRIM and evaluated it in terms of the correlations to the topography-induced gravity fields (always above 0.98 up to degree 169). We will present our most recent solution, where further improvements are demostrated from the optimisation of the parametrisation and non-gravitational force modeling. Although convenient for the initialization of GRAIL data processing, the use of the dynamic GNI1B positions is not entirely satisfactory. The ongoing implementation of DSN Doppler data processing into the Bernese GNSS Software will allow us to contribute a fully stand-alone solution.

Acknowledgements

We are grateful to the Planetary Data System (PDS) team for making GRAIL inter-satellite Ka-band and DSN tracking data available. This study has been funded with the support of the Swiss National Science Foundation (SNSF).

References

[1] Zuber, M. T. et al..: Gravity Field of the Moon from the Gravity Recovery and Interior Laboratory (GRAIL) Mission, Science, 2013.

[2] Asmar, S. W. et al..: The Scientific Measurement System of the Gravity Recovery and Interior Laboratory (GRAIL) Mission, Space Science Reviews, 2013.

[3] Beutler, G. and Jäggi, A. and Mervart, L. and Meyer, U.: The celestial mechanics approach, Journal of Geodesy, 2010.

[4] Dach, R. et al.: Bernese GPS Software - Version 5.0, Astronomical Institute, University of Bern, 2007.

[5] Lemoine, F. G. et al.: High-degree gravity models from GRAIL primary mission data, Journal of Geophysical Research (Planets), 2013.

[6] Konopliv, A. S. et al.: High-resolution lunar gravity fields from the GRAIL Primary and Extended Missions, Geophysical Research Letters, 2014.

EPSC Abstracts
Vol. 10, EPSC2015-685, 2015
European Planetary Science Congress 2015

GRAIL gravity field recovery using the short-arc integral equation technique: development of the latest Graz lunar gravity field model (GrazLGM)

S. Krauss (1), B. Klinger (2), O. Baur (1), and T. Mayr-Gürr (2)

(1) Austrian Academy of Sciences, Space Research Institute, Schmiedlstrasse 6, 8042-Graz, Austria (sandro.krauss@oeaw.ac.at, oliver.baur@oeaw.ac.at)

Please make sure that your pdf conversion results in a document with a page size of 237 x 180 mm!

(2) Graz University of Technology, Institute of Geodesy , Steyrergasse 30/III, 8010-Graz, Austria (beate.klinger@tugraz.at, mayer-guerr@tugraz.at)

Abstract

We present an updated version of the lunar gravity field model GrazLGM300a,b [1,2] based on inter-satellite Ka-band ranging (KBR) observations collected by the GRAIL mission. We propose to exploit the ranging measurements by an integral equation approach using short orbital arcs [4]. Compared to the predecessor model we increase the spectral resolution to degree and order 450 and refined the parameterization. Validation shows that the applied technique is well suited to recover the lunar gravity field.

1. Introduction

The NASA lunar science mission Gravity Recovery And Interior Laboratory (GRAIL) uses Ka-band range-rate measurements between the two GRAIL satellites to resolve the lunar gravity field with unprecedented resolution and accuracy. This satellite-to-satellite tracking technique is independent of the tracking capability from Earth, thus allowing data acquisition on the near side and the far side of the Moon. The GRAIL mission plays a key role to improve our understanding of the Moon's interior structure and its thermal evolution, as well as the evolution of the terrestrial planets in the solar system. For our current gravity field investigations we focus on data from the primary mission (March 1 to May 29, 2012).

2. Methods & Results

To determine the lunar gravity field we analyze the KBR observations within an integral equation approach using short orbital arcs. This method has already successfully applied to the recovery of the Earth's gravity field from data provided by the GRACE mission [6]. The basic idea is to reformulate Newton's equation of motion in the inertial space as a boundary value problem:

$$\ddot{\boldsymbol{r}}(t) = \boldsymbol{g}(t) + \boldsymbol{a}(t) = \boldsymbol{g}(t) + \boldsymbol{a}_b(t) + \boldsymbol{a}_t(t) + \boldsymbol{a}_n(t) + \boldsymbol{a}_r(t)$$

In doing so, the total acceleration acting on both GRAIL satellites can be split into the Moon's gravitational attraction on the satellite $\boldsymbol{g(t)}$ and additional perturbing forces, including third-body accelerations $\boldsymbol{a_b(t)}$, accelerations due to solid Moon tides $\boldsymbol{a_t(t)}$, non-gravitational accelerations $\boldsymbol{a_n(t)}$ and relativistic effects $\boldsymbol{a_r(t)}$. In this contribution we pay particular attention to processing details associated with the error structure of the observations (covariance functions) and the spectral increase of the model. On this basis we computed a refined version of the lunar gravity field model GrazLGM300b [2]. Finally, a validation with recent GRAIL models computed at NASA-GSFC [1] and NASA-JPL [5] is performed.

Acknowledgement

The data used in this study were made freely available by NASA; GRAIL orbit and inter-satellite information was retrieved from the Planetary Data System (PDS, http://geo.pds.nasa.gov/missions/grail).

References

[1] Krauss S. et al.: Development of the lunar gravity field model GrazLGM300a. VGI Special issue: Austrian contribution to the XXVI General Assembly of the IUGG, accepted, 2015.

[2] Krauss S. et al.: Development of the lunar gravity field model GrazLGM300b in the framework of project GRAZIL. Presented at the EGU meeting, Vienna, Austria, 2015.

[3] Lemoine, F.G., Goossens, S., Sabaka, T.J., et al. (2014): GRGM900C: A degree 900 lunar gravity model from GRAIL primary and extended mission data. Geophysical Research Letters, 3382-3389, doi: 10.1002/2014GL060027.

[4] Mayer-Gürr, T. (2006): Gravitationsfeldbestimmung aus der Analyse kurzer Bahnbögen am Beispiel der Satellitenmissionen CHAMP und GRACE. PhD Thesis, Rheinische Friedrich-Wilhelms-Universität zu Bonn.GRACE Science Team Meeting, Potsdam, Germany, 2014.

[5] Konopliv, A.S., Park, R.S., Yuan, D.N., et al. (2014): High resolution lunar gravity fields from the GRAIL primary and extended mission. Geophysical Research Letters 41, 1452-1458, doi: 10.1002/2013GL059066.

[6] Tapley, B.: GRACE measurements of mass variability in the Earth system. Science 305, 503-505, http://dx.doi.org/10.1126/science.1099192, 2004.

EPSC Abstracts
Vol. 10, EPSC2015-702, 2015
European Planetary Science Congress 2015

Lunar impact flashes: Results from 56 hours of video survey data observed by using one telescope

M. Ait Moulay Larbi (1,2), Z. Benkhaldoun(1), D. Baratoux (2), A. Daassou (1), S. Bouley (3)
(1) Laboratoire de Physique des Hautes Energies et Astrophysique, FSSM, Université Cadi Ayyad, Av. Prince My Abdallah,BP 2390, Marrakech, Maroc. (2) Université de Toulouse; UPS-OMP; IRAP; Toulouse, France
(3) IDES, UMR8148, Université Paris-Sud, 91405 Orsay Cedex,(mamoun.larbi@gmail.com)

Abstract

Primarily observations are performed during 2013 and 2014 at AGM observatory of Marrakech by using one SC telescope in the aim of observing sporadic meteoroids impacting the lunar dark side. Here, we report results from 56 hours of video survey.

1. Introduction

The impact of hyper-velocity centimeter-sized meteoroids on the moon yield moonquakes, melt the rocks, produce meter size craters and generates a plasma/vapor plume as bright and brief flash, which enhances eventually the lunar atmosphere. All these physical effects are now technically observable (e.g. Apollo, LROC, LADEE). Lunar impact detection provides the time and the position of the impact site with the best accuracy; and allows to estimates the energy, and the size of meteoroids and the craters produced. Future lunar explorations (lunar crust, atmosphere, new crater identification) will be more profitable if the independent determinations of the different parameters deduced are made in conjunction with more than one technique. Besides, the large monitored area provided by our Moon is favorable to better constraint the current impact rate on Earth-Moon environment and to characterize the upper size limit of meteoroids swarms. Moroccan observatories (Oukaimeden and AGM) are now involved in this research context, first detections from 2013 have been already presented and implications in lunar seismology are also discussed [1].

2. Observations and detections

A large part of observations was made during the first 4 months of 2013 and the latest four months of 2014. Several factors have prevented us to observe at the peak of meteor showers; including: unfavourable lunar phase and inadequate orbital encounter with most of the meteoroids swarms during the last two years, plus weather. More than 97% of our data was carried out in the best conditions. We monitor the night side of the lunar disc with a sensitive video camera working at interlaced mode (1 half-frame per 20 ms ; 1 frame per 40 ms) attached to a (0.33x or 0.63x) focal reducer + (35 or 20 cm) SC telescope. More details about the instrumental setup can be found in [1, 2,3]. The LunarScan software [4] is used on recorded videos to perform automated detections. The automatically detected transient events are then manually examined to eliminate false detections. Within the 56 hours data analysis; we have rejected several tens of hundreds of false detections.

Obviously, the most false detections are single half-frame duration (20ms) “cosmic ray and electronic noise”. Otherwise, they show motion across the field of view “sun glints from satellite and orbital debris”, or it is just a brilliant feature of the lunar surface (fig.1). Majority of lunar impacts are one frame flashes, and these flashes must be confirmed by at least two different observatories, other flashes can be easily identified based on typical characteristics of impact flashes in terms of intensity, spatial extension and duration. By using one telescope, we estimate to have missed more than tree one-frame flashes. Among the several hundreds of false detections, only four events were lasted more than one frame (20 ms) and simultaneously shown adequate brightness changes at the same pixels. Examining their light curves profile (sudden signal increase followed by a sharp decrease) plus photometric analysis one can notice undoubtedly that they are really impact flashes. The identification criteria and our survey results are consistent with more reliable statistics from NASA-MSFC [5].

Figure 1: Snapshots of typical false detections.

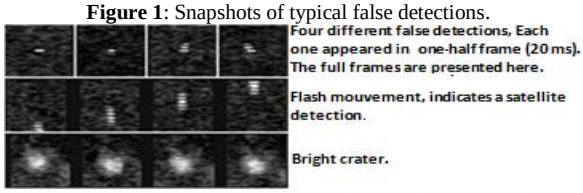

Figure 2: Sub-frames and characteristics of detected flashes. Each field present 20ms. Flashes 2 & 3 are not clearly visible on the last field, but visible on the original full-frame (40 ms).

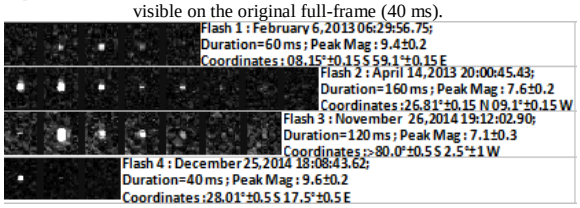

3. Analysis and Results

Characteristics of each flash are given in Figure 2 and derived parameters in Table 1. We noticed that the last three flashes have been observed very close to the equator. All Magnitudes and durations showed a consistency on the trend revealed in the work of [6] (the most luminous flashes persist more). Except that the photometric analysis indicated that Flash 3 was brighter than flash 2 which is the longest one. This can be explained by the fact that fastest meteoroids have capacity to produce bright and short flashes as clarified at the same work [6] in the case of the Leonid meteoroids impacts. So, we consider that the object producing the flash 3 was faster; however the other caused flash 2 is larger and more massive. This is consistent with

light curves analysis, the flash 2 has required more time during its expansion phase (this can be directly noticed in the Fig.2); while the flash 3 has quickly reached its maximum intensity. Since it is this phase that is considered in the calculation of energy, the flash 2 was found more energetic, subsequently generated with a more massive projectile.

Figure 3: Light curves of recorded flashes.

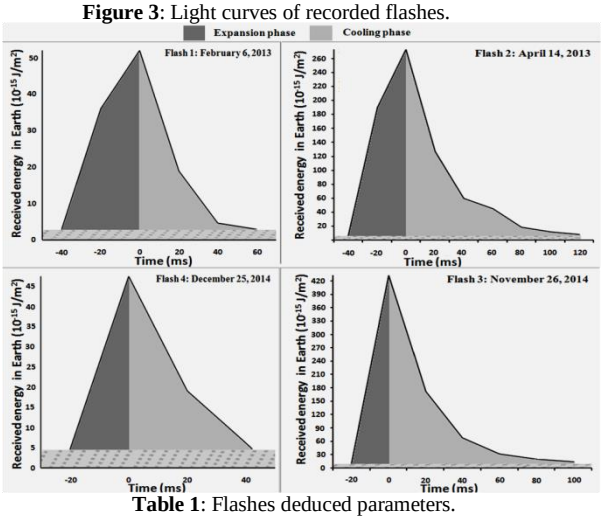

Table 1: Flashes deduced parameters.

	F 1	F 2	F3	F4
Impact luminous Energy (10^4 J)	8.2	43	35	4.5
Estimated impact Energy (10^7 J)	5.4	28.7	23.1	3.0
Estimated mass of impactor (kg)	0.4	2.1	1.2	0.15
Estimated crater diameter (m)	2.6	4.4	4.2	1.8

"Meteoroid speed of 16 km/s, a luminous efficiency of 1.5 10^{-3}, projectile density of 1.5 g/cm^{-3} and target density of 2.2 g/cm^{-3} are used in the calculation".

4. Implications for the impact rate

Lunar impact rate can be reached by considering the total survey time and the average surface monitored. Then, the terrestrial impact flux is obtained by calibrating the lunar rate in terms of Earth collecting area and correcting the impact energy by considering gravitational focusing [2, 3, 7].

New and old results of Earth-lunar system data flux are plotted in the figure 3. Our derived flux is relatively compatible with the extrapolation of lunar impact data given by Apollo seismic station [8]. We have converted bolides explosions rate in Earth to the lunar rate. Our data are more consistent with small fireballs flux [9] and a little compatible with extrapolation of large bolides flux [10]. Compared to other lunar flashes fluxes, our data are consistent with flux derived from [2] at low energy, but higher with a factor of 3 in energy between 10^8 and 10^9J. With the same differences approximately, our data are low in comparison with the rate obtained by [3, 11], note that this last rate supports the annual flux indicated by large impact events such as Tunguska and Chelyabinsk. The present discord may be simply due to difference in the approach taken to determine the energy of the impact in each work, something that can be minimized in the future.

Figure 4: our data rate (green dots) plotted with recent lunar flashes flux and different datasets presented in the lunar & terrestrial scale (error bars do not take into account the error associated with the luminous efficiency.

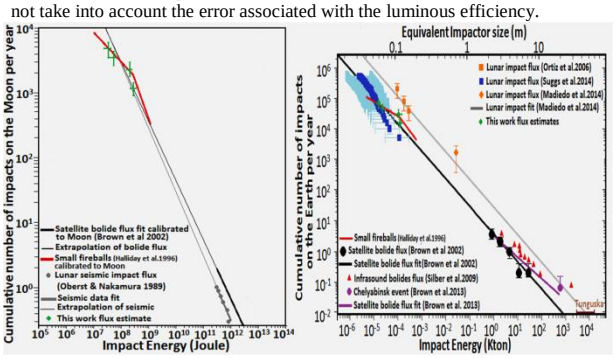

Impact flashes allows to monitor low-energy impacts (in the 10^7J range; provoked by~ 5 cm meteoroid; resulting~ 1.5 m crater). In addition, given the large monitored area, it helps also to keep an eye on the big explosions as the largest flash (8s, 15.6 TNT) observed by [3]. With more datasets, especially, if detections are matched with other techniques (seismic detection, new craters characterization); improvements and accurate estimation of the present impacts and characterization of the meteoroid impact hazards danger will certainly achieved, this will allow as well calibration of the partitioned energies, improve the energy calculation procedure and calibrate the scaling laws used.

5. Conclusion

Primarily results from our survey are discussed, and summarized characteristics of our detections are also presented. Our estimates indicate that about 12±3 craters that are larger than 1.5 m in diameter are created daily on our moon. Our first attempts were satisfactory, it allowed us to make confidence on our current progress in observational and analysis techniques, and to check whether our detection rate is consistent or not with other datasets. Given the time-consuming workload required to registering and analyzing the videos data, which is the main limitation to our capabilities, we wish to automate our instrumental setup in order to increase our detections and be in rendezvous with future lunar exploration.

Acknowledgements

The authors would like to thank the Partenariat Hubert Curien / Volubilis Program ("PHC24675QJ, Impact rate in the Earth-Moon System"). We are grateful to the Mr. Hila Omar and its company Atlas Golf Marrakech for putting at our disposal the mean of their observatory.

References

[1] Ait Moulay Larbi, M. et al., 2015, Earth Moon Planets 114.
[2] Suggs, R.M. et al., 2014 Icarus, 238:23.
[3] Madiedo, J. M. et al., 2014, MNRAS, 439 :3, 2364.
[4] Gural, P. Meteoroid environments workshop, MSFC 2007.
[5] Suggs, R., 2013. Lunar impacts and LADEE mission worshop.
[6] Bouley, S. et al. Icarus., 218, 115, 2012..
[7] Jones, J. & Poole, L.M.G, 2007, MNRAS, 375.
[8] Oberst, J. & Nakamura, Y,. 1989, LPSC 20,802.
[9] Halliday, I., et al, 1996,M&PS, 31,185-217.
[10] Brown, P. G. et al, 2002. Nature 420, 294-296
[11] Ortiz J.L. et al., 2006, Icarus, 184, 319.

EPSC Abstracts
Vol. 10, EPSC2015-738-1, 2015
European Planetary Science Congress 2015

Hydrogen at the Lunar Terminator

T. A. Livengood (1,2), G. Chin (2), R. Z. Sagdeev (3), I. G. Mitrofanov (4), W. V. Boynton (5), L. G. Evans (6), M. L. Litvak (4), T. P. McClanahan (2), A. B. Sanin (4), R. D. Starr (7), J. J. Su (3).
(1) CRESST, University of Maryland, USA (2) NASA Goddard Space Flight Center, USA (3) University of Maryland, USA (4) Institute for Space Research, Moscow, Russia (5) University of Arizona, USA (6) Computer Sciences Corporation, Lanham, MD, USA (7) Catholic University of America, Washington, DC, USA (timothy.a.livengood@nasa.gov)

Abstract

Suppression of the Moon's naturally occurring epithermal neutron leakage flux near the equatorial dawn terminator is consistent with the presence of diurnally varying quantities of hydrogen in the regolith with maximum concentration on the day side of the dawn terminator. This flux suppression has been observed using the Lunar Exploration Neutron Detector (LEND) on the polar-orbiting Lunar Reconnaissance Orbiter (LRO). The chemical form of hydrogen is not determined, but other remote sensing methods and elemental availability suggest water. The observed variability is interpreted as frost collecting in or on the cold nightside surface, thermally desorbing in sunlight during the lunar morning, and migrating away from the warm subsolar region across the nearby terminator to return to the lunar surface. The maximum concentration, averaged over the upper ~1 m of regolith to which neutron detection is sensitive, is estimated to be 0.0125±0.0022 weight-percent water-equivalent hydrogen (wt% WEH), yielding an accumulation of 190±30 ml recoverable water per square meter of regolith at each dawn. The source of hydrogen (water) must be in equilibrium with losses due to solar photolysis and escape. A chemical recycling process or self-shielding from solar UV must be assumed in order to bring the loss rate down to compatibility with possible sources, including solar wind or micrometeoroid delivery of hydrogen, which require near-complete retention of hydrogen, or outgassing of primordial volatiles, for which a plausible supply rate requires significantly less retention efficiency.

1. Introduction

Mineral hydration on the lunar surface has been detected in reflected near-IR and UV light, but the quantity is not well constrained [1,2,4,5]; it could be anything from a few microns thick layer of lightly hydrated material, to extending deep into the surface. The magnitude of hydration varies diurnally, with maximum near the terminators and minimum near noon. The Lunar Exploration Neutron Detector (LEND) on LRO can uses a different remote-sensing technique, measuring the flux of cosmic-ray induced neutrons from the lunar surface [3]. Neutron remote-sensing is insensitive to solar illumination and probes approximately a meter deep into the surface, enabling LEND to explore the concentration of hydrogen in the lunar surface at all times of the lunar day and night.

2. Results

The presence of hydrogen in the regolith results in suppressing the flux of epithermal neutrons (neutrons of energy near but greater than thermal), as scattering from protons efficiently degrades the energy of epithermal neutrons into the thermal regime. A cadmium foil intercepts such low-energy neutrons before reaching the detector. Maximum flux suppression for epithermal neutrons is found at about 06:35 local time and least flux suppression at 14:35. The maximum of low-energy epithermal neutron flux covers a period of about six hours of local time, starting at 14:35. The high-energy epithermal flux has a unique maximum that coincides with the beginning of the plateau in SETN signal. Contrast between the most flux-suppressed interval and the maximum flux is 5.6 times uncertainty. The observed distribution implies that the least-hydrogenated regolith appears in the mid- to late-afternoon while the most-hydrogenated regolith appears on the dayside of the dawn terminator. This distribution is partially consistent with observed mineral hydration [2,5], which shows peak hydration symmetrically near both dawn and dusk terminators and minimum at noon. Minimal neutron suppression at dusk suggests that the total column of hydrogenated regolith is very small, even though hydration in a thin surface layer may be comparable to the corresponding region near the dawn terminator.

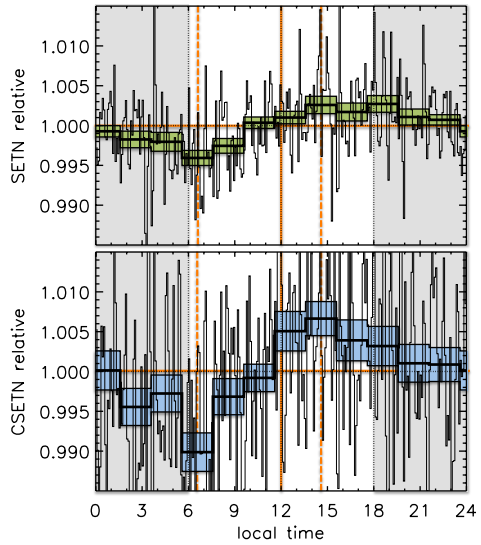

Figure 2: Neutron flux *vs.* local time for low energy (*upper*) and high energy (*lower*) epithermal neutrons. Gray indicates lunar night. Flux suppression near the dawn terminator, biased toward the day side.

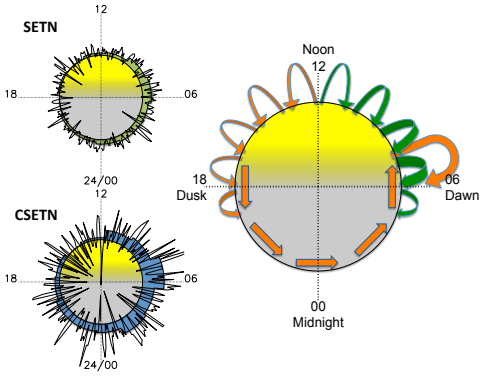

Figure 3: Hydrogen (water) distribution with local time and lateral transport. (*upper left*) Hydrogen concentration from low-energy epithermal neutron flux. (*lower left*) Hydrogen concentration from high-energy epithermal neutron flux. (*right*) Schematic of volatile migration (curved arrows) and transport in regolith by lunar rotation (tangential arrows). Volatiles migrate east (orange), condense onto night regolith, remobilize after dawn and migrate back to cold terminator. Volatiles that migrate west (green) are reinforced by thermally desorbed volatiles in the morning sector.

6. Summary and Conclusions

The distribution in local time of epithermal neutron flux is consistent with a maximum of hydrogen-bearing volatiles just after lunar dawn but widely distributed at lesser concentration up to the afternoon and extending across much of the lunar night. A distribution that is fixed near dawn despite lunar rotation requires a diurnal cycle in which volatiles desorb and migrate across the terminator to be readsorbed on the cold nightside surface. Only about 1% of the inventory at dawn will be in gas phase above the surface. The relative magnitude of response in the two LEND detector systems is consistent with hydrogen in a shallow layer of 3–15 cm depth, nominally ~6 cm.

Acknowledgements

Data are archived at http://wwwpds.wustl.edu. TAL was supported by NASA's Lunar Reconnaissance Orbiter project under NASA award number NNG06EO90A. The Russian co-authors were supported by grant No. 14-22-00249 of the Russian Scientific Foundation. The Russian Federal Space Agency supplied the LEND instrument to NASA and the LRO project.

References

[1] Clark, R. N.: Detection of Adsorbed Water and Hydroxyl on the Moon. *Science* **326**, 562–564, doi: 10.1126/science.1178105, 2009.

[2] Hendrix *et al.*: Indicator of hydration and weathering. *JGR-Planets* **117**, E12001 (8 pp), doi: 10.1029/2012JE004252, 2012.

[3] Mitrofanov *et al.*: Lunar Exploration Neutron Detector for the NASA Lunar Reconnaissance Orbiter. *Space Science Reviews* **150**, 183–207, doi: 10.1007/s11214-009-9608-4, 2010.

[4] Pieters *et al.*: Character and Spatial Distribution of OH/H2O on the Surface of the Moon Seen by M3 on Chandrayaan-1. *Science* **326**, 568–582, doi: 10.1126/science.1178658, 2009.

[5] Sunshine *et al.*: Temporal and Spatial Variability of Lunar Hydration As Observed by the Deep Impact Spacecraft. *Science* **326**, 565–568, doi: 10.1126/science.1179788, 2009.

EPSC Abstracts
Vol. 10, EPSC2015-739, 2015
European Planetary Science Congress 2015

NASA's Solar System Exploration Research Virtual Institute: Combining Science and Exploration

B. Bailey, G. Schmidt, D. Daou, Y. Pendleton
NASA Solar System Exploration Research Virtual Institute. NASA Ames Research Center. M/S 17-1. Moffett Field, CA, USA. 94035. (Brad.Bailey@nasa.gov, +01-650-604-2104)

Abstract

The NASA Solar System Exploration Research Virtual Institute (SSERVI) is a virtual institute focused on research at the intersection of science and exploration, training the next generation of lunar scientists, and community development. As part of the SSERVI mission, we act as a hub for opportunities that engage the larger scientific and exploration communities in order to form new interdisciplinary, research-focused collaborations.

This talk will describe the research efforts of the nine domestic teams that constitute the U.S. complement of the Institute and how we will engage the international science and exploration communities through workshops, conferences, online seminars and classes, student exchange programs and internships.

1. Introduction

NASA's Solar System Exploration Research Virtual Institute (SSERVI) represents a close collaboration between science, technology and exploration that will enable deeper understanding of the Moon and other airless bodies as we move further out of low-Earth orbit. The new Institute is centered on the scientific aspects of exploration as they pertain to the Moon, Near Earth Asteroids (NEAs) and the moons of Mars. The Institute focuses on interdisciplinary, exploration-related science centered around all airless bodies targeted as potential human destinations. Areas of study reported here will represent the broad spectrum of lunar, NEA, and Martian moon sciences encompassing investigations of the surface, interior, exosphere, and near-space environments as well as science uniquely enabled from these bodies.

We will provide a detailed look at research being conducted by each of the 9 domestic US teams as well as our 7 international partners. The research profile of the Institute integrates investigations of plasma physics, geology/geochemistry, technology integration, solar system origins/evolution, regolith geotechnical properties, analogues, volatiles, ISRU and exploration potential of the target bodies.

2. Summary and Conclusions

As the Institute's teams build upon their proposed research, new opportunities for both domestic and international partnerships will be generated that will produce exciting new results and generate new ideas for scientific and exploration endeavors. SSERVI enhances the widening knowledgebase of planetary research by acting as a bridge between several different groups and bringing together researchers from: 1) scientific and exploration communities, 2) multiple disciplines across the full range of planetary sciences, and 3) domestic and international communities and partnerships.

Acknowledgements

The authors would like to thank the hard work and dedication to all SSERVI Team members and International partners that work diligently to create an innovative and collaborative Institute.

EPSC Abstracts
Vol. 10, EPSC2015-752, 2015
European Planetary Science Congress 2015

Mechanism of formation of water molecules incorporated in near-surface lunar soil

A.Yu. Dubinskii (1) and S.I. Popel (1,2)
(1) Space Research Institute, Russian Academy of Sciences, Moscow, Russia, (2) Moscow Institute of Physics and Technology (State University), Dolgoprudnyi, Moscow region, Russia (popel@iki.rssi.ru / Fax: +7-495-3331248)

Abstract

A mechanism of the formation of water molecules incorporated in near-surface lunar soil is presented.

1. Introduction

Recent studies [1] based on the Lunar Reconnaissance Orbiter data and aimed at detecting the neutron fluxes that passed through the lunar surface regions in the southern hemisphere of the Moon revealed the presence of hydrogen-rich areas in the near-surface lunar region at latitudes exceeding 70°. The emergence of near-surface hydrogen-rich areas may be driven by the solar wind electrons and protons that impact the Moon, are absorbed by (implanted into) its surface, and form neutral atoms and molecules of hydrogen or chemical compounds that contain hydrogen, for example, in the form of hydroxyl groups [2]. This implanted hydrogen may accumulate at the lunar surface according to the following mechanism. The solar wind protons are absorbed by the lunar regolith particles at depths of up to 10^{-5} cm. At the end of the proton path they are chemically bound with atoms of the lunar regolith, in particular with oxygen atoms; as a result, tens of percent of oxygen atoms in the lunar soil regions that interact with the solar wind protons get bound into the OH hydroxyl groups. This implanted hydrogen rises to the lunar surface due to diffusion. The desorption of hydrogen bound in this way progresses very slowly at temperatures lower than 400 K that are typical for the lunar surface. As a result, the surface concentration of hydrogenous materials on the Moon may reach sufficiently large values (up to 10^{17} cm^{-2}) in several thousand years [2]. The hydrogen-rich lunar surface areas are more susceptible to photoemission than the surrounding regions [3], and this influences the process of charging the dust particles, their dynamics, and finally, the properties of the dusty plasma system at the Moon [4-6].

However, the results obtained by Mitrofanov et al. [1] are treated often as those which point at the presence of water ice in the near-surface lunar regions. Justification of such a treatment is important from the viewpoint of future lunar missions and exploration of the Moon, especially with taking into account very low probability of the existence of free water (say, not incorporated in near-surface lunar soil) on the Moon because of strong evaporation into atmosphereless space at day time and impossibility to condense at night time. Here, we present a possible mechanism of the formation of water molecules incorporated in the near-surface lunar soil.

2. Mechanism

In accordance with the conception [2], the energy of the solar wind proton is enough to uncouple a molecule of SiO_2 in the crystal lattice of quartz. Then the proton is coupled with an oxygen atom forming hydroxyl (OH-) group. However, the hydroxyl group remains coupled with a silicon atom presenting in the crystal lattice of SiO_2. Such a configuration is not related to the presence of water on the Moon.

The thermal energy is not sufficient to break chemical bonds in quartz. To explain the release of oxygen atoms from the crystal lattice of SiO_2 we consider sulfur compounds (e.g., Ag_2S) containing in the lunar regolith. Sulfur and oxygen atoms have similar structures of outer electron shell, although the size of the sulfur atom is larger than that of the oxygen one. Furthermore, the structure of the molecule Ag_2S is analogous to that of H_2O. This results in a possibility of substitution of oxygen atom in the crystal lattice of SiO_2 by sulfur atom and, correspondingly, in the release of oxygen atom in the regions of lunar near-surface soil where argentum sulphide contacts with silicon oxide. The mechanism of exchange between sulfur and oxygen is the following.

1) When a solar wind proton hits a region of lunar near-surface soil where argentum sulphide contacts with silicon oxide, Si-O bond breakage occurs, while hydrogen forms the hydroxyl group

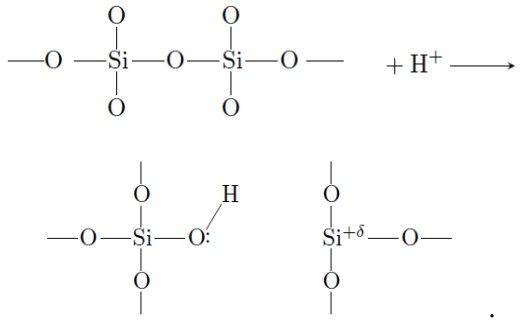

2) Then the interaction of argentum sulphide molecule is accompanied by the approach of sulphide and silicon atoms as well as argentum and oxygen those. The intermediate complex is formed

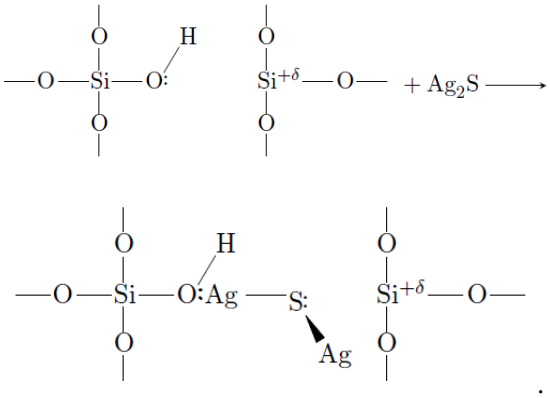

3) The integrated intermediate complex existing due to the covalent-hydrogen bonds is created. Then Ag-S bond breakage occurs

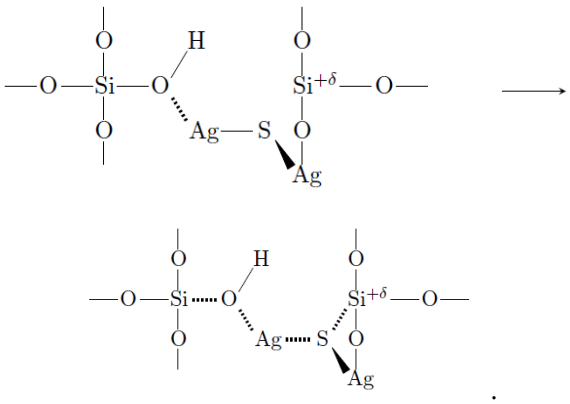

4) As a result, a molecule of argentum hydroxide AgOH is separated from the intermediate complex, and the separation of the argentum atom occurs.

3. Conclusions

Thus oxygen atoms are released (as a part of the molecule AgOH) from the crystal lattice of SiO_2. Argentum hydroxide can react relatively easily with hydrogen forming water and silver. This shows a possibility of the formation of water molecules incorporated in the near-surface lunar soil.

Acknowledgements

This work was carried out as part of the Russian Academy of Sciences Presidium program no. 9 “Experimental and Theoretical Research of Objects of the Solar System and Planetary Systems of Stars” and was supported by the Russian Foundation for Basic Research (project no. 15-02-05627-a).

References

[1] Mitrofanov, I.G., Sanin, A.B., Boynton, W.V., et al.: Hydrogen mapping of the lunar south pole using the LRO neutron detector experiment LEND, Science, Vol. 330, pp. 483-486, 2010.

[2] Starukhina, L.: Water detection on atmosphereless celestial bodies: alternative explanations of the observations, J. Geophys. Res., Vol. 106, pp. 14701-14710, 2001.

[3] Kolesnikov, E.K. and Manuilov, A.S.: The way to calculate electrostatic field intensity above lunar surface covered by hydrogen monolayer, Astron. Zh., Vol. 59, pp. 996-998, 1982.

[4] Popel, S.I., Kopnin, S.I., Golub', A.P., Dol'nikov, G.G., Zakharov, A.V., Zelenyi, L.M., and Izvekova, Yu.N.: Dusty plasma at the surface of the Moon, Solar System Research, Vol. 47, pp. 419-429, 2013.

[5] Popel, S.I., Morfill, G.E., Shukla, P.K., and Thomas, H.: Waves in a dusty plasma over the illuminated part of the Moon, J. Plasma Phys., Vol. 79, pp. 1071-1074, 2013.

[6] Popel, S.I., Golub', A.P., Izvekova, Yu.N., Afonin, V.V., Dol'nikov, G.G., Zakharov, A.V., Zelenyi, L.M., Lisin, E.A., and Petrov, O.F.: On the distributions of photoelectrons over the illuminated part of the Moon, JETP Lett., Vol. 99, pp. 115-120, 2014.

EPSC Abstracts
Vol. 10, EPSC2015-753, 2015
European Planetary Science Congress 2015

"NASA's Solar System Exploration Research Virtual Institute" – Expanded Goals and More Partners

D. Daou, G. K. Schmidt, Y. Pendleton, and B. E. Bailey for NASA SSERVI
Solar System Exploration Research Virtual Institute (SSERVI) (Doris.Daou@nasa.gov).

Abstract

The NASA Solar System Exploration Research Virtual Institute (SSERVI) has been pursuing international partnerships since its inception as the NASA Lunar Science Institute (NLSI), in order to both leverage the science being done by its domestic member institutions as well as to help lunar science and exploration become a greater global endeavor. The international partners of the Institute have pursued a broad program of lunar science stimulated by scientific partnerships enabled by the SSERVI community. Furthermore, regional partnerships have been formed such as the new pan-European lunar science consortium, which promises both new scientific approaches and mission concepts.

International partner membership requires long-term commitment from both the partner and SSERVI, together with tangible and specific plans for scientific interaction that will produce results of mutual benefit to both the institute's U.S. Teams and the international partner. International partners are invited to participate in all aspects of the Institute's activities and programs, on a basis of no exchange of funds. Through these activities, SSERVI researchers and international partners participate in sharing ideas, information, and data arising from their respective research efforts, and contribute to the training of young scientists.

This talk will present an overview of the Institute and the international nodes. We will also discuss the various processes to become a SSERVI partner as well as the opportunities available for collaborations with the SSERVI national teams.

1. Introduction

Recognizing that science and exploration go hand in hand, NASA has expnaded its successful NASA Lunar Science Institute (NLSI) to broaden its research base to other science and exploration destinations. NLSI officially changed to SSERVI in July 2013, and has continued to address basic and applied scientific questions fundamental to understanding the Moon, and added investigations related to Near Earth Asteroids, the Martian moons Phobos and Deimos, and the near space environments of these target bodies. SSERVI, supported by NASA's Science Mission Directorate and Human Exploration and Operations (HEO) Mission Directorate, is composed of an administrative office located at NASA Ames Research Center that oversees the operation of several research teams distributed across the United States and a growing number of international partners.

1.1 Mission Statement

SSERVI fosters collaborations within and among competitively selected domestic teams, the broader lunar science community, and multiple international partners in order to:

- Conduct basic and applied research fundamental to lunar and planetary sciences while advancing human exploration of the solar system,
- Conduct and catalyse collaborative research in lunar and planetary science, enabling cross-disciplinary partnerships throughout the science and exploration communities,
- Provide scientific, technical, and mission-relevant analyses for appropriate NASA programs, planning, and space missions as requested by NASA,
- Explore innovative ways of using information technology for scientific collaboration and information dissemination across geographic and contextual boundaries to stimulate inter- and cross-discipline research,

- Train the next generation of scientific explorers through research opportunities, and encourage global outreach through various participatory events and programs.

SSERVI recognizes the importance of stimulating science throughout the entire community, leveraging additional research by connecting others to the Institutes' currently funded teams. Most notably, SSERVI organizes and sponsors the annual Exploration Science Forum, held at Moffett Field, California, which brings together several hundred researchers to discuss topics ranging from modelling to mission science. The Director's Seminar Series brings the community together via monthly videoconferences that are archived for future reference. The Focus Groups mobilize expertise across the community on relevant topics developed at a grass roots level. The Institute's Workshops Without Walls, held in virtual space, provides travel-free conferences with recognized leaders on topics of current interest.

2. SSERVI International Partnerships

The NASA Solar System Exploration Research Virtual Institute (SSERVI) has a program of partnerships with international organizations to provide collaborative research opportunities for all members of the international science community. International partner membership requires long-term commitment from both the partner and the SSERVI, together with tangible and specific plans for scientific interaction that will produce results of mutual benefit to both the SSERVI U.S. teams and the international partner. The NASA SSERVI international partnerships program includes collaborative activities that address any of the objectives defined in the SSERVI Mission Statement. It is preferred that organizations proposing partnership represent a broad range of academic or research groups, able to represent the lunar science activity within a country. International partners are invited to participate in all aspects of the Institute's activities and programs, on a basis of no exchange of funds. Through these activities, SSERVI researchers and international partners participate in sharing ideas, information, and data arising from their respective research efforts, and contribute to the training of young scientists. Non-U.S. organizations can propose to become either Associate or Affiliate Members of the SSERVI, as described below. **Affiliate:** with non-government institutions; the majority of agreements will be Affiliate. **Associate:** a government-to-government agreement; this includes space agencies.

How to Apply to the International Partners Program

Proposal Development: Proposers to the SSERVI International Partners Program are requested to describe: 1) the organizational nature of the proposing group (e.g., academic, government agency, private, non-profit, consortium); 2) the themes of the scientific work currently being undertaken, together with plans for interacting with the SSERVI community in ways that will advance the goals of the SSERVI while providing mutual benefit to the international partner; and 3) the specific areas where productive near-term exchanges/partnerships are anticipated, and areas for longer-term cultivation of interactions. Proposers are encouraged to include science collaboration plans with existing SSERVI teams, research exchange plans, collaborative field studies, facility sharing opportunities, digital content exchanges, and focus group plans.

Proposal Review at SSERVI: SSERVI Central will review the proposal internally using the following criteria: 1) the relevance of the scientific work being undertaken to the lunar science objectives and its synergy with the SSERVI 2) the nature of funding/endorsement from proposal sponsors 3) the strength and level of government endorsement (Associate Membership) 4) the specific areas where productive near-term exchanges/partnerships are anticipated, and areas for longer-term cultivation of interactions 5) any other issues that the SSERVI deems relevant, including the strategic goals of NASA

NASA Headquarters Review: When the proposal is complete and satisfactory to both your team and the SSERVI, it is then forward it to NASA Headquarters, to both the Office of International and Interagency Relations (OIIR) and to Jim Green, Director of Planetary Sciences.

Extra Review for Associate Partnerships: After approval from OIIR and Jim Green, additional review is done at NASA HQ and potentially the U.S.

State Department. This review is coordinated by the OIIR. Depending on the country in question, this portion of the process can take a longer time.

Official Exchange of Letters: After the review at NASA HQ for Affiliate partnerships, Yvonne Pendleton (SSERVI Director) and Greg Schmidt (SSERVI Deputy Director) send an official letter of invitation to the primary partner institution. The letter is typically addressed to a senior official at the institution. After receiving this letter, the lead organization sends a formal letter reply accepting our offer, and the partnership is complete. For Associate partnerships, once the additional State Department review is complete, letters are sent between the heads of agencies for NASA and the partner institution and the partnership is complete. At this point, there can make plans for joint press announcements, a formal "signing" ceremony if desired, and other activities.

Learn More To learn more about our international program or to inquire about how to become a partner, contact: Greg Schmidt, Director of International Partnerships or Doris Daou, Deputy Director of International

3. Figures

4. Summary and Conclusions

The NASA Solar System Exploration Research Virtual Institute (SSERVI) is uniquely poised to bring people together via the realm of science, where the pinnacle of success is sharing results with the world. SSERVI's International Partnerships Program provides collaboration opportunities for researchers within the global science community, as well as the international education/public outreach community. International partners are invited to participate in all aspects of the Institutes activities and programs on a no-exchange-of-funds basis. Non-U.S. science organizations can propose to become either Associate or Affiliate members of the SSERVI on a no-exchange-of-funds basis. Affiliate partnerships are with non-government institutions; the majority of agreements will be Affiliate. Associate partnerships are government-to-government agreements; this includes space agencies.

EPSC Abstracts
Vol. 10, EPSC2015-854, 2015
European Planetary Science Congress 2015

The Widespread Distribution of Swirls in Lunar Reconnaissance Orbiter Camera Images

Brett W. Denevi (1), Mark S. Robinson (2), Aaron K. Boyd (2), and David T. Blewett (1)
(1) The Johns Hopkins University Applied Physics Laboratory, Laurel, MD, USA, (2) School of Earth and Space Exploration, Arizona State University, Tempe, AZ, USA. Email: brett.denevi@jhuapl.edu.

1. Introduction

Lunar swirls, the sinuous high- and low-reflectance features that cannot be mentioned without the associated adjective "enigmatic," are of interest because of their link to crustal magnetic anomalies [1,2]. These localized magnetic anomalies create mini-magnetospheres [3,4] and may alter the typical surface modification processes or result in altogether distinct processes that form the swirls. One hypothesis is that magnetic anomalies may provide some degree of shielding from the solar wind [1,2], which could impede space weathering due to solar wind sputtering. In this case, swirls would serve as a way to compare areas affected by typical lunar space weathering (solar wind plus micrometeoroid bombardment) to those where space weathering is dominated by micrometeoroid bombardment alone, providing a natural means to assess the relative contributions of these two processes to the alteration of fresh regolith. Alternately, magnetic anomalies may play a role in the sorting of soil grains, such that the high-reflectance portion of swirls may preferentially accumulate feldspar-rich dust [5] or soils with a lower component of nanophase iron [6]. Each of these scenarios presumes a pre-existing magnetic anomaly; swirls have also been suggested to be the result of recent cometary impacts in which the remanent magnetic field is generated by the impact event [7]. Here we map the distribution of swirls using ultraviolet and visible images from the Lunar Reconnaissance Orbiter Camera (LROC) Wide Angle Camera (WAC) [8,9]. We explore the relationship of the swirls to crustal magnetic anomalies [10], and examine regions with magnetic anomalies and no swirls.

2. Data and Methods

The WAC maps the Moon in seven filters from 321 to 689 nm [8]. Denevi et al. [11] found that WAC ratios isolate the steep ultraviolet slope (shortward of ~415 nm) common to fresh silicates, and thus delimit areas that are especially spectrally immature. WAC reflectance properties can also be used to separate fresh plagioclase-rich materials from their shocked or glassy equivalent in the highlands. Lunar swirls are characterized by this steep UV slope [11], such that a WAC color composite (415 nm, 321/415 nm, and 321/360 nm in red, green, and blue, respectively) reveals their locations (e.g., Fig. 1). We used this WAC composite sampled at 400 m/pixel as the basis for our mapping, noting the locations and margins of the high-reflectance portions of swirls based on their UV ratios and 415 nm reflectance values.

3. Distribution of Swirls

The WAC-based map (Fig. 2) reveals a generally greater extent and higher concentration of lunar swirls than prior mapping that was based on albedo alone. For example, we find a higher concentration of swirls than previously observed [7] in the northwestern portion of the South Pole–Aitken basin (e.g., Fig. 1), so that the three previously identified swirl groupings at Hopmann, Ingenii, and NW of Apollo [e.g., 12] are clearly seen to be one continuous group of swirls. The distribution of swirls in that region is similar, but not identical, to the distribution of magnetic anomalies (Fig. 2). A higher concentration of swirls is also seen in the Marginis region, and the Marginis and Firsov swirls are also clearly observed to be one continuous group in the WAC map. Swirls that have not been previously

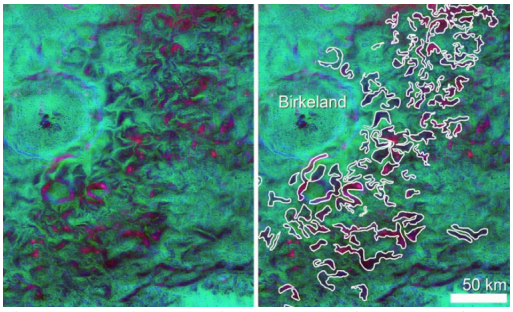

Fig. 1. WAC color composite (415 nm, 321/415 nm, 321/360 nm in red, green, and blue) where swirls appear blue–pink. Annotated version with swirls outlined on right. Scene centered at 31° S, 176° E.

recognized were found in the Crozier, Abel, and Dewar regions (Fig. 2). Each is associated with a local magnetic anomaly.

Nearly all major magnetic anomalies have associated swirls (Fig. 2). We examined the exceptions and found that several are obscured by fresh impact crater ejecta, (i.e., Tycho or Jackson craters), some are at high latitudes for which WAC ratio data is unreliable, and one has an associated bright diffuse patch (Descartes), as previously recognized [12]. However, there are several locations, the most prominent one to the northeast of the Orientale basin near Hartwig crater, where we find no evidence of a swirl in the WAC color composite nor a plausible cloaking mechanism.

For many of the swirls, the ultraviolet–visible color properties vary across the group. For example, in the Firsov and Gerasimovich regions, which vary little in terms of FeO content [13], the high-reflectance portion of swirls range from having a break in slope at 360 nm, consistent with fresh plagioclase-rich soil, to having a strong downturn at 415 nm, indicating shocked or glassy soil of plagioclase-rich composition, suggesting variations spectral character consistent with those observed around fresh highland impact craters. We further explore the characteristics of the mapped swirls for comparison with predictions based on the proposed models of formation.

References

[1] Hood L.L. and Schubert G. (1980) *Science*, *208*, 49–51. [2] Hood L.L. and Williams C.R. (1989) *LPSC 19,* 99–113. [3] Halekas J.S. et al. (2008) *PSS*, *56*, 941–946. [4] Wieser M. et al. (2010) *GRL*, *37*, L05103. [5] Garrick-Bethell I. et al. (2011) *Icarus*, *212*, 480–492. [6] Pieters C.M. et al. (2014) *LPSC 45*, Abs. 1408. [7] Schultz P.H. and Srnka L.J. (1980) *Nature*, *284*, 22–26. [8] Robinson M.S. et al. (2010) *Space Sci. Rev.*, *150*, 81–124. [9] Boyd A.K. et al. (2012) *LPSC 43*, Abs. 2795. [10] Richmond N.C. and Hood L.L. (2008) *JGR, 113*, E02010. [11] Denevi B.W. et al. (2014) *JGR*, *119*, 2013JE004527. [12] Blewett D.T. et al. (2011) *JGR*, *116*, doi:10.1029/2010JE004656. [13] Lawrence D.J. et al. (2002) *JGR*, *107*, 10.1029/2001JE001530.

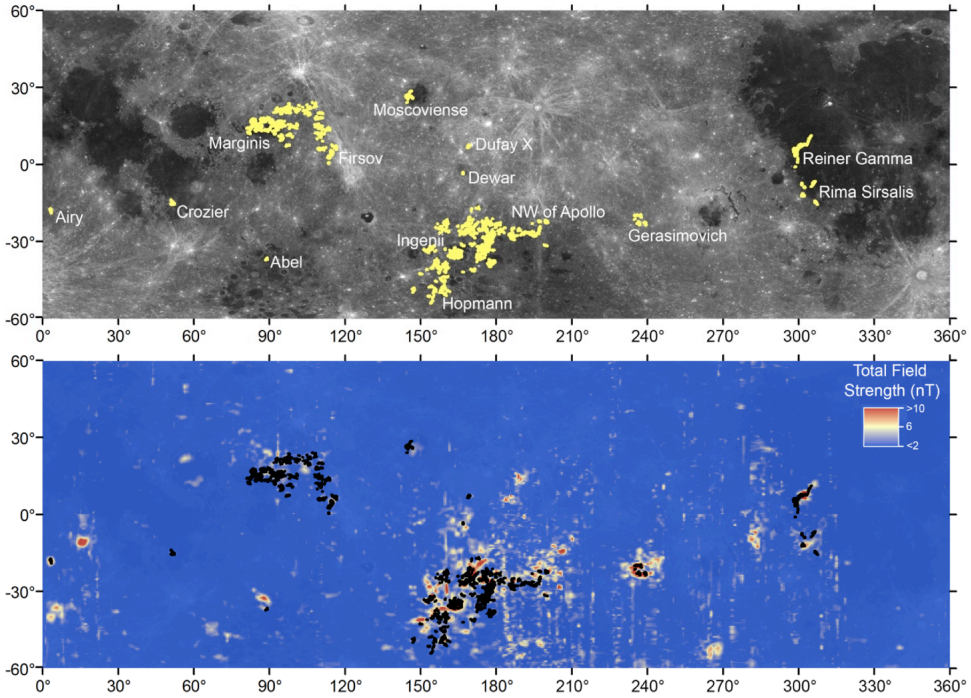

Fig. 2. Preliminary WAC map of lunar swirl locations, cropped to ±60° latitude where WAC color ratio data is most reliable. Top: Swirls shown in yellow on a WAC 415 nm reflectance basemap. Labels correspond to regions examined by Blewett et al. [12], plus Dufay X and Dewar. Bottom: Swirls shown in black on a map of total magnetic field strength from Lunar Prospector [10]. Note that the outlines of swirls are shown in bold to make them more visible at this scale, thus features are slightly exaggerated in size.

EPSC Abstracts
Vol. 10, EPSC2015-860, 2015
European Planetary Science Congress 2015

New Views of the Moon II 2008-2018. An initiative to integrate new lunar information into our fundamental understanding of the Moon and the next stages of international lunar exploration.

C.K. Shearer[1], C.R. Neal[2], B.L. Jolliff[3], M.A. Wieczorek[4], S. Mackwell[5] and S. Lawrence[6].[1]Institute of Meteoritics, Department of Earth and Planetary Sciences, University of New Mexico, Albuquerque, New Mexico 87131(cshearer@unm.edu), [2]University of Notre Dame, Notre Dame, Indiana, 46556, [3]Department of Earth and Planetary Sciences, Washington University in St. Louis, St. Louis, Missouri, 63130, [4]Insitut de Physique de Globe de Paris, Saint Maur, France, [5]Lunar and Planetary Institute, Houston, Texas, 77058. [6] School of Earth and Space Exploration, Arizona State University, Tempe, Arizona 85281.

1. Introduction

In 1998, the Curation and Analysis Planning Team for Extraterrestrial Materials (CAPTEM) sponsored a long-term initiative to improve our understanding of the Moon and its history by integrating all available types of data: in situ investigations, analyses of lunar samples, telescopic observations, and spacecraft datasets. This initiative, New Views of the Moon (NVM-I), was supported by NASA's Science Mission Directorate and the Lunar and Planetary Institute and guided principally by Brad Jolliff, Charles Shearer, Mark Wieczorek, and Clive Neal. The goals of the original NVM-I initiative were (1) to summarize new insights that have been gained about the Moon as a result of recent global data sets (Clementine, Lunar Prospector), and their integration with sample and other data; (2) to define current understanding of the Moon's geologic history, resources, and potential for scientific exploration; and (3) to communicate implications of knowledge gained from research and exploration of the Moon for planetary science and exploration beyond the Moon. The NVM-I initiative ultimately involved contributions and data synthesis from over 100 individual scientists and engineers at numerous workshops and special sessions at worldwide scientific meetings. NVM-I culminated in a book "New Views of the Moon" published in 2006 as volume 60 of Reviews in Mineralogy and Geochemistry published by the Mineralogical Society of America. In 2012, the book was translated into Chinese. NVM-I went to press prior to analysis of the data from missions flown since 2000, and before the major discoveries from sample analyses made this century.

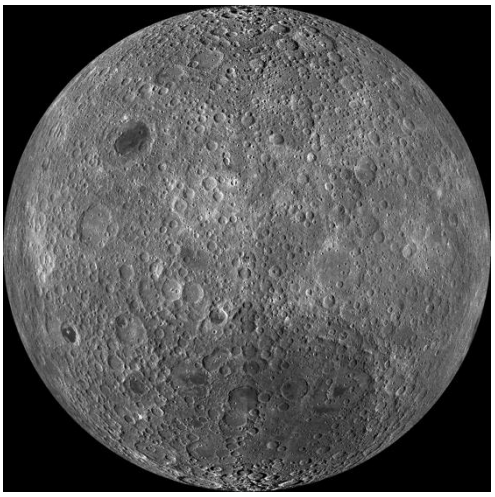

Figure 1. Mosaic of over 15,000 LRO Wide Angle Camera images showing the far side of the Moon including the South Pole-Aitken (SPA) basin.

Using new mission observations and new lunar sample measurements, incredible strides in lunar science have been made since NVM-I was published, We therefore propose to start a new international lunar science community initiative, the New Views of the Moon II (NVM-II), that will integrate these new observations and produce a richer understanding of our nearest neighbor in space, reveal new clues about the history of the Solar System as recorded on the Moon, and provide new information to define missions and investigations for a renewed exploration of the Moon with robotic and human missions.

2. A New Perspective from Missions

A key goal of NVM-II is to synthesize the results from recent lunar missions to build on the results of NVM-1. Subsequent to the publication of NVM-I, data from numerous missions exploring the interior and surface of the Moon have become available. These include SMART-1 (ESA), Kaguya (Japan), Chang'e 1, 2, 3 (China), Chandrayaan-1 (India), LRO, LCROSS, ARTEMIS, GRAIL, and LADEE (USA). These new datasets (e.g., Fig. 1) have redefined our view of the Moon with regards to lunar time-stratigraphy, lunar crustal evolution, terrain formation, cratering processes, tectonic and geochemical processes, volatile reservoirs, and resource potential. During the projected three-year duration of NVM-II a variety of additional missions are possible. Potential missions include new Chang'e missions, a mission to return samples from the SPA such as MoonRise, SELENE-2, a new series of Russian Luna missions, a South Korean lunar orbiter, human missions in cislunar space using the Orion spacecraft, surface missions designed for resource exploration and utilization, and commercial missions linked to the Google X-Prize.

3. New Perspective from Samples

Since 2006, using new or improved analytical approaches, sample studies have shed light on the nature, behaviour, and role of volatile reservoirs in the lunar mantle and crust, the age and evolution of the lunar highlands, age and origin of the Moon, and dynamical processes in the early Solar System. Ion microprobe studies of lunar volcanic glasses and apatite in mare basalts indicate H-bearing species are in higher abundance in the lunar interior than expected and that there are distinct endogenous volatile reservoirs in the lunar mantle. New age dates on lunar highlands rocks have identified a major lunar thermal event at approximately 4.35-4.38 Ga. Does this event represent the termination of the primordial differentiation of the Moon via the lunar magma ocean or is it a major mantle event such as the overturn of the lunar magma ocean cumulate pile? NVM-II is designed to help address this and other questions arising from recent sample studies while integrating with remotely sensed results.

4. A New Perspective from Engineering and Resource Utilization

The lunar missions this century have also generated new observations that directly enable future human missions to the Moon while providing a foundation for future human activity in the Earth-Moon system and beyond enabled by the identification of lunar resources. For example, the meter-scale Digital Terrain Models produced by LRO permit terrain referenced navigation as well as morphometric assessment of lunar terrains, enabling optimized hardware decisions and increasing the chance of mission success. In another example, new illumination maps now available for the Moon characterize the distribution and nature of volatile and solar resources on the lunar surface, permitting efficient future utilization of a variety of lunar resources to sustain human exploration and commerce beyond LEO and into the Solar System.

5. Proposal for a New International Lunar Initiative

The time is right to synthesize these new observations and to integrate them with our understanding of the Moon prior to 2006. NVM-II will build upon both NVM-I and the Lunar Sourcebook to produce a comprehensive new science and engineering assessment of the Moon. The initiative will consist of topical workshops, special meeting sessions, and Web-based resource collections, leading to a book product. Themes that will be included in the initiative are: Summary of 2001-2015 lunar missions and their goals, the origin of the Moon, initial differentiation and late accretion, impact chronology of the Moon, cratering processes and history, the constitution and structure of the lunar interior, lunar tectonics, lunar volatiles in the interior, volatiles on the lunar surface, exosphere and interactions with the lunar surface, lunar resources, lessons learned, and future exploration goals. NVM-II has already been presented to the Lunar Exploration Analysis Group in the Fall of 2014 and to the planetary community at the Lunar and Planetary Science Conference in the Spring of 2015. This abstract and presentation is a solicitation for input from the international lunar community.

EPSC Abstracts
Vol. 10, EPSC2015-896, 2015
European Planetary Science Congress 2015

Spatial distribution of steep slopes on the Moon

M. Kreslavsky (1,2) and **J. Head** (3)
(1) University of California - Santa Cruz, California, USA (2) Moscow State University of Geodesy and Cartography (MIIGAiK), Moscow, Russia (3) Brown University, Providence, Rhode Island, USA (mkreslav@uscs.edu)

1. Introduction

Statistical characterization of topographic slopes is a valuable tool for comparison of planetary landscapes and understanding of landscape evolution processes. The steepest slopes are of special interest because they are more sensitive to alteration; on the Moon with its generally old and stable surface, their sensitivity is important. Here we analyze global spatial distribution of the steepest slopes on the Moon.

2. Data processing

We used the entire set of LOLA data obtained during LRO operations in the circular orbit from September 2009 to December 2011 (LRO orbits 1005 – 11403). We excluded night-time data affected by the LOLA anomaly [1]. Each LOLA laser shot produced 5 elevation measurements for five spots, one in the center, and four around it at ~25 m separation. For each of ~6×10^8 successful laser shots we measured four 2D slopes (gradient vectors) at ~25 m baseline using four spot triplets. Then we selected and listed all ~6×10^6 slopes steeper than 32º.

There is a significant observational bias related to the steepest slopes in the LOLA data set: on steep and/or rough terrain, many LOLA data points are missing. Moreover, the proportion of missing data points is different for different spots. This leads to a strong bias in estimation of the absolute proportion of the steepest slopes among all measured slopes. This also means that it is impossible to study statistics of slope orientations. However, our analysis showed that the proportion of missing data points is a rather stable quantity for each spot; it does not depend on latitude and only very weakly changes through the mission. This means that the large-scale spatial variations of the proportion of steep slopes are detected reliably. In addition to this bias, there are some false elevation measurements not marked as bad in the LOLA data set and thus formally producing false

3. Results and Interpretation

3.1 Geological correlations.

Slopes steeper than 40º (Fig. 1, upper pane) are associated with young (Copernican, might be Eratosthenian) craters, which is natural, because such steep slopes should inevitably degrade with time. Slopes steeper than 35º (Fig. 1, middle) are also typical for craters of the Late Imbrian age, but not for older ones. Orientale basin, the youngest impact basin on the Moon, is well seen in the steep slope maps. The basin rings (Montes Rook and Montes Cordillera) have steep slopes, including those steeper than 40º. Montes Apenninus (a part of Imbrium basin outer ring) have some steep slopes just above 35º, however, slopes here never approach 40º. Old impact basins do not have any expression in the steepest slope maps; however, Crisium basin becomes visible in slopes above 32º (Fig. 1, lower pane). All these observations are consistent with global seismic shaking caused by basin-forming impacts as a major surface-shaping factor [2]: the latest basin-forming impacts (Orientale, Imbrium) effectively removed all slopes steeper than the static angle of repose over the whole Moon.

3.2 Global distribution.

Global distribution of steep slopes is highly inhomogeneous: southern farside (roughly coinciding with South Pole - Aitken basin) has much lower density of craters with steep slopes than other heavily cratered terrains. Smoothed (down to spherical harmonics of degree 2 or 3, Fig. 2) global distribution strongly correlates with similarly smoothed elevation and subkilometer-baseline topographic roughness [3]. These correlations are difficult to explain. Subkilometer-baseline topographic roughness is is

controlled by regolith gardening processes, while steep slopes are related to bedrock / megaregolith processes, therefore, variations in steep slopes and roughness are different phenomena. Correlation with the predicted impact rate [4] and therefore with expected number of post-Orientale craters is worse, although the amplitudes of steep slope concentration toward equator and toward the western hemisphere are comparable to the predicted for impact rate.

Acknowledgements

We greatly appreciate efforts of the LOLA team resulted in the excellent data set we used. The technical work on data analysis was carried out by M.K. at MIIGAiK under Russian Science Foundation support, project 14-22-00197.

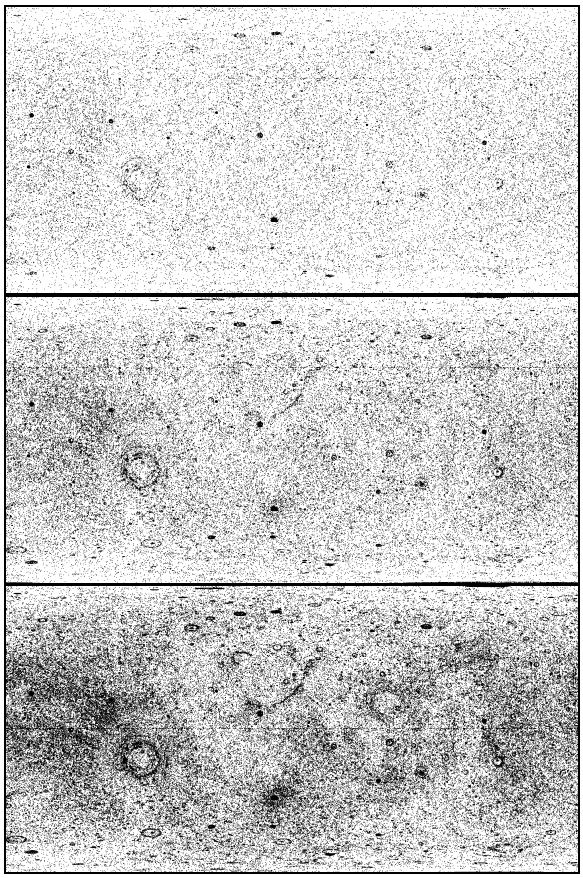

Figure 1: Distribution of locations (black dots) of slopes steeper than, top to bottom, 40º, 35º, and 32º. Global simple cylindrical projection centred at the sub-Earth point

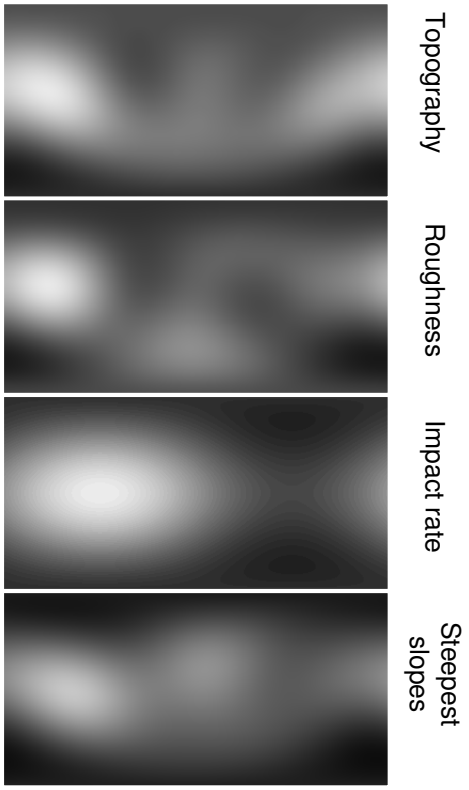

Figure 2: Global spatial distribution of elevation, topographic roughness, predicted modern impact rate [4], and proportion of slopes steeper than 35º, filtered down to spherical harmonics of degree 3. Global simple cylindrical projection centred at the sub-Earth point

References

[1] Smith, D. E., and 19 colleagues: Initial observations from the Lunar Orbiter Laser Altimeter (LOLA), Geophys. Res. Lett. Vol. 37, CiteID L18204, 2010.

[2] Kreslavsky, M., Head, J.: New observational evidence of global seismic effects of basin-forming impacts on the Moon from Lunar Reconnaissance Orbiter Lunar Orbiter Laser Altimeter data, J. Geophys. Res., Vol. 117, CiteID E00H24, 2012.

[4] Le Feuvre, M., Wieczorek, M.: Nonuniform cratering of the Moon and a revised crater chronology of the inner Solar System, Icarus, Vol. 214, p. 1-20, 2011.

[3] Kreslavsky, M., J. Head, G. Neumann, M. Rosenburg, O. Aharonson, D. Smith, and M. Zuber: Lunar topographic roughness maps from Lunar Orbiter Laser Altimeter (LOLA) data: Scale dependence and correlation with geologic features and units, Icarus, Vol. 226, p. 52-66, 2013.

EPSC Abstracts
Vol. 10, EPSC2015-916, 2015
European Planetary Science Congress 2015

The International Lunar Decade Declaration

V. Beldavs (1), B. Foing (2), D. Bland, and J. Crisafulli for the International Lunar Decade Working Group (3)
(1) FOTONIKA-LV national science center of the University of Latvia (vid.beldavs@fotonika-lv.eu / phone +371-27862021)
(2) ILEWG & ESTEC, (3) List of International Lunar Decade Working Group members at https://ildwg.wordpress.com/

Abstract

The International Lunar Decade Declaration was discussed at the conference held November 9-13, 2014 in Hawaii "The Next Giant Leap: Leveraging Lunar Assets for Sustainable Pathways to Space" – http://2014giantleap.aerospacehawaii.info/ and accepted by a core group that forms the International Lunar Decade Working Group (ILDWG) that is seeking to make the proposed global event and decade long process a reality. The Declaration will be updated from time to time by members of the ILDWG reflecting new knowledge and fresh perspectives that bear on building a global consortium with a mission to progress from lunar exploration to the transformation of the Moon into a wealth generating platform for the expansion of humankind into the solar system. When key organizations have endorsed the idea and joined the effort the text of the Declaration will be considered final. An earlier International Lunar Decade proposal was issued at the 8th ICEUM Conference in 2006 in Beijing together with 13 specific initiatives for lunar exploration[1,2,3]. These initiatives have been largely implemented with coordination among the different space agencies involved provided by the International Lunar Exploration Working Group [2,3]. The Second International Lunar Decade from 2015 reflects current trends towards increasing involvement of commercial firms in space, particularly seeking opportunities beyond low Earth orbit. The central vision of the International Lunar Decade is to build the foundations for a sustainable space economy through international collaboration concurrently addressing

- Lunar exploration and building a shared knowledge base;
- Policy development that enables collaborative research and development leading to lunar mining and industrial and commercial development;
- Infrastructure on the Moon and in cislunar space (communications, transport, energy systems, way-stations, other) that reduces costs, lowers risks and speeds up the time to profitable operations;
- Enabling technologies needed for lunar operations (robotic and human), lunar mining, materials processing, manufacturing, transportation, life support and other.

The current text of the International Lunar Decade, and update information can be found at.https://ildwg.wordpress.com/

References

[1] Planetary Society Press Release 31-03-2015 from http://www.planetary.org/pressroom/releases/2006/0708_Planetary_Society_Calls_for.html [2] ILEWG : http://sci.esa.int/ilewg ; [3] Foing, B. H.; Wu, J.; Iceum8 Participants, Beijing Lunar Declaration 2006, Advances in Space Research, Volume 42, Issue 2, p. 244-245. (online at http://sci.esa.int/ilewg/38863-iceum8-beijing-2006declaration/)

EPSC Abstracts
Vol. 10, EPSC2015-917, 2015
European Planetary Science Congress 2015

Strategy for the International Lunar Decade

V. Beldavs (1), D. Dunlop(2), B. Foing(3) for the International Lunar Decade Working Group(4)
(1) FOTONIKA-LV national science center of the University of Latvia (vid.beldavs@fotonika-lv.eu / phone +371-27862021)
(2) NSS, (3) ILEWG & ESTEC, (4)ILDWG members and their affiliations can be found at https://ildwg.wordpress.com/

Abstract

ILD is a global event and process for international collaboration in space initiated by the International Lunar Exploration Working Group (ILEWG), the National Space Society and the National Science Centre FOTONIKA-LV of the University of Latvia. ILD is planned for launch in 2017, the 60th anniversary of the International Geophysical Year that marked the dawn of the space age with the launch of Sputnik. ILD is envisioned as a decade long process of international collaboration with lunar exploration concurrent with development of policies, key enabling technologies and infrastructures on the Moon and in cislunar space leading towards an eventual goal of industrial development of the Moon and economic activity beyond Earth orbit [1]. This second International Lunar Decade will build on the foundations of the ILD first proposed in by the Planetary Society in 2006 at International Conference on Exploration and Utilisation of the Moon (ICEUM), was endorsed by ICEUM participants [3], and then by ILEWG, COSPAR and other organizations. Starting in 2007, the work plan included a series of recommendations for lunar exploration missions coordinated through the ILEWG agencies and COSPAR. Advances in technology such as CubeSats and 3D printing and fundamental changes in mind-set marked by initiatives such as the Google Lunar-X prize and asteroid mining ventures have made industrial development of the Moon a thinkable proposition. The ILD to be launched in 2017 is intended to set the stage for the Moon to become a wealth generating platform for human expansion into the solar system. ILD is being organized to engage existing organizations involved in space collaboration such as COSPAR, COPUOS, ISECG, technical and scientific organizations and others that address space policy, space law, space security, governance and related concerns. Additional organizations will be involved that deal with structures, ecosystems, financing, economic development and health and life support and related concerns. The Moon Treaty (1979) will be reviewed for its applicability to the development of the international regime that will be required to govern mining, industrial development and commercial activities on the Moon. ILD has already been a significant topic in several international conferences. Through this and many other conferences to follow the initial organizers expect that key organizations will see a role for their activities within the ILD process, endorse it and start to shape implementation plans. This report will focus on overall strategies for the ILD process to fully engage multiple countries and organizations building towards a shared vision through a diversity of scientific, technical and cultural perspectives. Public outreach and involvement of the public, particularly youth and schools will be an important component of the overall strategy. The activities of the International Lunar Decade Working Group can be followed at https://ildwg.wordpress.com/

References

[1] V. Beldavs, “The International Lunar Decade: Scenarios for long term collaboration in space development, The Space Review, retrieved 2015-05-01 from http://www.thespacereview.com/article/2728/1; [2] ILEWG website: http://sci.esa.int/ilewg ; [3] Foing, B. H.; Wu, J.; Iceum8 Participants, Beijing Lunar Declaration 2006, Advances in Space Research, Volume 42, Issue 2, p. 244-245. (online at http://sci.esa.int/ilewg/38863-iceum8-beijing-2006declaration/)

EPSC Abstracts
Vol. 10, EPSC2015-934, 2015
European Planetary Science Congress 2015

ILEWG Report and Introduction to EPSC session on Lunar Science and Exploration

B. Foing
ESA/ESTEC & ILEWG, postbus 299, 2200 AG Noordwijk, NL (Bernard.Foing@esa.int)

Abstract

We shall introduce the TP4 session on Lunar Science and Exploration and present a status report of ILEWG/COSPAR International Lunar Exploration Working Group to EPSC 2015.

1. Lunar session description

This TP4 session will highlight latest lunar science and exploration results, and recent missions.

It will address key questions on lunar geochemistry, geophysics, evolution, environment, volatiles relevant for planetary research.

We plan overview talks, contributed oral or poster presentations and workshop discussions.

In the last decade, an international fleet of orbiters (SMANRT-1, Kaguya, Chang'E1 & 2, Chandrayaan-1, LRO/LCROSS, Artemis, LADEE, GRAIL) has unveiled new faces of the Moon with new discoveries and questions. The Chang'e 3 lander and rover have opened a new lunar decade of surface activities towards a lunar robotic village with strong opportunities for science and exploration, and preparation for humans.

We shall discuss EPSC community inputs developing ILEWG/COSPAR, ISECG and other global roadmaps for robotic/human exploration.

How can the community support and prepare for upcoming lunar landers or orbital missions? The workshop will include the discussion of strategic measurements needed for exploration, and of possible science, instruments, terrestrial field work and simulation preparations.

2. ILEWG report

The International Lunar Exploration Working Group (ILEWG) was established in April 1995 at a meeting in Hamburg, Germany. As established in its charter, this working group reports to COSPAR and is charged with developing an international strategy for the exploration of the Moon. It discusses coordination between missions, and a road map for future international lunar exploration and utilisation. It fosters information exchange or potential and real future lunar robotic and human missions, as well as for new scientific and exploration information about the Moon.

We refer to COSPAR and ILEWG ICEUM and lunar conferences and declarations [1-19], present the GLUC/ICEUM11 declaration and give a report on ongoing relevant ILEWG community activities. We discuss how lunar missions SMART-1, Kaguya, Chang'E1&2, Chandrayaan-1, LCROSS, LRO, GRAIL, LADEE, Chang'E3 and upcoming missions contribute to lunar exploration objectives & roadmap.

References

[1] 1st International Lunar Workshop, Balsiger H. et al., Editors, European Space Agency, 1994. ESA-SP-1170.
[2] 2nd International Lunar Workshop, Kyoto, H. Mizutani, editor, Japan Space Forum Publisher, 1997.
[3] 3rd International Lunar Workshop, Moscow 1998, E. Galimov, editor.
[4] ICEUM4, ESTEC, 2000, ESA SP-462, B.H. Foing & M. Perry, editors.
[5] ICEUM5, Hawaii Nov 2003, Durst S.M. et al, Editors, Vol 108, 1-576 pp, Science and Technology Series, American Astronautical Society, 2004.
[6] ICEUM6, Udaipur 2004, Bhandari N., Editor, Journal Earth System Science, India, 114, No6, Dec 2005, pp. 573-841.
[7] ICEUM7, Toronto Sept 2005, sci.esa.int/ilewg.

[8] ICEUM8, Beijing July 2006, Journal of Chinese Society of Astronautics, Vol. 28 Sup., 2007, Ji W., Editor.
[9] ICEUM9, Sorrento, Italy, Foing B., Espinasse S., Kosters G., Editors. http://sci.esa.int/iceum9, Dec. 2007), and declaration http://sci.esa.int/ilewg/41506-iceum9-sorrento-2007-lunar-declaration/
[11] Ehrenfreund, P., Foing, B.H., Cellino, A. Editors, The Moon and Near Earth Objects, ASR Vol 37, 1, 2006.
[12] Foing, B.H. et al editors, 'Astronomy and Space Science from the Moon', ASR 14, 6, 1994.
[13] Ip W.-H., Foing, B.H., Masson Ph.L., editors, The Moon and Mars, ASR Vol 23, 11, 1999.
[14] Foing, B.H. et al, editor, Lunar Exploration, Planetary and Space Science, Vol 50, 14-15, 2002.
[15] Foing, B.H., Heather, D. editors, 'Lunar Exploration 2000', ASR Vol 30, Nr 8, 2002.
[16] Huntress, W. et al 'The next steps in exploring deep space - A cosmic study by the IAA', Acta Astronautica, Vol 58, Issues 6-7, 2006, p302-377.
[17] ICEUM10 Cape Canaveral declaration http://sci.esa.int/ilewg/43654-declaration-iceum10-leag-srr-florida-2008/
[18] ICEUM11-Global Lunar Beijing Declaration http://sci.esa.int/ilewg/47170-gluc-iceum11-beijing-2010lunar-declaration/
[19] Ehrenfreund P. et al (COSPAR planetary exploration panel report) 2012, ASR Vol 49, Nr 1, pp. 2-48.